Coherent control of molecular dynamics

2003 Rep. Prog. Phys. 66 859

(http://iopscience.iop.org/0034-4885/66/6/201)

INSTITUTE OF PHYSICS PUBLISHING REPORTS ON PROGRESS IN PHYSICS

Rep. Prog. Phys. **66** (2003) 859–942 PII: S0034-4885(03)12601-2

Coherent control of molecular dynamics

Moshe Shapiro[1,3,4] **and Paul Brumer**[2]

[1] Department of Chemical Physics, The Weizmann Institute, Rehovot 76100, Israel
[2] Chemical Physics Theory Group, Department of Chemistry, 80 St George St., University of Toronto, Toronto, Canada, M5S 3H6

E-mail: Moshe.Shapiro@weizmann.ac.il and pbrumer@tikva.chem.utoronto.ca

Received 9 January 2003
Published 12 May 2003
Online at stacks.iop.org/RoPP/66/859

Abstract

We review the principles and some recent advances in the theory of coherent control of molecular processes and discuss some of its experimental realizations. Amongst the topics discussed are: bichromatic and pump-dump control; the interference between N-photons and M-photon processes; the optical conversion of a mixture of left- and right-handed chiral molecules into an ensemble containing molecules of the handedness of choice; control of collisional processes; control over chaotic dynamics; effects of decoherence; the solution of the non-degenerate quantum control problem; and control over spontaneous emission and other decay processes.

[3] Author to whom correspondence should be addressed.
[4] Also at: Departments of Chemistry and Physics, The University of British Columbia, Vancouver Canada, V6T1Z1.

0034-4885/03/060859+84$90.00

1. Introduction

One of the central questions in physical science is the extent to which the future is determined by the present. Quantum mechanics, although a probabilistic theory, gives a deterministic answer to this question: the wavefunction of an isolated system at present completely determines the system wavefunction in the future. This is basically due to the fact that the Schrödinger equation is a first order differential equation in the time variable.

Thus, in order to predict future probabilities, all we need to do is to numerically solve the time dependent Schrödinger equation from the present to the future. Assuming that the integration of the Schrödinger equation is possible, and hence, that given the present we are able to predict future probabilities, a more ambitious question can then be asked: given an initial wavefunction at present, what dynamics (e.g. the Hamiltonian) guarantees a particular, desired outcome in the future? This question constitutes the essence of the field now called quantum control [1, 2].

Developments over the past fifteen years make clear that such control is based on the fundamental principle of coherent control (CC) [3–14], i.e. that control can be achieved by manipulating quantum interferences that arise when the desired final state is reached through a number of indistinguishable pathways. Such interferences can often be manipulated by simply varying aspects of radiation incident on the system, as described in detail below. This CC methodology is the subject of this review.

We note, for completeness, that obtaining maximal control to achieve a desired target may well necessitate a means of tuning the system and the laser parameters to optimally achieve the desired objective. This is the subject of optimal control, which is discussed elsewhere [1, 2, 15–26].

2. Preliminaries

2.1. Photo-excitation of a molecule with a pulse of light

Consider a molecule interacting with a pulse of coherent light where the light is described in terms of a purely classical electric field $\boldsymbol{E}(z, t)$ propagating along the z-axis:

$$\boldsymbol{E}(z, t) = \hat{\varepsilon}\varepsilon(z, t), \tag{1}$$

where

$$\varepsilon(z, t) = \int_{-\infty}^{\infty} \mathrm{d}\omega\, \epsilon(\omega) \exp\left[-\mathrm{i}\omega\left(t - \frac{z}{c}\right)\right] \tag{2}$$

is the strength of the field and $\hat{\varepsilon}$ is the polarization direction vector. The quantity ω denotes the frequency. The dynamics of the system is described by a time dependent Hamiltonian, $H(t) = H_M + H_{\mathrm{MR}}$, where H_M is the (radiation free) material Hamiltonian and H_{MR} is the matter-radiation interaction, given in the dipole approximation as

$$H_{\mathrm{MR}} = -\boldsymbol{d} \cdot \boldsymbol{E}(z, t). \tag{3}$$

The dynamics of the radiation-free molecule is fully described by the (discrete or continuous) set of energy eigenvalues and eigenfunctions, denoted, respectively, as E_n and $|E_n\rangle$, of the material Hamiltonian H_M:

$$H_M|E_n\rangle = E_n|E_n\rangle. \tag{4}$$

Given E_n and $|E_n\rangle$, the full time dependent Schrödinger equation

$$\frac{\mathrm{i}\hbar\partial|\Psi(t)\rangle}{\partial t} = H|\Psi(t)\rangle \tag{5}$$

can be solved by expanding $|\Psi(t)\rangle$ in terms of $|E_n\rangle$:

$$|\Psi(t)\rangle = \sum_n b_n(t)|E_n\rangle \exp\left(-\frac{\mathrm{i}E_n t}{\hbar}\right) \tag{6}$$

with the $b_n(t)$ coefficients given (using the orthonormality of the $|E_n\rangle$ basis functions), as the solution of a set of first order differential equations:

$$\frac{\mathrm{d}b_m(t)}{\mathrm{d}t} = \left(\frac{1}{i\hbar}\right)\sum_n b_n(t)\exp(\mathrm{i}\omega_{m,n}t)\langle E_m|H_{\mathrm{MR}}(t)|E_n\rangle. \tag{7}$$

Here, $\omega_{m,n} \equiv (E_m - E_n)/\hbar$.

Consider first the case where the molecule is initially ($t = -\infty$) in a single state $|E_1\rangle$, i.e. where

$$b_1(t=-\infty) = 1 \qquad \text{and} \qquad b_k(t=-\infty) = 0 \quad \text{for } k \neq 1. \tag{8}$$

Formally integrating equation (7), while neglecting all coefficients on the right-hand side save for $b_1(t)$, we obtain that,

$$b_m(t) = \int_{-\infty}^{t} b_1(t)\exp(\mathrm{i}\omega_{m,1}t)\langle E_m|H_{\mathrm{MR}}(t)|E_1\rangle. \tag{9}$$

If the perturbation is weak we can also assume that $b_1(t) = 1$ at all times, to obtain that,

$$\begin{aligned} b_m(t) &= -\frac{\mathrm{d}_{m,1}}{\mathrm{i}\hbar}\int_{-\infty}^{t}\mathrm{d}t'\exp[\mathrm{i}\omega_{m,1}t']\varepsilon(z,t') \\ &= -\frac{\mathrm{d}_{m,1}}{\mathrm{i}\hbar}\int_{-\infty}^{\infty}\mathrm{d}\omega\,\bar{\epsilon}(\omega)\int_{-\infty}^{t}\mathrm{d}t'\exp[\mathrm{i}(\omega_{m,1}-\omega)t'], \end{aligned} \tag{10}$$

where

$$\mathrm{d}_{m,1} \equiv \langle E_m|\hat{\varepsilon}\cdot\boldsymbol{d}|E_1\rangle \qquad \text{and} \qquad \bar{\epsilon}(\omega) \equiv \epsilon(\omega)\exp\left[\frac{\mathrm{i}\omega z}{c}\right]. \tag{11}$$

Here, $\hat{\varepsilon}\cdot\boldsymbol{d}$ is the projection of the transition-dipole operator along the electric field direction.

Equation (10) provides the expansion coefficients at any time t. If our interest is in observing or controlling the final product states (as it is in photodissociation) then we only require the wavefunction $\Psi(t)$ as $t \to +\infty$. In this limit, we can insert the equality

$$\int_{-\infty}^{\infty}\mathrm{d}t'\exp[\mathrm{i}(\omega_{m,1}-\omega)t'] = 2\pi\,\delta(\omega_{m,1}-\omega) \tag{12}$$

into equation (10) to obtain

$$b_m(+\infty) = \frac{2\pi\,\mathrm{i}}{\hbar}\bar{\epsilon}(\omega_{m,1})\mathrm{d}_{m,1} = \frac{2\pi\,\mathrm{i}}{\hbar}|\epsilon(\omega_{m,1})|\mathrm{d}_{m,1}\exp\left[\mathrm{i}\left(\phi(\omega_{m,1}) + \frac{\omega_{m,1}z}{c}\right)\right], \tag{13}$$

where ϕ is defined as the phase of $\epsilon(\omega)$, i.e., $\epsilon(\omega) = |\epsilon(\omega)|\exp(i\phi(\omega))$.

Equation (13) clearly shows that in preparing the state $|E_m\rangle$, the light field has imparted both a magnitude as well as a phase to $\Psi(t)$.

2.2. Photodissociation

Photodissociation results when the energy eigenstates reached by photon absorption are in the continuum. When the spectrum is continuous we have to use the scattering wavefunctions as the states of matter. These are defined as eigenstates $|E, \boldsymbol{m}\rangle$ of the material Hamiltonian with

continuous energy eigenvalues E, i.e.

$$[E - H_M]|E, \boldsymbol{m}\rangle = 0 \tag{14}$$

with normalization chosen as

$$\langle E', \boldsymbol{m}|E, \boldsymbol{n}\rangle = \delta(E - E')\delta_{\boldsymbol{m},\boldsymbol{n}}. \tag{15}$$

The index $\boldsymbol{m}$ designates a collection of additional quantum numbers that may be necessary to completely specify the state. In particular, if we regard the state $|E, \boldsymbol{m}\rangle$ as representing a collisional or a dissociation process, then $\boldsymbol{m}$ includes the chemical identity as well as all the internal (electronic, vibrational, rotational, etc) quantum numbers of the molecules that participate in the collision, before (or after) the event (see, e.g. [27]).

Using equations (6) and (13), it is evident that after the pulse is over the portion of the wavepacket excited to a continuous segment of the spectrum is given by

$$|\Psi'(t)\rangle = \left(\frac{2\pi \mathrm{i}}{\hbar}\right) \sum_{\boldsymbol{n}} \int \mathrm{d}E\, \bar{\epsilon}(\omega_{E,1}) \langle E, \boldsymbol{n}|\hat{\epsilon} \cdot \boldsymbol{d}|E_1\rangle |E, \boldsymbol{n}\rangle \exp\left(-\frac{\mathrm{i}Et}{\hbar}\right). \tag{16}$$

Consider then the long-time properties of equation (16). In order to do so we need to relate the eigenstates of H_M to the eigenstates that describe the freely moving fragments at the end of the process. We take as an example a triatomic molecule ABC, which fragments at the end of the process to yield, say, the $A + BC$ channel. Factorizing out the ABC centre-of-mass motion, we partition the remaining part of H_M into three parts

$$H_M = K_{\boldsymbol{R}} + K_{\boldsymbol{r}} + W(\boldsymbol{R}, \boldsymbol{r}). \tag{17}$$

Here, $\boldsymbol{R}$ is the radius vector separating A and the BC centre-of-mass, $\boldsymbol{r}$ is the $B - C$ separation; $W(\boldsymbol{R}, \boldsymbol{r})$ is the total potential energy of A, B and C, and

$$K_{\boldsymbol{R}} = \frac{-\hbar^2}{2\mu} \nabla^2_{\boldsymbol{R}}, \tag{18}$$

$$K_{\boldsymbol{r}} = \frac{-\hbar^2}{2m} \nabla^2_{\boldsymbol{r}} \tag{19}$$

are the kinetic energy operators in the $\boldsymbol{R}$ and $\boldsymbol{r}$ variables, with μ and m being the reduced masses,

$$\mu = \frac{m_A(m_B + m_C)}{(m_A + m_B + m_C)}, \qquad m = \frac{m_B m_C}{(m_B + m_C)}. \tag{20}$$

Denoting by $v(r)$ the asymptotic limit of $W(\boldsymbol{R}, \boldsymbol{r})$ as A separates from $B - C$,

$$v(r) = \lim_{R \to \infty} W(\boldsymbol{R}, \boldsymbol{r}), \tag{21}$$

it is clear that the $A - BC$ interaction potential, defined by

$$V(\boldsymbol{R}, \boldsymbol{r}) \equiv W(\boldsymbol{R}, \boldsymbol{r}) - v(r) \tag{22}$$

vanishes as $R \to \infty$,

$$\lim_{R \to \infty} V(\boldsymbol{R}, \boldsymbol{r}) = 0. \tag{23}$$

Defining the $B - C$ Hamiltonian as

$$h_{\boldsymbol{r}} \equiv K_{\boldsymbol{r}} + v(r), \tag{24}$$

the triatomic Hamiltonian of equation (17) can now be divided, using equation (22), into three parts,

$$H_M = K_{\boldsymbol{R}} + h_{\boldsymbol{r}} + V(\boldsymbol{R}, \boldsymbol{r}). \tag{25}$$

In the absence of the interaction potential $V(\boldsymbol{R}, \boldsymbol{r})$ the two free fragments A and BC described by the free Hamiltonian

$$H_0 \equiv K_{\boldsymbol{R}} + h_{\boldsymbol{r}} \tag{26}$$

move independently of one another. The eigenstates of H_0, $|E, \boldsymbol{n}; 0\rangle$, satisfying

$$[E - H_0]|E, \boldsymbol{n}; 0\rangle = 0 \tag{27}$$

are given as products

$$|E, \boldsymbol{n}; 0\rangle = |e_{\boldsymbol{n}}\rangle|E - e_{\boldsymbol{n}}\rangle. \tag{28}$$

Here, $|e_{\boldsymbol{n}}\rangle$, the internal states, satisfy the eigenvalue relation,

$$[e_{\boldsymbol{n}} - h_{\boldsymbol{r}}]|e_{\boldsymbol{n}}\rangle = 0 \tag{29}$$

with $e_{\boldsymbol{n}}$ being the internal (electronic, vibrational, rotational) energy of the $B - C$ diatomic. The $|E - e_{\boldsymbol{n}}\rangle$ states, satisfying the eigenvalue relation,

$$[E - e_{\boldsymbol{n}} - K_{\boldsymbol{R}}]|E - e_{\boldsymbol{n}}\rangle = 0, \tag{30}$$

describe the free (translational) motion of A relative to BC.

The eigenstates $|E, \boldsymbol{n}\rangle$ of the fully interacting Hamiltonian H_M and associated boundary conditions are related to $|E, \boldsymbol{n}; 0\rangle$ via the Lippmann–Schwinger equations,

$$|E, \boldsymbol{n}^{\pm}\rangle = |E, \boldsymbol{n}; 0\rangle + \lim_{\epsilon \to 0}[E \pm \mathrm{i}\epsilon - H_0]^{-1} V |E, \boldsymbol{n}^{\pm}\rangle. \tag{31}$$

The 'plus' solutions are called the outgoing scattering states, and the 'minus' solutions are called the incoming scattering states, and relate to different boundary conditions, as shown below.

We now use the Lippmann–Schwinger equation to explore the long-time behaviour of the wavepacket $\Psi(t)$ created with the laser pulse. We can use either the outgoing or incoming states as the basis set for expanding $\Psi(t)$. Substituting equation (31) in (16), we obtain that

$$|\Psi'(t)\rangle = \left(\frac{2\pi\mathrm{i}}{\hbar}\right) \sum_{\boldsymbol{n}} \int \mathrm{d}E \, \exp\left(-\frac{\mathrm{i}Et}{\hbar}\right) \bar{\epsilon}(\omega_{E,1}) \langle E, \boldsymbol{n}^{\pm}|\hat{\varepsilon} \cdot \boldsymbol{d}|E_1\rangle \times \{|E, \boldsymbol{n}; 0\rangle + [E \pm \mathrm{i}\epsilon - H_0]^{-1} V |E, \boldsymbol{n}^{\pm}\rangle\}. \tag{32}$$

Using the spectral resolution of $[E \pm \mathrm{i}\epsilon - H_0]^{-1}$ we have from equation (32) that the amplitude for finding a free state $|E', \boldsymbol{m}; 0|$ at time t is given by

$$\langle E', \boldsymbol{m}; 0|\Psi'(t)\rangle = \left(\frac{2\pi\mathrm{i}}{\hbar}\right) \sum_{\boldsymbol{n}} \int \mathrm{d}E \, \exp\left(-\frac{\mathrm{i}Et}{\hbar}\right) \bar{\epsilon}(\omega_{E,1}) \langle E, \boldsymbol{n}^{\pm}|\hat{\varepsilon} \cdot \boldsymbol{d}|E_1\rangle \times \left\{\langle E'\boldsymbol{m}; 0|E, \boldsymbol{n}; 0\rangle + [E \pm \mathrm{i}\epsilon - E']^{-1} \langle E'\boldsymbol{m}; 0|V|E, \boldsymbol{n}^{\pm}\rangle\right\}. \tag{33}$$

Using the normalization of continuum states (equation (15)), we have that

$$\langle E', \boldsymbol{m}; 0|\Psi'(t)\rangle = \frac{2\pi\mathrm{i}}{\hbar} \exp\left(-\frac{\mathrm{i}E't}{\hbar}\right) \bar{\epsilon}(\omega_{E',1}) \langle E', \boldsymbol{m}^{\pm}|\hat{\varepsilon} \cdot \boldsymbol{d}|E_1\rangle + \frac{2\pi\mathrm{i}}{\hbar} \sum_{\boldsymbol{n}} \int \mathrm{d}E \, \exp\left(-\frac{\mathrm{i}Et}{\hbar}\right) \times \bar{\epsilon}(\omega_{E,1}) \langle E, \boldsymbol{n}^{\pm}|\hat{\varepsilon} \cdot \boldsymbol{d}|E_1\rangle [E \pm \mathrm{i}\epsilon - E']^{-1} \langle E'\boldsymbol{m}; 0|V|E, \boldsymbol{n}^{\pm}\rangle. \tag{34}$$

In the $t \to \infty$ limit the integration over E can be performed analytically by contour integration. It is easy to show by supplementing the real-E integration by a semi-circle in the lower-half complex E-plane, that when using the '$-$' solutions the second term vanishes and we obtain that,

$$\lim_{t\to\infty} \langle E', \boldsymbol{m}; 0|\Psi'(t)\rangle = \left(\frac{2\pi \mathrm{i}}{\hbar}\right) \bar{\epsilon}(\omega_{E',1}) \exp\left(-\frac{\mathrm{i}E't}{\hbar}\right) \langle E', \boldsymbol{m}^-|\hat{\epsilon}\cdot\boldsymbol{d}|E_1\rangle. \tag{35}$$

Thus, the coefficients of expansion of the excited wavepacket in terms of the $|E, \boldsymbol{m}^-\rangle$ states, yield directly the probability-amplitude of observing states $|E, \boldsymbol{m}; 0\rangle$ *in the distant future*. Hence, the 'minus' states are the natural basis functions to employ in photodissociation problems.

This treatment assumes that the product comprises a single arrangement channel, i.e. the formation of $A + BC$ as the final product. The extension of this formalism to multiple product arrangements, e.g. where $A + BC$ and $AB + C$ are products of ABC photodissociation, or where $A + BC$ collide to form $A + BC$ and $A + BC$, requires: (a) the addition of a channel label $q = 1, 2, \ldots$ to the descriptor of the state, so that $|E, \boldsymbol{m}, q; 0\rangle$ corresponds to arrangement q; and (b) rewriting equations (17)–(31) to partition the Hamiltonian in a fashion appropriate to the final arrangement of interest. Thus, for example, for the $AB + C$ arrangement, the vector $\boldsymbol{R}$ defines the AB to C distance, $\boldsymbol{r}$ defines the $A - B$ separation, etc.

The photodissociation probability into the state characterized by $\boldsymbol{n}$ at energy E, $P_{\boldsymbol{n}}(E|\mathrm{i})$, when starting in state $|E_\mathrm{i}\rangle$ is given by the square of $A_{\boldsymbol{n}}(E|\mathrm{i})$, the photodissociation amplitude for observing the free state $\exp(-\mathrm{i}Et/\hbar)|E, \boldsymbol{n}; 0\rangle$ in the long-time limit. That is,

$$P_{\boldsymbol{n}}(E|\mathrm{i}) = |A_{\boldsymbol{n}}(E|\mathrm{i})|^2, \tag{36}$$

with $A_{\boldsymbol{n}}(E|\mathrm{i})$ defined as

$$A_{\boldsymbol{n}}(E|\mathrm{i}) = \lim_{t\to\infty} \exp\left(\frac{\mathrm{i}Et}{\hbar}\right) \langle E, \boldsymbol{n}; 0|\Psi(t)\rangle. \tag{37}$$

Because the bound and continuum wavefunctions usually belong to different electronic manifolds, they are orthogonal to one another and the only term that contributes to $A_{\boldsymbol{n}}(E|\mathrm{i})$ derives from Ψ', the excited part of the wavepacket. It follows from the boundary conditions on $|E, \boldsymbol{n}^-\rangle$ (equation (35)), that the $t \to \infty$ limit of equation (32) can be written as

$$|\Psi'(t \to \infty)\rangle = \frac{2\pi \mathrm{i}}{\hbar} \sum_{\boldsymbol{n}} \int \mathrm{d}E\, \bar{\epsilon}(\omega_{E,i}) |E, \boldsymbol{n}; 0\rangle \langle E, \boldsymbol{n}^-|\mathrm{d}_{e,g}|E_i\rangle \exp\left(-\frac{\mathrm{i}Et}{\hbar}\right), \tag{38}$$

where $\mathrm{d}_{e,g} \equiv \langle e|\hat{\epsilon}\cdot\boldsymbol{d}|g\rangle$, with $|g\rangle$ and $|e\rangle$ being the ground and an excited electronic state, respectively. Using the orthonormality of the $|E, \boldsymbol{n}; 0\rangle$ functions, we obtain from equation (37) that

$$A_{\boldsymbol{n}}(E|\mathrm{i}) = \frac{2\pi \mathrm{i}}{\hbar} \bar{\epsilon}(\omega_{E,i}) \langle E, \boldsymbol{n}^-|\mathrm{d}_{e,g}|E_i\rangle. \tag{39}$$

Note that by using incoming states, we have shown that the coefficient of the state $|E, \boldsymbol{n}^-\rangle$ at time $t = 0$ in equation (38) is exactly $A_{\boldsymbol{n}}(E|\mathrm{i})$, the long-time photodissociation amplitude. Thus, we obtain the crucial insight that the probability of obtaining product in the state $|E, \boldsymbol{n}; 0\rangle$ is given solely by the probability of preparing the state $|E, \boldsymbol{n}^-\rangle$ at the time of preparation.

3. Weak-field CC

The traditional scenario of molecular excitation and subsequent system evolution whose theory was developed in the preceding section, affords little opportunity to control the outcome

of molecular events. In order to understand why this is so and how the problem may be overcome [28] we note that even beyond the weak perturbation limit the probability of dissociation into a particular product state at any given time is given as

$$P_{\boldsymbol{m}}(E)(t) = |\langle e_{\boldsymbol{m}}|\langle \boldsymbol{k}_{\boldsymbol{m}}|\Psi(t)\rangle|^2. \tag{40}$$

Using the expansion of the wavepacket

$$|\Psi(t)\rangle = b_1(t)\exp\left(\frac{-\mathrm{i}E_1 t}{\hbar}\right)|E_1\rangle + \sum_{\boldsymbol{n}}\int \mathrm{d}E\, b_{E,\boldsymbol{n}}(t)\exp\left(\frac{-\mathrm{i}Et}{\hbar}\right)|E,\boldsymbol{n}^-\rangle$$

we have that

$$\begin{aligned}\langle e_{\boldsymbol{m}}|\langle \boldsymbol{k}_{\boldsymbol{m}}|\Psi(t)\rangle &= b_1(t)\langle e_{\boldsymbol{m}}|\langle \boldsymbol{k}_{\boldsymbol{m}}|E_1\rangle\exp\left(-\frac{\mathrm{i}E_1 t}{\hbar}\right)\\ &\quad+\sum_{\boldsymbol{n}}\int \mathrm{d}E\, b_{E,\boldsymbol{n}}(t)\langle e_{\boldsymbol{m}}|\langle \boldsymbol{k}_{\boldsymbol{m}}|E,\boldsymbol{n}^-\rangle\exp\left(-\frac{\mathrm{i}Et}{\hbar}\right).\end{aligned} \tag{41}$$

Assuming that $\langle e_{\boldsymbol{m}}|E_1\rangle = 0$, (e.g. the two-states belong to different electronic states), it follows from equation (41) that in the long-time limit

$$P_m(E) = |\langle e_{\boldsymbol{m}}|\langle \boldsymbol{k}_{\boldsymbol{m}}|\Psi(t\to\infty)\rangle|^2 = |b_{E,\boldsymbol{m}}(t\to\infty)|^2. \tag{42}$$

It follows from equation (9) extended to continuum states, and assuming that the light field is in near-resonance with only the bound-free transition frequencies $\omega_{E,1}$, that

$$b_{E,\boldsymbol{n}}(t) = \frac{\mathrm{i}}{\hbar}\langle E,\boldsymbol{n}^-|\hat{\boldsymbol{\varepsilon}}\cdot\boldsymbol{d}|E_1\rangle\int_{-\infty}^{t}\mathrm{d}t'\varepsilon(t')\exp(-\mathrm{i}\omega_{E,1}t)b_1(t'). \tag{43}$$

Hence,

$$\frac{P_{\boldsymbol{n}}(E)}{P_{\boldsymbol{m}}(E)} = \left|\frac{b_{E,\boldsymbol{n}}(\infty)}{b_{E,\boldsymbol{m}}(\infty)}\right|^2 = \left|\frac{\langle E,\boldsymbol{n}^-|\hat{\boldsymbol{\varepsilon}}\cdot\boldsymbol{d}|E_1\rangle}{\langle E,\boldsymbol{m}^-|\hat{\boldsymbol{\varepsilon}}\cdot\boldsymbol{d}|E_1\rangle}\right|^2. \tag{44}$$

Thus, the branching ratios at a fixed energy E, control over which is generally sought, are independent of the external field(s). Hence, varying the parameters of the external field(s) will have no effect on the asymptotic branching ratios. That is, there is no way we can control the product ratios of the photodissociation event. This result, which coincides with that of perturbation theory, holds true as long as there is only one initial-state $|E_1\rangle$ that is excited to the continuum.

The above argument motivates the idea that the way to control photodissociation is to use more than one initial-state, or in greater generality, to use multiple excitation pathways. In this section, we demonstrate that such a strategy allows us to actively influence and control which photodissociation product is formed. These ideas, which introduce the notion of 'CC', will be later shown to hold true for any dynamical process, not just for photodissociation.

3.1. Photodissociation from a superposition state

We introduce the basic principles of CC through a series of examples. In particular, we extend the treatment of section 2.2 to the photodissociation of a non-stationary superposition of bound states, $|\chi(0)| = \sum_{j=1}^{N} a_j|E_j\rangle\exp(-\mathrm{i}E_j t/\hbar)$. Numerous experimental techniques can be used to create such a state. Whatever the method of preparation, the amplitude and phase of the coefficients a_j are functions of the experimentally controllable parameters used in creating the superposition.

Repeating the treatment of weak-field photodissociation given in section 2.2, but now for an initial superposition state, gives the same result as trivially replacing, in the

final result (equation (16)), the single initial-state $|E_1\rangle \exp(-\mathrm{i}E_1 t/\hbar)$ by the superposition $\sum_{j=1}^{N} a_j |E_j\rangle \exp(-\mathrm{i}E_j t/\hbar)$. Thus, at the end of the excitation pulse the system wavefunction at time t is given by

$$|\Psi(t)\rangle = \sum_{j=1}^{N} a_j |E_j\rangle \exp\left(-\frac{\mathrm{i}E_j t}{\hbar}\right) + \left(\frac{2\pi \mathrm{i}}{\hbar}\right) \sum_{j=1}^{N} a_j \times \sum_{\boldsymbol{n}} \int \mathrm{d}E\, \bar{\epsilon}(\omega_{E,j}) \langle E, \boldsymbol{n}^- | \mathrm{d}_{e,g} | E_j \rangle |E_0, \boldsymbol{n}^-\rangle \exp\left(-\frac{\mathrm{i}Et}{\hbar}\right), \tag{45}$$

where $\omega_{E,j} \equiv (E - E_j)/\hbar$. The probability $P_{\boldsymbol{n}}(E)$ of being in the final state $|E, \boldsymbol{n}; 0\rangle$ is $P_{\boldsymbol{n}}(E) = |A_{\boldsymbol{n}}(E)|^2$, where the probability-amplitude $A_{\boldsymbol{n}}(E)$ is given by (using equations (15) and (37))]

$$A_{\boldsymbol{n}}(E) = \lim_{t\to\infty} \exp\left(\frac{\mathrm{i}Et}{\hbar}\right) \langle E, \boldsymbol{n}; 0 | \Psi(t)\rangle = \frac{2\pi \mathrm{i}}{\hbar} \sum_{j=1}^{N} a_j \bar{\epsilon}(\omega_{E,j}) \langle E, \boldsymbol{n}^- | \mathrm{d}_{e,g} | E_j \rangle. \tag{46}$$

Of particular interest is the probability of being in a complete subspace of states, denoted by the label q; that is, in all states $\boldsymbol{m}$ associated with a fixed q, where $\boldsymbol{n} = (\boldsymbol{m}, q)$. Summing over $\boldsymbol{m}$ we obtain that,

$$P_q(E) = \sum_{\boldsymbol{m}} P_{\boldsymbol{m},q}(E) = \sum_{\boldsymbol{m}} |A_{\boldsymbol{m},q}(E)|^2. \tag{47}$$

Inserting $A_{\boldsymbol{m},q}(E)$ from equation (46) gives

$$P_q(E) = \left(\frac{2\pi}{\hbar}\right)^2 \sum_{i,j=1}^{N} [a_i a_j^* \bar{\epsilon}(\omega_{E,i}) \bar{\epsilon}^*(\omega_{E,j})] \mathrm{d}_q(ji), \tag{48}$$

where

$$\mathrm{d}_q(ji) = \sum_{\boldsymbol{m}} \langle E_j | \mathrm{d}_{g,e} | E, \boldsymbol{m}, q^-\rangle \langle E, \boldsymbol{m}, q^- | \mathrm{d}_{e,g} | E_i \rangle \tag{49}$$

and $\mathrm{d}_{g,e} = \mathrm{d}_{e,g}^*$. The branching ratio between two channels at energy E, $R_{q,q'}(E)$, which we control below is then,

$$R_{q,q'}(E) = \frac{P_q(E)}{P_{q'}(E)}. \tag{50}$$

Consider then the nature of $P_q(E)$ (equation (48)). The diagonal terms ($i = j$) give the standard probability, at energy E, of photodissociation out of a bound state $|E_j\rangle$ to produce a product in channel q. The off-diagonal terms ($i \neq j$) correspond to interference terms between these photodissociation routes. These interference terms describe the constructive enhancement, or destructive cancellation, of product formation in subspace q. Equation (48) is important in practice because the interference terms have coefficients $[a_i a_j^* \bar{\epsilon}(\omega_{E,i}) \bar{\epsilon}^*(\omega_{E,j})]$ whose magnitude and sign depend upon experimentally controllable parameters. Thus, the experimentalist can manipulate laboratory parameters and, in doing so, alter the interference term and hence control the reaction product yield. This control scenario can also be extended to the domain of moderately strong fields [29].

Equation (48) displays an important feature. That is, the entire control map, i.e. $P_q(E)$ or $R_{q,q'}(E)$ as a function of the control parameters, is a function of very few molecular parameters, i.e. the $\mathrm{d}_q(ji)$. As a consequence, the experimentalist need only determine these few parameters in order to produce the entire control map. This statement constitutes the weak-field version of 'Adaptive Feedback Control' [30–35]. In the general strong field regime, a numerical non-linear search procedure must be performed to achieve a desired optimization. However, in the

weak-field regime, because of the simple bilinear dependence of each $P_q(E)$ on the $a_j\bar{\epsilon}(\omega_{E,j})$ experimental parameters, we need only carry out $q \times N^2$ measurements to determine all the $\mathrm{d}_q(ji)$ coefficients. Once these coefficients are known, the bilinear $P_q(E)$ function can be analytically interpolated to give any desired branching ratio between, and including, the extrema of $R_{q,q'}(E)$.

3.2. Bichromatic control

Experimentally attaining control via equation (48) requires a light source containing N frequencies ω_i, $(i = 1, \ldots, N)$. Both pulsed excitation with a source whose frequency width encompasses these frequencies, as well as excitation with N continuous wave (cw) lasers of frequencies $\omega_i = \omega_{E,i}$, $(i = 1 \ldots N)$ are possible approaches, as depicted in figure 1. Here, we focus on $N = 2$, i.e. the effect of two cw lasers on a system in a superposition of two-states (figure 1(*c*)), a scenario that we call 'bichromatic control'.

Consider then two parallel cw fields of frequencies ω_1 and ω_2 incident on a molecule. The light–molecule interaction potential (equation (3)) is then

$$H_{\mathrm{MR}}(t) = -\sum_{i=1}^{2} 2\boldsymbol{d}\cdot\hat{\epsilon}\mathrm{Re}[\bar{\epsilon}(\omega_i)\exp(-\mathrm{i}\omega_i t)]. \tag{51}$$

Tuning the ω_1 and ω_2 frequencies such that, $\omega_2 - \omega_1 = (E_1 - E_2)/\hbar$, we have that $P_q(E)$ of equation (48), at energy $E = E_1 + \hbar\omega_1 = E_2 + \hbar\omega_2$, has only two contributions, corresponding to the excitations shown in figure 1(*c*). The quantities $P_q(E = E_1 + \hbar\omega_1)$ and $R_{q,q'}(E)$ are therefore given by [3, 7, 12–14]

$$\left(\frac{\hbar}{2\pi}\right)^2 P_q(E = E_1 + \hbar\omega_1) = |a_1|^2|\bar{\epsilon}(\omega_1)|^2\mathrm{d}_q(11) + |a_2|^2|\bar{\epsilon}(\omega_2)|^2\mathrm{d}_q(22) + 2\mathrm{Re}[a_1 a_2^*\bar{\epsilon}(\omega_1)\bar{\epsilon}^*(\omega_2)\mathrm{d}_q(12)], \tag{52}$$

$$R_{q,q'}(E) = \frac{|\mathrm{d}_q(11)| + x^2|\mathrm{d}_q(22)| + 2x\cos(\theta_1 - \theta_2 + \alpha_q(12))|\mathrm{d}_q(12)|}{|\mathrm{d}_{q'}(11)| + x^2|\mathrm{d}_{q'}(22)| + 2x\cos(\theta_1 - \theta_2 + \alpha_{q'}(12))|\mathrm{d}_{q'}(12)|}, \tag{53}$$

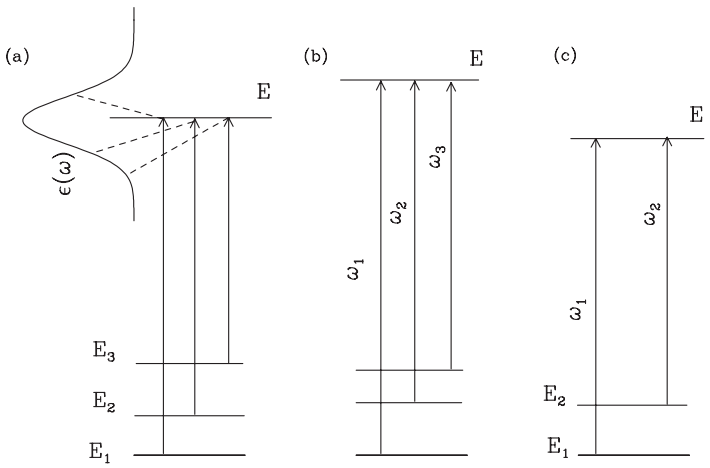

Figure 1. Photodissociation of a superposition of N levels using (*a*) a pulsed light source ($N = 3$ is shown); (*b*) N cw lasers ($N = 3$ is shown), and (*c*) $N = 2$ with two cw lasers.

where $\alpha_q(ij)$ and θ_j are defined via

$$\begin{aligned} \mathrm{d}_q(ij) &= |\mathrm{d}_q(ij)| \exp(\mathrm{i}\alpha_q(ij)), \qquad x = \frac{|\bar{\epsilon}(\omega_2)a_2|}{|\bar{\epsilon}(\omega_1)a_1|}, \\ \tan\theta_j &= \frac{\mathrm{Im}[\bar{\epsilon}(\omega_j)a_j]}{\mathrm{Re}[\bar{\epsilon}(\omega_j)a_j]}. \end{aligned} \tag{54}$$

For convenience, we have introduced the control variables $\Delta\theta = \theta_1 - \theta_2$ and $s = x^2/[x^2 + 1]$. The range $0 \leqslant s \leqslant 1$ covers all possible values of relative laser intensities. Varying $\Delta\theta$ or s, changes the interference term and thus gives us control over the dissociation probabilities. These changes may be accomplished either by varying the coefficients of the initial superposition state, $\{a_j\}$, or by changing the intensity and relative phases of the dissociation lasers. Note, in particular, that varying $\Delta\theta$ corresponds to just varying a phase. The dependence of the yield on $\Delta\theta$ hence emphasizes the quantum-interference-based nature of the control.

As an example of this approach we consider control over the relative probability of forming $^2P_{3/2}$ vs $^2P_{1/2}$ atomic iodine, denoted I and I*, in the dissociation of methyl iodide in the regime of 266 nm,

$$\mathrm{CH_3} + \mathrm{I}^*(^2P_{1/2}) \leftarrow \mathrm{CH_3I} \rightarrow \mathrm{CH_3} + \mathrm{I}(^2P_{3/2}). \tag{55}$$

This reaction is an example of electronic branching of photodissociation products. The results reported below are for a non-rotating two-dimensional model [36, 37] in which the H_3 centre-of-mass, the C and the I atoms are assumed to lie on a straight line.

Typical results for the control of the I vs I* channel are shown in figure 2, as contour plots of the yield of CH_3 + I as a function of the control parameters. Two cases are shown: photodissociation out of the two superposition states $|\chi(0)\rangle = a_1|E_1\rangle + a_2|E_2\rangle$ (figure 2(a)) and $|\chi(0)\rangle = a_1|E_1\rangle + a_3|E_3\rangle$ (figure 2(b)). Here, $|E_1\rangle$ is the ground state and $|E_2\rangle$ and $|E_3\rangle$ correspond to states with one and two quanta of excitation in the C–I bond. The results show a large range of possible control. For example, the yield changes in figure 2(b) from 30% to 70% as one varies s at small $\theta_1 - \theta_2$. In addition, a comparison of the two figures shows that the topology of the control plot depends strongly on the states that comprise the superposition state.

3.2.1. Energy averaging and satellite contributions. In general, experiments measure energy averaged quantities such as

$$P_q = \int \mathrm{d}E\, P_q(E), \qquad R_{q,q'} = \frac{P_q}{P_{q'}}, \tag{56}$$

since products are not distinguished on the basis of total energy. As such, it is necessary to compute photodissociation to all energies. For the case considered above, two-states irradiated with two cw fields of frequencies ω_1 and ω_2, $P_q(E)$ (equation (48)) is non-zero at three energies: $E = E_1 + \hbar\omega_1 = E_2 + \hbar\omega_2$, $E' = E_1 + \hbar\omega_2$ and $E'' = E_2 + \hbar\omega_1$.

The contribution from the first of these energies $P_q(E = E_1 + \hbar\omega_1)$ is given in equation (52) and shown on the left-hand side of figure 3. The remaining contributions, shown on the right-hand side of figure 3, are

$$\begin{aligned} P_q(E' = E_1 + \hbar\omega_2) &= \left(\frac{2\pi}{\hbar}\right)^2 |a_1\bar{\epsilon}(\omega_2)|^2 \mathrm{d}_q(11), \\ P_q(E'' = E_2 + \hbar\omega_1) &= \left(\frac{2\pi}{\hbar}\right)^2 |a_1\bar{\epsilon}(\omega_1)|^2 \mathrm{d}_q(22). \end{aligned} \tag{57}$$

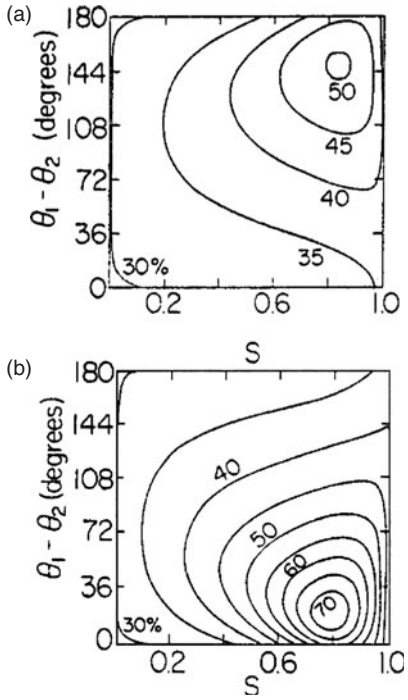

Figure 2. Contour plot of the yield of CH_3 + I from the photodissociation of CH_3I from a superposition of states at $\omega_1 = 37\,593.9\,\mathrm{cm}^{-1}$. (*a*) $|\chi(0)\rangle = a_1|E_1\rangle + a_2|E_2\rangle$, (*b*) $|\chi(0)\rangle = a_1|E_1\rangle + a_3|E_3\rangle$. Taken from figure 1, [3].

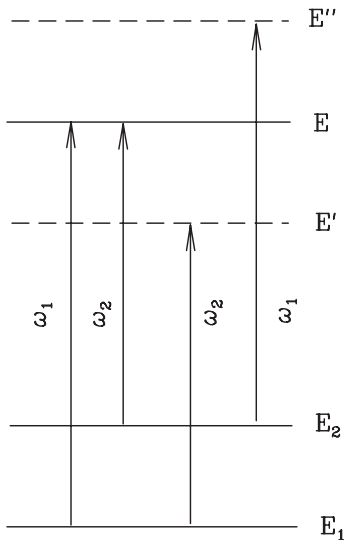

Figure 3. Contributions for two levels photodissociated by two frequencies. The interference terms correspond to total energy $= E$. The satellite terms correspond to total energies $= E'$ and E''.

Thus, the overall P_q for $N = 2$ is given by

$$P_q = P_q(E = E_1 + \hbar\omega_1) + P_q(E' = E_1 + \hbar\omega_2) + P_q(E'' = E_2 + \hbar\omega_1). \quad (58)$$

The latter two terms correspond to traditional photodissociation terms without associated interference contributions and provide uncontrollable photodissociation terms that we call 'satellites'. In this, and all CC scenarios discussed below, it is important to attempt to reduce the relative magnitude of the satellite terms in order to increase overall controllability.

We make the general observation that interference between terms of different energies contain oscillatory $\exp[\mathrm{i}(E_1 - E_2)t/\hbar]$ terms that average out to zero with time. (This is not to say that the oscillatory interference term cannot be put to good use. See, e.g. a proposal for generating terahertz radiation [38] using such oscillatory terms and a related experiment [39]).

4. The principle of CC and 'mode-selective chemistry'

Control of the type discussed above, in which quantum interference effects are used to constructively or destructively alter product properties, is called coherent control (CC). Photodissociation of a superposition state, the scenario described above, will be seen to be just one particular implementation of a general principle of CC: i.e. that coherently driving a state with phase coherence through multiple, coherent, indistinguishable, optical excitation routes to the same final state allows for the possibility of control. This procedure has a well-known analogy, the interference between paths as a beam of either particles or of light passes through a double slit. In that case interference between two coherent beams leads to spatial patterns of enhanced or reduced probabilities on an observation screen. In the case of CC the overall coherence of a pure state plus laser source allows for the constructive or destructive manipulation of probabilities in product channels. Active control results because the excitation process explicitly imparts experimentally controllable phase and amplitude information to the molecule.

As mentioned above, in general control can only arise from energetically degenerate states. Another way of seeing this is to note that products of states of different energies E and E' appearing in the square of the wavepacket of equation (45) cannot contribute to any measurement where the total energy is resolved. Such a measurement, which filters out all the wavepacket components save those belonging to a given value of E, eliminates all the $E \neq E'$ products. Alternatively, we note that two-states of different energy are in principle distinguishable. Hence, they cannot interfere with one another.

Numerous other scenarios can be designed that rely upon the essential CC principle. Several are discussed in the following sections.

We note that there is an alternative approach to the control of chemical reactions, called 'mode-selective chemistry', which does not rely upon quantum interferences. When applied to photodissociation, this approach would entail attempting to excite specific bonds in the molecule (e.g. the A–B bond in the A–B–C molecule) in order to produce a specific product (e.g. the $A + B - C$ product in the given example). Mode-selective chemistry, though very useful under favourable circumstances ([40–46], see [47] for a review), is of limited scope, because in most cases the chemical bond we wish to excite is strongly coupled to other bonds (i.e. the 'local mode' corresponding to excitation of one bond is not an eigenstate of the system Hamiltonian). As a consequence, most excitations result in the production of a highly delocalized wavepacket that entails excitation of many bonds. This phenomenon, is called intramolecular vibrational redistribution (IVR).

5. Interference between N-photon and M-photon routes

Another important example of CC introduces the possibility of quantum interference arising through competitive optical routes in the excitation of a single bound state to an energy E. Specifically, we consider the photodissociation of a single state via two pathways, an N-photon and an M-photon dissociation route. The N vs M scenarios are of two types, N and M of the same parity (i.e. both N and M odd or both even) or of opposite parity. The latter allows for control over the differential photodissociation cross-sections (i.e. scattering into different angles), or control of the integral cross-sections of systems lacking an inversion centre ('chiral' systems), whereas the former allows for control over both the integral and differential cross-sections. For simplicity, we focus on the two lowest order cases $(N, M) = (1, 2)$ and $(N, M) = (1, 3)$.

5.1. One vs three-photon interference

Consider [48] a molecule initially in state $|E_i\rangle$ subjected to two co-propagating cw fields of frequencies ω_1 and ω_3, with $\omega_3 = 3\omega_1$. The interaction potential is given by

$$H_{\mathrm{MR}}(t) = -2\boldsymbol{d} \cdot \mathrm{Re}[\hat{\epsilon}_3\bar{\epsilon}_3 \exp(-\mathrm{i}\omega_3 t) + \hat{\epsilon}_1\bar{\epsilon}_1 \exp(-\mathrm{i}\omega_1 t)], \tag{59}$$

where $\bar{\epsilon}_i \equiv \bar{\epsilon}(\omega_i)$.

We assume the following physics: (a) the dipole transitions within electronic states are negligible compared to those between electronic states; (b) the fields are sufficiently weak to allow the use of perturbation theory, and (c) $E_i + 2\hbar\omega_1$ is below the dissociation threshold, with dissociation occurring from the excited electronic state. The lowest order perturbation theory expression for the one-photon or three-photon dissociation amplitude $A_{\boldsymbol{m},q}(E = E_i + \hbar\omega_3)$ is

$$\begin{aligned} A_{\boldsymbol{m},q}(E = E_i + \hbar\omega_3) = \left(\frac{2\pi\mathrm{i}}{\hbar}\right) [&\delta(\omega_3 - \omega_{E,i})\bar{\epsilon}_3\langle E, \boldsymbol{m}, q^-|\mathrm{d}_{e,g}|E_i\rangle \\ &+\delta(3\omega_1 - \omega_{E,i})\bar{\epsilon}_1^3\langle E, \boldsymbol{m}, q^-|T_{e,g}|E_i\rangle], \end{aligned} \tag{60}$$

where, $T_{e,g}$ is the three-photon transition operator, given in third order perturbation theory as

$$T_{e,g} = \sum_{e'e''} \mathrm{d}_{e,e'}(E_i - H_{e'} + 2\hbar\omega_1)^{-1}\mathrm{d}_{e',e''}(E_i - H_{e''} + \hbar\omega_1)^{-1}\mathrm{d}_{e'',g}. \tag{61}$$

The probability to produce fragments q at a fixed energy E is therefore

$$P_q(E) = \sum_{\boldsymbol{m}} |A_{\boldsymbol{m},q}(E_i + \hbar\omega_3)|^2 = P_q^{(1)}(E) + P_q^{(3)}(E) + P_q^{(13)}(E), \tag{62}$$

where the one-photon photodissociation probability is

$$P_q^{(1)}(E) = \left(\frac{2\pi}{\hbar}\right)^2 |\bar{\epsilon}_3|^2 \sum_{\boldsymbol{m}} |\langle E, \boldsymbol{m}, q^-|\mathrm{d}_{e,g}|E_i\rangle|^2, \tag{63}$$

the three-photon dissociation probability is

$$P_q^{(3)}(E) = \left(\frac{2\pi}{\hbar}\right)^2 |\bar{\epsilon}_1|^6 \sum_{\boldsymbol{m}} |\langle E, \boldsymbol{m}, q^-|T_{e,g}|E_i\rangle|^2 \tag{64}$$

and the one-photon three-photon interference term is

$$P_q^{(13)}(E) = \left(\frac{2\pi}{\hbar}\right)^2 \left[\bar{\epsilon}_3\bar{\epsilon}_1^3 \sum_{\boldsymbol{m}} \langle E_i|T_{g,e}|E, \boldsymbol{m}, q^-\rangle\langle E, \boldsymbol{m}, q^-|\mathrm{d}_{e,g}|E_i\rangle + \mathrm{c.c.}\right], \tag{65}$$

where c.c. designates the complex conjugate.

As in our discussion of the photodissociation of a superposition state (section 3.1) we define a 'molecular' interference-amplitude $|F_q^{(13)}|$ and a 'molecular' phase $\alpha_q(13)$ as

$$|F_q^{(13)}| \exp[\mathrm{i}\alpha_q(13)] = \sum_{\boldsymbol{m}} \langle E_i | T_{g,e} | E, \boldsymbol{m}, q^- \rangle \langle E, \boldsymbol{m}, q^- | \mathrm{d}_{e,g} | E_i \rangle. \tag{66}$$

Recognizing that $\bar{\epsilon}_i$ is a complex number, $\bar{\epsilon}_i = |\bar{\epsilon}_i| \mathrm{e}^{\mathrm{i}\phi_i}$ we can write the above interference term as

$$P_q^{(13)}(E) = -2 \left(\frac{2\pi}{\hbar} \right)^2 |\bar{\epsilon}_3 \bar{\epsilon}_1^3| \cos(\phi_3 - 3\phi_1 + \alpha_q(13)) |F_q^{(13)}|. \tag{67}$$

The branching ratio $R_{qq'}(E)$ for channels q and q', (see equation (50)) can now be written as

$$R_{qq'}(E) = \frac{F_q^{(11)} - 2x \cos[\phi_3 - 3\phi_1 + \alpha_q(13)] \epsilon_0^2 |F_q^{(13)}| + x^2 \epsilon_0^4 F_q^{(33)}}{F_{q'}^{(11)} - 2x \cos[\phi_3 - 3\phi_1 + \alpha_{q'}(13)] \epsilon_0^2 |F_{q'}^{(13)}| + x^2 \epsilon_0^4 F_{q'}^{(33)}}, \tag{68}$$

where

$$F_q^{(11)} = \left(\frac{\hbar}{\pi |\bar{\epsilon}_3|} \right)^2 P_q^{(1)}(E), \qquad F_q^{(33)} = \left(\frac{\hbar}{\pi |\bar{\epsilon}_1|^3} \right)^2 P_q^{(3)}(E), \qquad x = \frac{|\bar{\epsilon}_1|^3}{\epsilon_0^2 |\bar{\epsilon}_3|}, \tag{69}$$

where ϵ_0 is defined as a single unit of electric field; x is therefore a dimensionless parameter.

The numerator and denominator of equation (68) each display the canonical form for CC, i.e. a form similar to equation (53) in which there are independent contributions from more than one route, modulated by an interference term. Since the interference term is controllable through variation of the (x and $\phi_3 - 3\phi_1$) laboratory parameters, so too is the branching ratio $R_{qq'}(E)$. Thus, the principle upon which this control scenario is based is the same as that in section 3.1 but the interference is introduced in an entirely different way.

The three-photon vs one-photon scenario has been experimentally realized by Elliott *et al* in atoms [49], and by Gordon and co-workers [50–54] in a series of experiments on HCl and CO. In the case of HCl, shown in figure 4, the molecule was excited to an intermediate $^3\Sigma^-(\Omega^+)$ vib-rotational resonance, using a combination of three ω_1 ($\lambda_1 = 336$ nm) photons and one ω_3 ($\lambda_3 = 112$ nm) photon. The ω_3 beam was generated from an ω_1 beam by tripling in a Kr gas cell. Ionization of the intermediate state takes place by absorption of one additional ω_1 photon. The relative phase of the light fields was varied by passing the ω_1 and ω_3 beams through a second Ar or H_2 ('tuning') gas cell of variable pressure.

The HCl experiments verified the predictions of CC theory concerning the sinusoidal dependence of the ionization rates on the relative phase of the two exciting lasers. The HCl experiment also verified the prediction of the dependence of the strength of the sinusoidal modulation of the ionization current on the relative laser field intensities. Similar demonstrations for ammonia, trimethylamine, triethylamine, cyclooctatetraene, and 1,1-dimethylhydrazine by Bersohn and co-workers [55] have been reported.

Gordon has also demonstrated [52] control of ionization in H_2S, in a jet with a large distribution of j-states. Although in this case both a dissociation and an ionization channel are possible, i.e. $H_2S^+ \leftarrow H_2S \rightarrow H + HS$, no discrimination between the possible outcomes of the photoexcitation has been observed: the signals of all final channels oscillate in phase as the relative phase $\phi_3 - 3\phi_1$ is varied.

By contrast, in the $HI^+ \leftarrow HI \rightarrow H + I$ case, control over the production of different channels, specifically the HI^+ vs the H + I channels, has been observed [53, 54]. The experimental results, shown in figure 5, are highly significant as, contrary to the H_2S case, the modulations in the I^+ signal are seen to be out of phase with those of the HI^+ signal. Thus, control overdifferent reaction products has been demonstrated. That is, by changing $\phi_3 - 3\phi_1$,

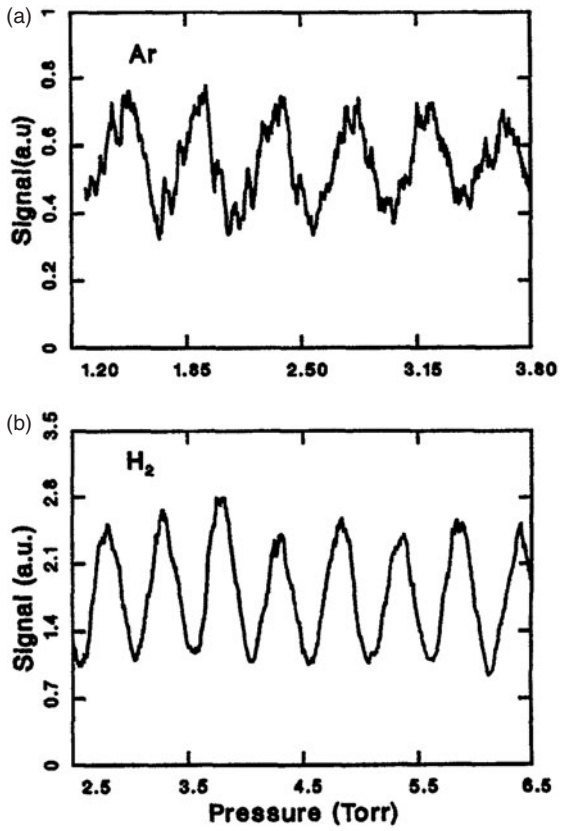

Figure 4. Ionization signal for the HCl $R(2)$ transition as a function of pressure in the tuning cell, using either (*a*) Ar or (*b*) H_2 to control the relative phases of ω_1 and ω_3. Taken from figure 2, [50].

the phase difference between the ω_3 and the ω_1 laser fields, through the change in the pressure of the H_2 gas in the tuning cell, different I^+/HI^+ ratios are attained.

The quantitative nature of the observed control depends upon the values of $F_q^{(13)}$ and the 'molecular phase', α_q. In particular, the value of $\alpha_q - \alpha_{q'}$ dictates the shift between the peaks in $P_q(E)$ and $P_{q'}(E)$. For example, a molecular case where $\alpha_q - \alpha_{q'} \approx 0$ (e.g. in the $H_2S^+ \leftarrow H_2S \rightarrow H + HS$ case discussed above) shows less discrimination between channels than does a molecular case where $\alpha_q - \alpha_{q'} = \pi$. Hence, the relationship between the nature of the dynamics and the α_q values is of interest, a topic studied in detail by Gordon *et al* [56].

A crucial aspect of these experiments is the requirement that the two co-propagating ω_1 and ω_3 beams satisfy the 'phase-matching' condition $\boldsymbol{k}_3 = 3\boldsymbol{k}_1$. As a result, equation (68) no longer depends upon the spatial coordinate z and the interference term is independent of the position in space.

The above results show that it is possible to control the integral cross-section into channel q via one-photon vs three-photon absorption. A similar result obtains for any N-photon vs M-photon absorption scenario where N and M are of the same parity. In addition, these scenarios allow for control over differential cross-sections as well. To see this, consider rewriting equations (63)–(66) so that it applies to the probability of observing the product in channel q, but at a fixed scattering angle. Then the sum over the channel indices $\boldsymbol{m}$ no longer

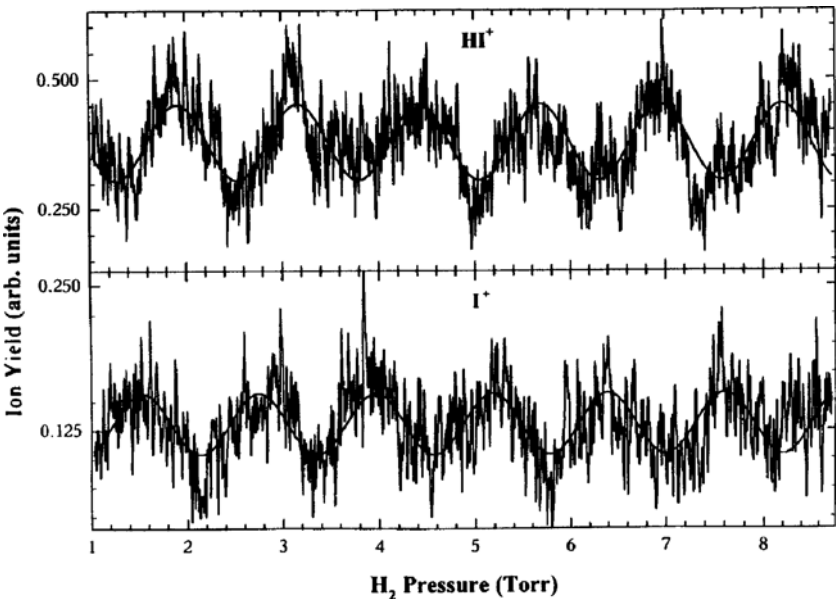

Figure 5. Modulation of the HI^+ and I^+ signals as a function of the difference between the one- and three-photon phases (proportional to the H_2 pressure in the cell used to phase shift the beams). Taken from figure 3, [53].

includes an integral over scattering angles. The resultant cross term $P^{(13)}$ is non-zero so that varying properties of the lasers will indeed alter the differential cross-section into channel q.

5.2. One vs two-photon interference: symmetry breaking

Although scenarios for interference between an N-photon route and an M-photon route, where N, M are of the same parity, allow for control over both the differential and integral photodissociation cross-sections, this is not the case when N and M are of different parity. In this case, only control over the differential cross-section is possible. However, the control is such that it leads to the breaking of the usual backward–forward symmetry. This is but one example of the breaking of symmetry afforded via CC techniques. A more spectacular example, that of chiral (asymmetric) synthesis, is presented in section 10.

In order to understand why control over the total cross-section is lost and how the backward–forward symmetry is broken we analyse in some detail the simplest case in this class, namely the interference between a one-photon and a two-photon absorption process [57]. Consider irradiating a molecule by a field composed of two modes, ω_2 and ω_1, with $\omega_2 = 2\omega_1$, for which the light–matter interaction is

$$H_{\mathrm{MR}}(t) = -2\boldsymbol{d} \cdot \mathrm{Re}[\hat{\epsilon}_2\bar{\epsilon}_2 \exp(-\mathrm{i}\omega_2 t) + \hat{\epsilon}_1\bar{\epsilon}_1 \exp(-\mathrm{i}\omega_1 t)]. \tag{70}$$

The amplitude for the combined one-photon, two-photon absorption process is,

$$A_{q,\boldsymbol{m}}(E = E_i + \hbar\omega_2) = \left(\frac{2\pi\mathrm{i}}{\hbar}\right)\delta(\omega_2 - \omega_{E,i})[\bar{\epsilon}_2\langle E, \boldsymbol{m}, q^-|\mathrm{d}_{e,g}|E_i\rangle + \bar{\epsilon}_1^2\langle E, \boldsymbol{m}, q^-|D_{e,g}|E_i\rangle], \tag{71}$$

where $D_{e,g}$ is the two-photon transition operator, defined as,

$$D_{e,g} = \sum_{e'} \mathrm{d}_{e,e'}(E_i - H_{e'} + \hbar\omega_1)^{-1}\mathrm{d}_{e',g} \tag{72}$$

and we implicitly assume that $E_i + \hbar\omega_1$ is below the threshold for photodissociation.

Suppressing for the moment all channel indices $\boldsymbol{m}$ (which can be readily included), save for the final direction $\hat{\boldsymbol{k}}$, we square the amplitude to obtain $P_q(E, \hat{\boldsymbol{k}})$, the probability of photodissociation into channel q at angles $\hat{\boldsymbol{k}} \equiv (\theta_k, \phi_k)$,

$$P_q(E, \hat{\boldsymbol{k}}) = |A_q(\hat{\boldsymbol{k}}, E_i + \hbar\omega_2)|^2 = P_q^{(1)}(E, \hat{\boldsymbol{k}}) + P_q^{(12)}(E, \hat{\boldsymbol{k}}) + P_q^{(2)}(E, \hat{\boldsymbol{k}}), \tag{73}$$

where

$$\begin{aligned}
P_q^{(1)}(E, \hat{\boldsymbol{k}}) &= \left(\frac{2\pi}{\hbar}\right)^2 |\bar{\epsilon}_2|^2 |\langle E, \hat{\boldsymbol{k}}, q^-|\mathrm{d}_{e,g}|E_i\rangle|^2, \\
P_q^{(2)}(E, \hat{\boldsymbol{k}}) &= \left(\frac{2\pi}{\hbar}\right)^2 |\bar{\epsilon}_1|^4 |\langle E, \hat{\boldsymbol{k}}, q^-|D_{e,g}|E_i\rangle|^2, \\
P_q^{(12)}(E, \hat{\boldsymbol{k}}) &= -2\left(\frac{2\pi}{\hbar}\right)^2 |\bar{\epsilon}_2\bar{\epsilon}_1^2| \cos[\phi_2 - 2\phi_1 + \alpha_q(12; \hat{\boldsymbol{k}})] |F_q^{(12)}(\hat{\boldsymbol{k}})|
\end{aligned} \tag{74}$$

with the amplitude $|F_q^{(12)}(\hat{\boldsymbol{k}})|$ and phase $\alpha_q(12; \hat{\boldsymbol{k}})$ defined by

$$|F_q^{(12)}(\hat{\boldsymbol{k}})| \exp(\mathrm{i}\alpha_q(12; \hat{\boldsymbol{k}})) = \langle E_i|D_{g,e}|E, \hat{\boldsymbol{k}}, q^-\rangle\langle E, \hat{\boldsymbol{k}}, q^-|\mathrm{d}_{e,g}|E_i\rangle. \tag{75}$$

The interference term $P_q^{(12)}(E, \hat{\boldsymbol{k}})$ is generally non-zero, so that control over the differential cross-section is possible. Consider, however, the integral cross-section into channel q, i.e.

$$P_q(E) = \int \mathrm{d}\hat{\boldsymbol{k}} \;\; P_q(E, \hat{\boldsymbol{k}}) \tag{76}$$

and focus on the contribution from $P_q^{(12)}(E, \hat{\boldsymbol{k}})$. That is, consider

$$\begin{aligned}
P_q^{(12)}(E) &= \int \mathrm{d}\hat{\boldsymbol{k}} |F_q^{(12)}(\hat{\boldsymbol{k}})| \exp(\mathrm{i}\alpha_q(12; \hat{\boldsymbol{k}})) \\
&= \int \mathrm{d}\hat{\boldsymbol{k}} \langle E_i, J_i, M_i|D_{g,e}|E, \hat{\boldsymbol{k}}, q^-\rangle\langle E, \hat{\boldsymbol{k}}, q^-|\mathrm{d}_{e,g}|E_i, J_i, M_i\rangle,
\end{aligned} \tag{77}$$

where we have explicitly inserted the angular momentum characteristics of the initial-state. Using the definition of $D_{g,e}$ and inserting unity in terms of the states $|E_j, J_j, M_j\rangle$ of the intermediate electronic states gives

$$\begin{aligned}
P_q^{(12)}(E) = \sum_{j,e'} \int \mathrm{d}\hat{\boldsymbol{k}} [\hbar\omega_1 + E_i - E_j]^{-1} &\langle E_i, J_i, M_i|\mathrm{d}_{g,e'}|E_j, J_j, M_j\rangle \\
&\times \langle E_j, J_j, M_j|\mathrm{d}_{e',e}|E, \hat{\boldsymbol{k}}, q^-\rangle\langle E, \hat{\boldsymbol{k}}, q^-|\mathrm{d}_{e,g}|E_i, J_i, M_i\rangle.
\end{aligned} \tag{78}$$

For convenience, consider the case of diatomic dissociation. Examination of the selection rules shows that when the transition-dipole operators $\boldsymbol{d}_{e,g}$ and $\boldsymbol{d}_{e',e}$ are parallel to the nuclear axis, the two-photon amplitude is non-zero only if $J_j - J_i = \pm 2, 0$. By contrast, in this case the one-photon matrix element $\langle E_i, J_i, M_i|\mathrm{d}_{g,e'}|E_j, J_j, M_j\rangle$ is non-zero only if $J_j - J_i = \pm 1$. Since these two conditions are contradictory, $P_q^{12}(E)$ is zero. Hence, CC over integral cross-sections is not possible using the one vs two-photon scenario.

This result holds true even when the transition-dipole operators are perpendicular to the nuclear axis. Thus, lack of control over the integral cross-section in the 1 vs 2 scenario will also occur in polyatomic molecules and for any N- vs M-photon process where N and M are

of different parities. The loss of integral control emanates from the fact that the total parity of any molecular wavefunction is reversed each time a photon is absorbed, since the parity of each photon is negative and the total parity of the photon + molecule system must be conserved. Thus, the parity of a molecular state resulting from a given initial-state absorbing an odd number (N) of photons is opposite that resulting from the absorption of an even number (M) of photons by the same initial-state. The integrated interference term that reflects the overlap integral between such states is zero.

However, these features do not prevent control over the differential cross-sections for N and M of different parity, because no integration over angles is required. In fact, because the continuum state $|E, \hat{\boldsymbol{k}}, q^-\rangle$ accessed via multiphoton pathways of opposite parity has contributions from angular momentum states of opposite parity, the probability of seeing products in a given direction $\hat{\boldsymbol{k}}$ is not the same as the probability of observing products in the opposite direction $-\hat{\boldsymbol{k}}$. That is, the 'forward–backward' symmetry has been broken. This as shown below to be but one example of symmetry breaking induced by many CC scenarios. Several theoretical papers have analysed this phenomenon [57–60]. One particularly interesting example is control over right- vs left-handed enantiomers, discussed in detail in section 10.

The experimental implementation of the one-plus-two-photon absorption scenario have taken a variety of forms [61–66]. For example, Corkum and co-workers [64] have carried out one vs two-photon absorption in crafted quantum wells in an experiment depicted schematically in figure 6. As shown in figure 7, by varying $\phi_2 - 2\phi_1$, the relative phase between the second harmonic and twice that of the fundamental frequency (at 10.6 μm), the experimentalists were able to direct the electronic current to move in either the forward or backward direction, or to generate a current that was equally probable in both directions.

Related results were obtained with molecules. For example, following the theoretical predictions of Charron *et al* [67, 68], displayed in figure 8 on the photodissociation of H_2^+, Dimauro *et al* [65] performed an experiment (shown schematically in figure 9) to control product directionality in HD^+ dissociation to $H+D^+$ and H^++D. Here, a combination of a one-photon process, induced by the second harmonic, and a two-photon process, induced by the

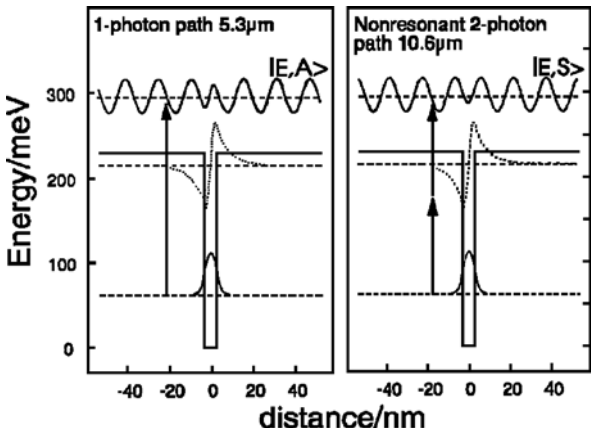

Figure 6. Energy band diagram of a 55 A GaAs/$Ga_{0.74}Al_{0.26}As$ QW and wave functions of the states implied in a 5.3 μm single-photon pathway and a 10.6 μm two-photon process. Neither dephasing nor reflections of the electronic waves on the neighbour quantum wells are considered in this simplified figure. Taken from figure 1, [64].

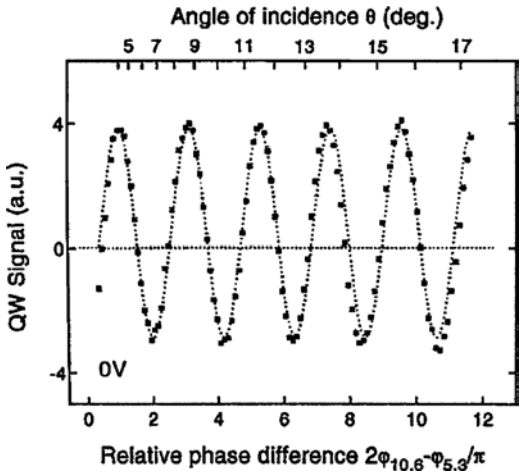

Figure 7. An experiment showing the integrated quantum well response vs the relative laser phase. Dashed line: sinusoidal fit. Taken from figure 4, [64].

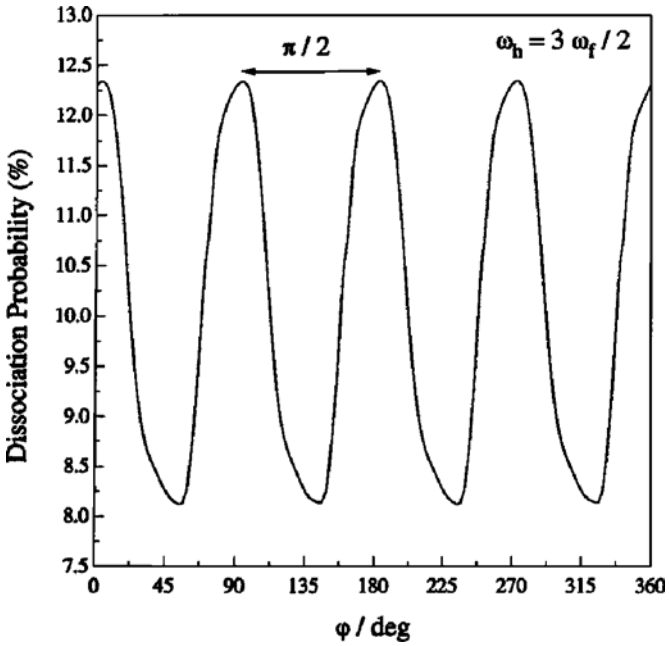

Figure 8. The computed H^+ current resulting from the photodissociation of H_2^+ as a function of $\varphi = \phi_2 - 2\phi_1$, the difference between the second harmonic phase and twice the phase of the fundamental photon. Taken from figure 6, [68].

fundamental frequency, were used to excite the molecule to a repulsive $2p\sigma$ state yielding either the $H + D^+$ or the $D + H^+$ products. The results of the experiment are shown in figure 10. We see that the angle at which the ions appear can be varied by changing the $\phi_2 - 2\phi_1$ relative phase.

It is interesting to note (see figure 10(*b*)) that the ratio between the H^+ and D^+ ions does not vary with the relative phase. This is partly in agreement with the analysis presented above that,

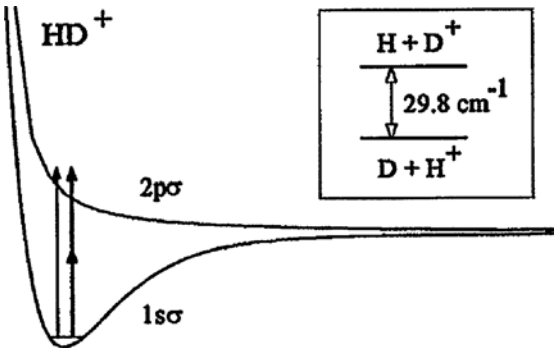

Figure 9. Potential curves for the $1s\sigma$ and $2p\sigma$ states of HD^+. In the homonuclear case (H_2^+), the two-states are asymptotically degenerate; the degeneracy is lifted in the heteronuclear case by $29.8\,cm^{-1}$ (inset). Taken from figure 1, [65].

within lowest order perturbation theory, the ratio between integral cross-sections of different channels cannot be controlled by an N- vs M-photon scenario when N and M possess different parities. This means that, within the confines of perturbation theory, when we average over all angles we should find a phase independent H^+/D^+ branching ratio. This argument does not, however, explain why this lack of discrimination should hold for each and every angle: as can be seen from figure 10(a), the H^+/D^+ ratio is independent of the dissociation angle. Moreover, an argument based on low order perturbation theory is not expected to hold in the long wavelength regime where multiple photon transitions are involved, and isotopic discrimination is therefore expected to occur [68].

We conclude that in the short wavelength regime what is being affected in the dissociation of HD^+ is the motion of the (lone) electron. The electron is seen to direct itself towards the forward or backward directions in the laboratory frame as the $\phi_2 - 2\phi_1$ relative phase is varied. Since the experiment monitored only dissociative events where the electron is still bound to the molecule, the electron simply 'rides' on whatever ion happens to be pointing in its preferred laboratory direction. If, while the molecule is rotating and dissociating, the electron finds the D^+ nucleus pointing in its preferred direction, it attaches itself to the deuteron and the neutral D atom will emerge in that direction (with the H^+ ion emerging in the opposite direction). The situation is reversed if the proton happens to be moving in the direction preferred by the electron.

These conclusions, that even if ionization does not occur, it is often the electron that is being controlled rather than the nuclei, follow the work of Aubanel and Bandrauk [69] who have shown such electronic control in the photodissociation of Cl_2. The case for electronic control is naturally stronger when the lasers are intense enough to ionize the molecule. In that case the interference between the one-photon and two-photon processes has been shown to affect the ionization yield [70]. Additional theoretical and experimental work on the control of atomic phenomena in $\omega+2\omega$ and $\omega+3\omega$ scenario has been reviewed in detail by Ehlotzky [71].

6. Pump-dump control: few level excitation

Control of the dynamics via a pump-dump scenario was first introduced by Tannor, Rice and Kosloff [16, 17, 72] with insight afforded by localized wave packets [73], an approach that is associated with many level excitation, and which is reviewed in detail in [2]. Here, we only discuss the few levels case shown qualitatively in figure 11. It can be regarded as a useful

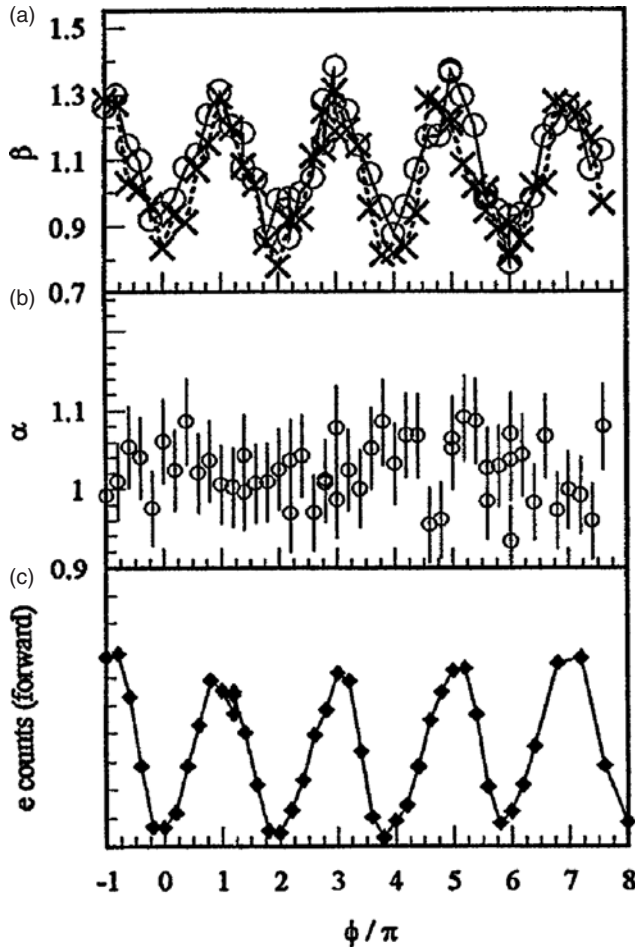

Figure 10. (*a*) The forward/backward yield ratios of H^+, $\beta_{H^+} = \mathrm{H}_f^+/\mathrm{H}_b^+$ (○), and of D^+, $\beta_{D^+} = \mathrm{D}_f^+/\mathrm{D}_b^+$ (×), of protons and deuterons in the dissociation of HD^+ vs $\phi = \phi_2 - 2\phi_1$, the difference between the phase of the second harmonic phase and twice the phase of the fundamental photon. (b) Plot of the ratio of isotopes, α, vs ϕ. The uncertainty is indicated by the error bars. (c) The yield of the photoelectron arising from the $\mathrm{Kr} \xrightarrow{\hbar\omega_3, 3\hbar\omega_1} \mathrm{Kr}^+ + \mathrm{e}^-$ photoionization moving towards the detector vs ϕ. The modulations were used to calibrate ϕ. Taken from figure 3, [65].

extension of the scenario outlined in section 3.1, in which the initial superposition of bound states is prepared with one laser pulse and subsequently dissociated with another.

Consider a molecule, initially ($t = 0$) in an eigenstate $|E_1\rangle$ of the molecular Hamiltonian H_M that is subjected to two transform limited light pulses, termed the 'pump' and 'dump' pulses. These pulses are assumed to be temporally separated by a time delay Δ_d. The electric field consists of two temporally separated pulses $\boldsymbol{E}_x(\tau), \boldsymbol{E}_d(\tau)$ (where τ is the retarded time $(t - z/c)$) (figure 12). For both pulses the electric field is of the form $\boldsymbol{E}(\tau) = 2\epsilon\varepsilon(\tau)\cos(\omega_0\tau)$, which is a parameterization of equation (2). Here, ω_0 is the carrier frequency and $\varepsilon(\tau)$ describes the pulse envelope. Thus, the molecule is subjected to the field,

$$\boldsymbol{E}(\tau) = \boldsymbol{E}_x(\tau) + \boldsymbol{E}_d(\tau). \tag{79}$$

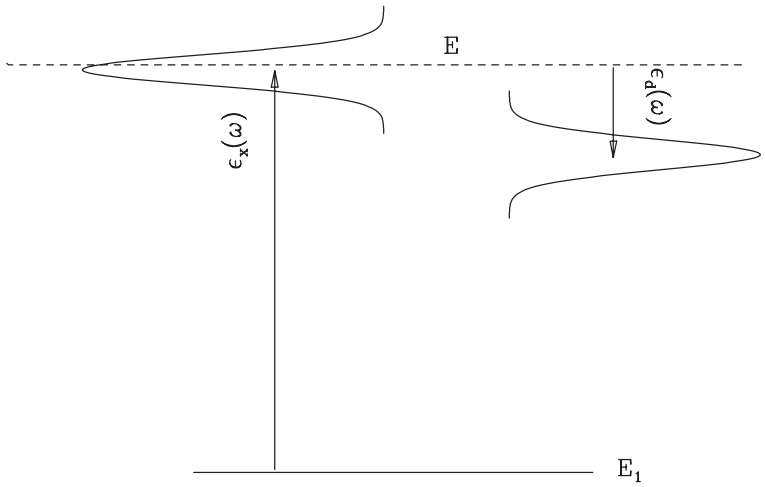

Figure 11. Pump-dump control scenario.

For convenience, we use Gaussian pulses that peak at $t = t_x$ and t_d, respectively. In particular, the excitation pulse is of the form

$$\boldsymbol{E}_x(\tau) = \frac{1}{2}\hat{\varepsilon}_x \epsilon_x \exp[-\mathrm{i}(\omega_x \tau + \delta_x)] \exp\left[-\frac{(\tau - t_x)^2}{\tau_x^2}\right], \tag{80}$$

where the Gaussian pulse is spread with width τ_x about time t_x and carries an overall phase δ_x. The associated frequency profile is given by the Fourier transform of equation (80):

$$\epsilon_x(\omega) = \left(\frac{\sqrt{\pi}}{2}\right) \epsilon_x \tau_x \exp[-\mathrm{i}(\omega_x - \omega)t_x] \exp\left[-\frac{\tau_x^2(\omega_x - \omega)^2}{4}\right] \exp(-\mathrm{i}\delta_x). \tag{81}$$

Further, we define $\bar{\epsilon}_x(\omega)$ as in equation (11), with $\phi(\omega) = (\omega - \omega_x)t_x - \delta_x$.

The analogous quantities for the dissociation laser, $\boldsymbol{E}_d(\tau)$, $\epsilon_d(\omega)$ and $\bar{\epsilon}_d(\omega)$ are defined similarly, with the parameters t_d and ω_d replacing t_x and ω_x, etc. The pump pulse $\boldsymbol{E}_x(\tau)$

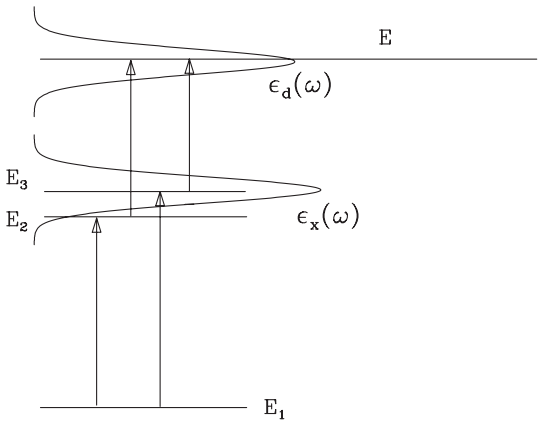

Figure 12. Interfering 2 two-photon pathways to energy E contained in the pump-dump control scheme of figure 11. The ϵ_x, ϵ_d labels indicate whether the excitation or dissociation laser is causing the indicated transition.

induces a transition to a linear combination of the eigenstates $|E_i\rangle$ of the excited electronic state. The pump pulse may be chosen to encompass any number of states. Here, we choose the pump pulse sufficiently narrow to excite only two of these states, $|E_2\rangle$ and $|E_3\rangle$. The dump pulse $\boldsymbol{E}_d(\tau)$ dissociates the molecule by further exciting it to the continuous part of the spectrum. Both fields are chosen sufficiently weak for perturbation theory to be valid.

Since the two pulses are temporally distinct, it is convenient to deal with their effects consecutively. After the first pulse is over, the superposition state prepared by the $\boldsymbol{E}_x(\tau)$ pulse, whose width is chosen to encompass just the two levels $|E_2\rangle$ and $|E_3\rangle$, is given in first order perturbation theory as

$$|\phi(t)\rangle = |E_1\rangle \mathrm{e}^{-\mathrm{i}E_1 t/\hbar} + b_2|E_2\rangle \mathrm{e}^{-\mathrm{i}E_2 t/\hbar} + b_3|E_3\rangle \mathrm{e}^{-\mathrm{i}E_3 t/\hbar}, \tag{82}$$

where (equation (10))

$$b_k = \left(\frac{2\pi \mathrm{i}}{\hbar}\right) \langle E_k|\hat{\epsilon}\cdot\boldsymbol{d}|E_1\rangle \bar{\epsilon}_x(\omega_{k,1}), \qquad k = 2, 3 \tag{83}$$

with $\omega_{k,1} \equiv (E_k - E_1)/\hbar$.

After a delay time of $\Delta_d \equiv t_d - t_x$ the system is subjected to the $\boldsymbol{E}_d(\tau)$ pulse. It follows from equation (82) that after this delay time each preparation coefficient has picked up an extra factor of $\mathrm{e}^{-\mathrm{i}E_k\Delta_d/\hbar}$, $k = 2, 3$. Hence, the phase of b_2 relative to b_3 at that time increases by $[-(E_2 - E_3)\Delta_d/\hbar = \omega_{3,2}\Delta_d]$. Thus, the natural two-state time evolution controls the relative phase of the two terms, replacing the externally controlled relative laser phase of the two-frequency control scenario of section 3.1.

After the action and subsequent decay of the $\boldsymbol{E}_d(\tau)$ pulse, the system wavefunction is:

$$|\psi(t)\rangle = |\phi(t)\rangle + \sum_{n,q} \int \mathrm{d}E\, b_{E,\boldsymbol{m},q}(t)|E, \boldsymbol{m}, q^-\rangle \mathrm{e}^{-\mathrm{i}Et/\hbar}. \tag{84}$$

In accord with equations (36)–(39), the probability of observing the q product at total energy E in the remote future is therefore

$$P_q(E) = \sum_{\boldsymbol{m}} |b_{E,\boldsymbol{m},q}(t=\infty)|^2 = \left(\frac{2\pi}{\hbar}\right)^2 \sum_{\boldsymbol{m}} \left| \sum_{k=2,3} b_k \langle E, \boldsymbol{m}, q^-|\mathrm{d}_{e,g}|E_k\rangle \bar{\epsilon}_d(\omega_{EE_k})\right|^2, \tag{85}$$

where $\omega_{EE_k} = (E - E_k)/\hbar$, b_k is given by equation (83), and where $\bar{\epsilon}_d(\omega)$ is given via an expression analogous to equation (81).

Expanding the square and using the Gaussian pulse shape (equations (80) and (81)) gives,

$$\begin{aligned} P_q(E) = \left(\frac{2\pi}{\hbar}\right)^2 & [|b_2|^2 \mathrm{d}_q(22)\bar{\epsilon}_2^2 + |b_3|^2 \mathrm{d}_q(33)\bar{\epsilon}_3^2 \\ & + 2|b_2 b_3^* \bar{\epsilon}_2 \bar{\epsilon}_3^* \mathrm{d}_q(32)| \cos(\omega_{3,2}\Delta_d + \alpha_q(32) + \chi)], \end{aligned} \tag{86}$$

where $\bar{\epsilon}_i = |\bar{\epsilon}_d(\omega_{EE_i})|$, $\omega_{3,2} = (E_3 - E_2)/\hbar$ and the phases χ, $\alpha_q(32)$ are defined via

$$\begin{aligned} & \langle E_1|\mathrm{d}_{e,g}|E_g\rangle\langle E_g|\mathrm{d}_{g,e}|E_2\rangle \equiv |\langle E_1|\mathrm{d}_{e,g}|E_g\rangle\langle E_g|\mathrm{d}_{g,e}|E_2\rangle| \mathrm{e}^{\mathrm{i}\chi}, \\ & \mathrm{d}_q(ki) \equiv |\mathrm{d}_q(ki)| \mathrm{e}^{\mathrm{i}\alpha_q(ki)} = \sum_{\boldsymbol{m}} \langle E_k|\mathrm{d}_{g,e}|E, \hat{\boldsymbol{m}}, q^-\rangle\langle E, \boldsymbol{m}, q^-|\mathrm{d}_{e,g}|E_i\rangle. \end{aligned} \tag{87}$$

Integrating equation (86) over E to encompass the full width of the second pulse yields the final expressions for the quantities we wish to control: P_q, the probability of forming channel q, and $R_{q,q'}$, the ratio of product probabilities into q vs q' (see equation (56)).

Examination of equation (86) makes clear that $R_{q,q'}$ can be varied by changing the delay time $\Delta_d = (t_d - t_x)$ or the ratio $x = |b_2/b_3|$; the latter is most conveniently done by detuning

the initial excitation pulse. Note that, once again, as in the scenarios above, the z dependence of P_q vanishes due to cancellation between the excitation and dump steps. In addition, the phases δ_x, δ_d do not appear in the final $R_{q,q'}$ expression, so that the relative phases of the two pulses do not affect the result.

This approach was applied to realistic systems such as the control of the Br to Br* branching ratio in the photodissociation of IBr [74], and the control of Li_2 photodissociation [75]. To gain insight into the control afforded by this scenario we also applied it to a model of the photodissociation of a hypothetical collinear DH_2 complex [76]:

$$H + HD \leftarrow DH_2 \rightarrow D + H_2. \tag{88}$$

The first pulse is used to excite a pair of states in an electronic state supporting bound states and the second pulse to dissociate the system by de-exciting it back to the ground state, above the dissociation threshold.

The model potentials used in the DH_2 [76] are shown in figure 13 and typical control results are shown in figure 14. Specifically, figure 14 contours of equal DH yield as a function of $E_x - E_{\rm av}$ and Δ_d. Here $(E_x - E_{\rm av})$ measures the deviation of the central excitation energy of the pump pulse from the mean energy $E_{\rm av}$ of the pair of bound states that it excites. The DH yield is shown to vary significantly, from 16% to 72%, as the control parameters are varied. This is an extreme range of control, especially if one considers that the product channels only differ by a mass factor.

The pump-dump scheme described above has also been applied to the control of the

$$D + OH \leftarrow HOD \rightarrow H + OD$$

dissociation reaction, proceeding via the B^1A' excited state of HOD. In this case, both asymptotic channels have identical potential energy surfaces so that control over the relative yield is challenging. To consider the extent of possible control we excite an initial superposition of the $(0, 2, 0)$ and $(1, 0, 0)$ states of ground state HOD ($(0, 2, 0)$ denotes two quanta in the bend mode and $(1, 0, 0)$ denotes one quantum of excitation of the OD stretch). A subsequent pulse dissociates HOD via the B^1A' continuum. A typical result is displayed in figure 15, which shows contours of constant percentage yield of H + OD (i.e. 100P(OD + H)/[P(OD + H) + P(OH + D)]) as a function of the time delay Δ_d and of the detuning of the pump laser pulse $E_x - E_{\rm av}$. Features of this result are of note. First, significant variations of yield ratio accompany changes in $(E_x - E_{\rm av})$. Second, the dependence of the yield ratio on the time delay is weak. The former feature merely reflects a natural preference, on the part of either of the two excited states $|E_2\rangle, |E_3\rangle$ to favour production of OD over OH. Changing $E_x - E_{\rm av}$ changes the relative contribution of each of these two-states thereby changing the yield ratio. Thus, changes in yield ratio with changes in $E_x - E_{\rm av}$ is not due to CC. Rather, quantum interference effects are reflected in variations of the yield ratio with changes in Δ_d. The fact that this is weak is indeed a reflection of the similarity of the two product channels.

Contrary to the approach discussed here, which relies heavily on the interference generated between a very small number of energy levels, the approach of Tannor and Rice [16, 72] and Tannor *et al* [17] is based on localized wavepackets, which are a superposition of many levels.

7. Control of chaotic dynamics

Studies in classical non-linear mechanics have shown that typical systems lie between two limits: that of integrable dynamics and that of chaotic dynamics [78–80]. In the integrable

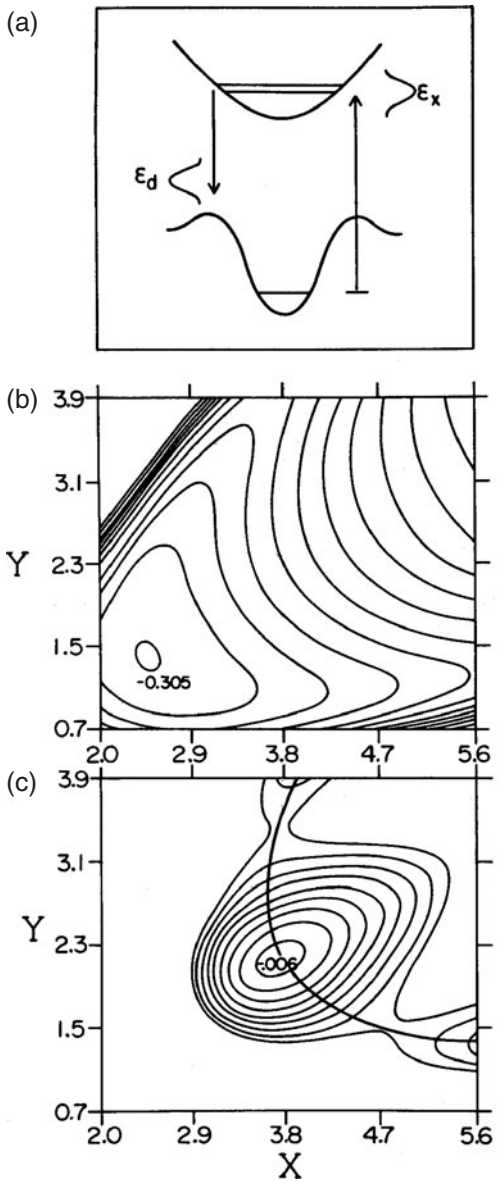

Figure 13. (*a*) Schematic diagram of a pump-dump scheme to control the model $DH + H \leftarrow DH_2 \rightarrow D + H_2$ branching photodissociation reaction. Here, ϵ_x is the excitation pulse and ϵ_d is the dump pulse. (*b*) Ground potential surface. Contour lines are spaced by 0.02 a.u., increasing outwards from the indicated minimum. (*c*) Excited potential surface. Contour lines are spaced by 0.0098 a.u., increasing outwards from the indicated minimum. The reaction coordinate *S* is shown as a thick line that is chosen here as to coincide with the minimum energy path connecting the DH + H and the $D + H_2$ products. Taken from figure 1, [76].

case, the dynamics of a system of *N* degrees of freedom possesses *N* conserved integrals of motion and is stable with respect to small external perturbations. In the chaotic case, the system dynamics usually possesses only symmetry based integrals of motion, such as the total energy and angular momentum, and the dynamics is extremely sensitive to initial conditions

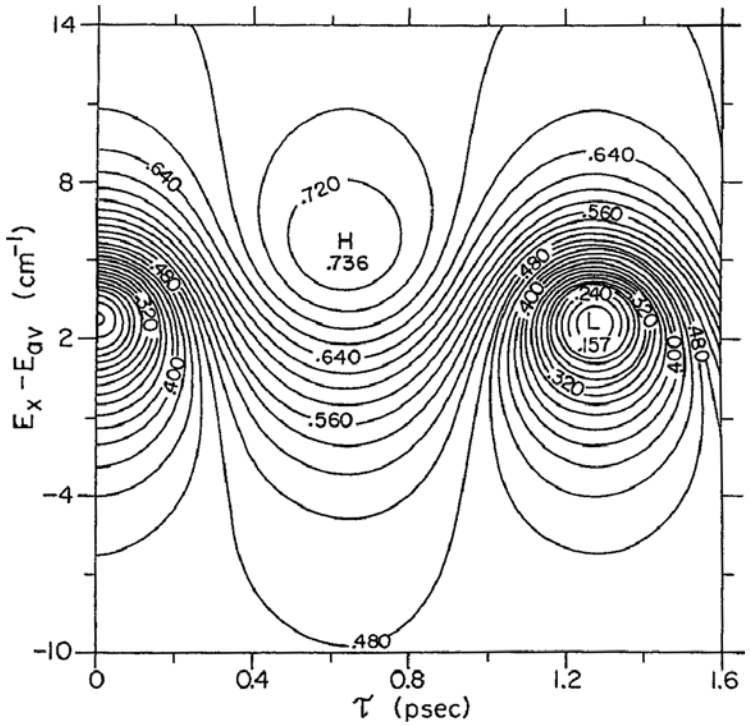

Figure 14. Contour plot of the DH yield as a function of the detuning of the exciting pulse $E_x - E_{\rm av}$, and the delay variable $\tau \equiv \Delta_d$. The actual delay is $(8.44 + 2.11n)$ ps $+ \tau$, where n is an arbitrary positive integer that is chosen high enough to eliminate any overlap between the pulses. Here, the initially created superposition state is between levels 56 and 57 ($E_1 = 0.323\,849$ a.u., $E_2 = 0.323\,968$ a.u.) of the excited surface. The letters H and L denote the positions of the absolute maxima and minima, whose magnitudes are explicitly shown. Taken from figure 6, [14].

and external perturbations. Even in the absence of external perturbations, a classical chaotic system 'loses memory' of the initial-state exponentially fast. This categorization extends to quantum mechanics in the sense that a system is said to be quantum mechanically chaotic if its classical counterpart is classically chaotic. Numerous computational studies (e.g. [81]) have shown that quantum systems do display characteristics of classical chaos if they are sufficiently close to the classical limit, a manifestation of the correspondence principle [82]. It is expected that the vast majority of realistic systems are sufficiently complex so as to display some degree of classically chaotic behaviour.

Considering the sensitivity of classical chaotic systems to external perturbations, and the ubiquitous nature of chaotic dynamics in larger systems, it is important to establish that quantum mechanics allows for control in chaotic systems as well.

One simple molecular system that displays quantum chaos is the rotational excitation of a diatomic molecule using pulsed microwave radiation [83]. Under the conditions adopted below this system is a molecular analogue of the 'delta-kicked rotor', i.e. a rotor that is periodically kicked by a delta function potential, which is a paradigm for chaotic dynamics [84, 85]. The observed energy absorption of such systems is called 'quantum chaotic diffusion'. There are numerous manifestations of this quantum chaotic diffusion including the application to molecules below and implementations in terms of atom optics [86], etc. Hence, this system is of quite general interest.

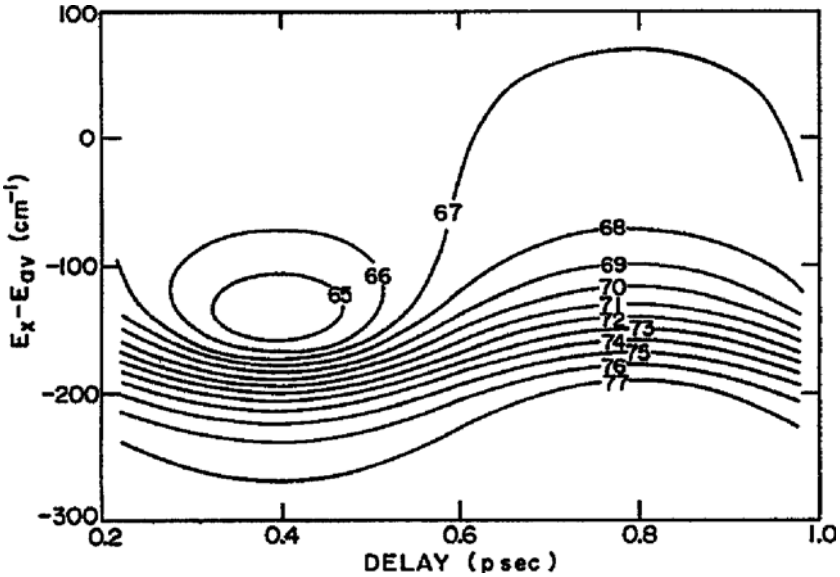

Figure 15. Percentage yield of the H + OD channel in the photodissociation of the DOH(0, 2, 0 + 1, 0, 0) superposition state. The excitation pulse band width is $50\,\mathrm{cm}^{-1}$, the dissociation pulse bandwidth is $50\,\mathrm{cm}^{-1}$, and the enter frequency is $71\,600\,\mathrm{cm}^{-1}$. The ordinate is the detuning of the excitation pulse ω_x from the energy centre of the (0, 2, 0) and (1, 0, 0) states. Taken from figure 3, [77].

If the orientation of a diatomic molecule is described by two angles θ and ϕ [87], then the corresponding Hamiltonian is

$$H = \frac{\hat{J}^2}{2I} + \boldsymbol{d}\cdot\boldsymbol{E}_0\cos\theta\sum_n \Delta\left(\frac{t}{T} - n\right), \tag{89}$$

where $\hat{J}$ is the angular momentum operator in three dimensions:

$$\hat{J}^2 = -\hbar^2\left[\frac{1}{\sin\theta}\frac{\partial}{\partial\theta}\left[\sin\theta\frac{\partial}{\partial\theta}\right] + \frac{1}{\sin^2\theta}\frac{\partial^2}{\partial\phi^2}\right]. \tag{90}$$

Here, $\boldsymbol{d}$ is the molecular electric dipole moment, $\boldsymbol{E}_0$ is the amplitude of the driving field whose polarization direction defines the z direction, I is the moment of inertia of the molecule about an axis perpendicular to the symmetry axis, and $\Delta(t/T - n)$ is the pulse shape function of the form

$$\Delta\left(\frac{t}{T} - n\right) = 1 + 2\sum_{m=1}^{m=7}\cos\left[2m\pi\left(\frac{t}{T} - n - \frac{1}{2}\right)\right]. \tag{91}$$

Eigenstates of the Hamiltonian H are $|n_J, m_J\rangle$, where n_J is the angular momentum quantum number with projection m_J along the z-axis.

As shown by Fishman [83], the kicked CsI molecule is particularly appropriate candidate for this study since it has a large dipole moment (that increases the molecule–field coupling strength), and the rotation–vibration coupling is small at low excitation energies so that one may consider solely rotational excitation. We consider then the dynamics of CsI in the indicated pulsed field, in a parameter range known to display classical chaos [88].

To demonstrate control of chaotic dynamics consider an initial superposition state of the form

$$|\psi(0)\rangle = \cos\alpha|j_1, 0\rangle + \sin\alpha\exp(-\mathrm{i}\beta)|j_2, 0\rangle. \tag{92}$$

This system is now subjected to pulsed microwave irradiation, and the rotational energy absorption is measured in terms of a dimensionless rotational energy $\tilde{E} \equiv \sum_j P_j j(j+1)\tau^2/2$, $\tau = \hbar T/I$, where P_j, the occupation probability of the $|j, 0\rangle$ state.

To anticipate the result note from equations (89) and (91) that the Hamiltonian is strictly periodic in time with the time evolution operator over one period T denoted $\hat{F}$. Thus, there exists a description of the dynamics in terms of this operator:

$$|\psi(nT)\rangle = \hat{F}^{n-1}|\psi((n-1)T)\rangle = \hat{F}^n|\psi(0)\rangle, \tag{93}$$

where n is an integer.

The operator $\hat{F}$ can be formally diagonalized by a unitary transformation $\underline{\underline{\mathrm{U}}}$ so that,

$$\langle j_a, 0|\hat{F}|j_b, 0\rangle = \sum_{j_c} \exp(-\mathrm{i}\phi_{j_c}) U^*_{j_c, j_a} U_{j_c, j_b}, \tag{94}$$

where $U_{j_c, j_a} \equiv \langle j_c, 0|\hat{U}|j_a, 0\rangle$ ($j_a = 0, 1, 2, \ldots$) is the eigenvector with eigenphase ϕ_{j_c}. Moreover, since the basis states $|j, 0\rangle$ are time-reversal invariant, one can prove that the matrix elements U_{j_c, j_b} can be chosen as real numbers [89], i.e.

$$U^*_{j_c, j_a} = U_{j_c, j_a}, \qquad j_a,\ j_c = 0, 1, 2, \ldots. \tag{95}$$

Further, evaluating $\tilde{E}$ at $t = NT$ with equations (92), (94) and (95) give

$$\begin{aligned}
\frac{2\tilde{E}}{\tau^2} &= \langle\psi(0)|\hat{F}^{-N}\frac{\hat{J}^2}{\hbar^2}\hat{F}^N|\psi(0)\rangle \\
&= \cos^2\alpha \sum_{j j_a j_b} j(j+1) U_{j_a j_1} U_{j_b j} U_{j_a j} U_{j_b j_1} \mathrm{e}^{\mathrm{i}N(\phi_{j_a} - \phi_{j_b})} \\
&\quad + \sin^2\alpha \sum_{j j_a j_b} j(j+1) U_{j_a j_2} U_{j_b j} U_{j_a j} U_{j_b j_2} \mathrm{e}^{\mathrm{i}N(\phi_{j_a} - \phi_{j_b})} \\
&\quad + \frac{\sin(2\alpha)}{2}\left(\mathrm{e}^{-\mathrm{i}\beta} \sum_{j j_a j_b} j(j+1) U_{j_a j_1} U_{j_b j_2} U_{j_a j} U_{j_b j} \mathrm{e}^{\mathrm{i}N(\phi_{j_a} - \phi_{j_b})} + \text{c.c.}\right).
\end{aligned} \tag{96}$$

Evidently, the first two terms are incoherent since they do not depend on the value of the phase β in equation (92). They represent quantum dynamics associated with each of the states $|j_1, 0\rangle$ and $|j_2, 0\rangle$ independently. The last two terms represent interference effects due to initial-state coherence between $|j_1, 0\rangle$ and $|j_2, 0\rangle$. Hence, the absorption of rotational energy in this system, i.e. quantum chaotic diffusion, can be controlled by manipulating the quantum phase β in the initial-state, which corresponds to manipulating the interference term in equation (96).

Figure 16 shows a representative example of phase control in this system. In the chosen parameter region the underlying classical dynamics of rotational excitation is strongly chaotic [88] and the excitation is far off-resonance, with many levels excited. Using $j_1 = 1$ and $j_2 = 2$ to create the initial superposition state $(|1, 0\rangle \pm |2, 0\rangle)/\sqrt{2}$, i.e. $\alpha = \pi/4$ and $\beta = 0, \pi$ in equation (92) gives the results shown in figure 16. It displays striking phase control. That is, $(|1, 0\rangle - |2, 0\rangle)/\sqrt{2}$ shows almost no energy absorption at all, whereas the $(|1, 0\rangle + |2, 0\rangle)/\sqrt{2}$ case shows extraordinarily fast energy absorption [88] before it essentially stops at $t \approx 10T$. Note (1) that this huge difference is achieved solely by changing the initial

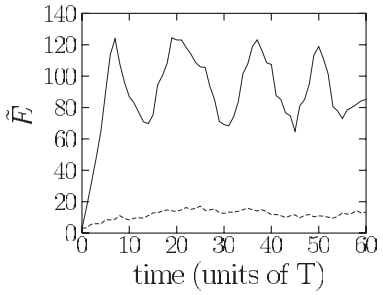

Figure 16. The dimensionless rotational energy of the kicked diatomic molecule $\tilde{E} = \sum_j P_j j(j+1)\tau^2/2$ vs time (in units of T). Solid line and dashed lines are for the initial-states $(|1,0\rangle + |2,0\rangle)/2^{1/2}$ and $(|1,0\rangle - |2,0\rangle)/2^{1/2}$, respectively, for $\tau = 1.2$, $k = 4.8$. From figure 2, [88].

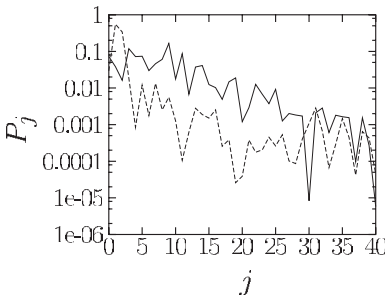

Figure 17. The occupation probability P_j vs the rotational quantum number j at $t = 60T$. Solid line and dashed lines are for the initial-states $(|1,0\rangle + |2,0\rangle)/2^{1/2}$ and $(|1,0\rangle - |2,0\rangle)/2^{1/2}$, respectively, for $\tau = 1.2$, $k = 4.8$. From figure 3, [88].

relative phase between the two participating states $|1,0\rangle$ and $|2,0\rangle$ in the initial superposition state, and (2) that by contrast, each of $|1,0\rangle$ or $|2,0\rangle$ individually would give very similar diffusion behaviour lying between the solid and dashed lines in figure 16. This shows that the two participating states $|1,0\rangle$ and $|2,0\rangle$ can either constructively or destructively interfere with one another, even though the underlying classical dynamics is strongly chaotic. A detail of the respective wavefunctions at $t = 60T$ is shown in figure 17 in terms of the occupation probability P_j vs j. One sees vividly that changing β from 0 to π alters the occupation probability of many states by almost an order of magnitude.

The quantum dynamics of the kicked molecule depends on two parameters, $\tau \equiv \hbar T/I$ and $k \equiv \boldsymbol{d}\cdot\boldsymbol{E}_0/\hbar$. However, as shown elsewhere [88] the classical dynamics depends solely in the product $k\tau$. Thus, by decreasing the magnitude of $\tau \equiv \hbar T/I$ while keeping $k\tau$ fixed, we can approach the classical limit while keeping the underlying classical dynamics unaffected. This is a useful tool to show that the demonstrated phase control is indeed quantal in nature. Specifically we show, in figure 18, the CsI quantum dynamics after reducing the effective Planck constant τ by 50 times, while keeping $k\tau$ constant. Here, with $\tau = 0.024$ and $k = 240$, the energy diffusion only shows slight dependence on β. That is, the phase control disappears, clearly demonstrating the quantum nature of the control.

The ideas here have been extended in a number of ways to include various types of pulse sequences that allow for a wide range of control [90], (including faster-than-anamolous diffusion) over energy absorption in the kicked rotor systems and their analogues.

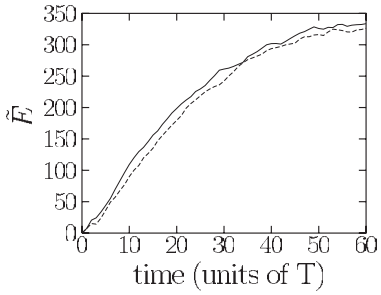

Figure 18. The occupation probability P_j vs the rotational quantum number j at $t = 60T$. Solid line and dashed lines are for the initial-states $(|1,0\rangle + |2,0\rangle)/2^{1/2}$ and $(|1,0\rangle - |2,0\rangle)/2^{1/2}$, respectively, for $\tau = 1.2$, $k = 4.8$. From figure 5, [88].

8. CC of collisions

The results described above deal with control of unimolecular processes, i.e. processes that begin with a single molecule that subsequently undergoes excitation and dynamics. However, the vast majority of chemical reactions occur via two-body collisions ('bimolecular' processes), e.g.

$$A + B \rightarrow C + D, \tag{97}$$

where A, B, C, D are, in general, molecules of mass M_A, M_B, M_C and M_D. Here, C and D can be identical to A and B (non-reactive scattering) or different from A and B (reactive scattering). We label $A+B$ as arrangement q and $C+D$ as arrangement q'. Below we describe CC of collisions ([91–94], [95][5], [96–98]).

The cross-section $\sigma_E(\boldsymbol{n}, q'; \boldsymbol{m}, q)$ for scattering between the asymptotic states $|E, q, \boldsymbol{m}; 0\rangle$ of $A + B$ (labelled q) and $|E, q', \boldsymbol{n}; 0\rangle$ of $C + D$ (labelled q') is given by

$$\sigma_E(\boldsymbol{n}, q'; \boldsymbol{m}, q) = |\langle E, q', \boldsymbol{n}^- | V_q | E, q, \boldsymbol{m}; 0\rangle|^2. \tag{98}$$

Here $|E, q', \boldsymbol{n}^-\rangle$ denotes the incoming scattering solutions associated with product in state $|E, q', \boldsymbol{n}; 0\rangle$ and V_q is the component of the total potential that vanishes as the A to B distance becomes arbitrarily large. The cross-section for scattering into arrangement q', independent of the product internal state $\boldsymbol{n}$, is then

$$\sigma_E(q'; \boldsymbol{m}, q) = \sum_{\boldsymbol{n}} |\langle E, q', \boldsymbol{n}^- | V_q | E, q, \boldsymbol{m}; 0\rangle|^2. \tag{99}$$

Assorted other cross-sections may be defined, depending upon which of the elements of $\boldsymbol{n}$ are summed over. For example, by not including the scattering angles θ, ϕ in the sum we obtain $\sigma_E(q', \theta, \phi; \boldsymbol{m}, q)$, corresponding to scattering into the q' product channel and into scattering angles (θ, ϕ). Similarly, $\sigma_E(q', \theta; \boldsymbol{m}, q)$ is the traditional differential cross-section $\sigma_E(q', \theta; \boldsymbol{m}, q) = \int_0^{2\pi} \mathrm{d}\phi\, \sigma_E(q', \theta, \phi; \boldsymbol{m}, q)$ into angle θ.

Note that the above formalism is in the the centre-of-mass coordinate system, i.e. it arises in scattering theory after separating out the motion of the centre-of-mass of $A - B$, a feature discussed in greater detail in section 8.1.

[5] An erratum clarifies that the results shown in [94] are valid at $\phi = 0$ and that control over the total cross-section is not possible when building the initial superposition from helicity states.

Control of collisions is achieved by constructing an initial-state $|E, q, \{a_{\boldsymbol{m}}\}\rangle$ composed of a superposition of N energetically degenerate asymptotic states $|E, q, \boldsymbol{m}; 0\rangle$:

$$|E, q, \{a_{\boldsymbol{m}}\}\rangle = \sum_{\boldsymbol{m}} a_{\boldsymbol{m}} |E, q, \boldsymbol{m}; 0\rangle. \tag{100}$$

The cross-section associated with using equation (100) as the initial-state, obtained by replacing $|E, q, \boldsymbol{m}; 0\rangle$ by equation (100) in (98), is

$$\begin{aligned}\sigma_E(\boldsymbol{n}, q'; \{a_{\boldsymbol{m}}\}, q) &= \left| \langle E, q', \boldsymbol{n}^- | V_q \sum_{\boldsymbol{m}} a_{\boldsymbol{m}} |E, q, \boldsymbol{m}; 0\rangle \right|^2 \\ &= \sum_{\boldsymbol{m}} |a_{\boldsymbol{m}}|^2 |\langle E, q', \boldsymbol{n}^- | V_q | E, q, \boldsymbol{m}; 0\rangle|^2 \\ &\quad + \sum_{\boldsymbol{m}'} \sum_{\boldsymbol{m} \neq \boldsymbol{m}'} a_{\boldsymbol{m}} a^*_{\boldsymbol{m}'} \langle E, q, \boldsymbol{m}'; 0 | V_q | E, q', \boldsymbol{n}^- \rangle \langle E, q', \boldsymbol{n}^- | V_q | E, q, \boldsymbol{m}; 0\rangle \\ &\equiv \sum_{\boldsymbol{m}} |a_{\boldsymbol{m}}|^2 \sigma(\boldsymbol{n}, q'; \boldsymbol{m}, q) + \sum_{\boldsymbol{m}'} \sum_{\boldsymbol{m} \neq \boldsymbol{m}'} a_{\boldsymbol{m}} a^*_{\boldsymbol{m}'} \sigma(\boldsymbol{n}, q'; \boldsymbol{m}', \boldsymbol{m}, q),\end{aligned} \tag{101}$$

where $\sigma(\boldsymbol{n}, q'; \boldsymbol{m}', \boldsymbol{m}, q)$ is defined via equation (101). The total cross-section into arrangement q' is then given by

$$\sigma_E(q'; \{a_{\boldsymbol{m}}\}, q) = \sum_{\boldsymbol{n}} \sigma_E(\boldsymbol{n}, q'; \{a_{\boldsymbol{m}}\}, q). \tag{102}$$

Note that equation (101), and hence equation (102), are of a standard CC form, i.e. direct contributions from each individual member of the superposition, proportional to $|a_{\boldsymbol{m}}|^2$, plus interference terms that are proportional to $a_{\boldsymbol{m}} a^*_{\boldsymbol{m}'}$. It is clear that if we control the $a_{\boldsymbol{m}}$, through assorted preparation methods, then we can control the interference term, and hence the scattering cross-section.

8.1. Issues in the preparation of the scattering superposition

To describe how the required superposition state (equation (100)) can be constructed in the laboratory requires some introductory remarks. Note first that equations (98)–(102) and the $|E, q, \boldsymbol{m}; 0\rangle$ states are understood to be in the centre-of-mass coordinate system and describe the relative translational motion as well as the internal state of A and B. In typical $A-B$ scattering, separating out the centre-of-mass motion comes about in a straightforward way. That is, let $\boldsymbol{r}_A$ and $\boldsymbol{r}_B$ denote the laboratory position of A and B and $\hbar\boldsymbol{k}^A$, $\hbar\boldsymbol{k}^B$ denote their laboratory momenta. The relative momentum $\boldsymbol{k}$, relative coordinate $\boldsymbol{r}$, centre-of-mass momentum $\boldsymbol{K}$ and position $\boldsymbol{R}_{\rm cm}$ are defined as

$$\begin{aligned}\boldsymbol{K} &= \boldsymbol{k}^A + \boldsymbol{k}^B, \qquad & \boldsymbol{R}_{\rm cm} &= \frac{(M_A \boldsymbol{r}_A + M_B \boldsymbol{r}_B)}{(M_A + M_B)} \\ \boldsymbol{k} &= \frac{(M_B \boldsymbol{k}^A - M_A \boldsymbol{k}^B)}{(M_A + M_B)}, & \boldsymbol{r} &= \boldsymbol{r}_A - \boldsymbol{r}_B.\end{aligned} \tag{103}$$

In the case where A and B are initially in internal states $|\phi_A(i)\rangle$ and $|\phi_B(j)\rangle$, of energies $e_A(i)$ and $e_B(j)$, and the initial A and B translational motion are described by plane waves of momenta $\boldsymbol{k}_i^A$ and $\boldsymbol{k}_j^B$ then the incident wavefunction $\psi_{\rm in}$ is the product

$$\begin{aligned}\psi_{\rm in} &= |\phi_A(i)\rangle |\phi_B(j)\rangle \exp(\mathrm{i}\boldsymbol{k}_i^A \cdot \boldsymbol{r}_A) \exp(\mathrm{i}\boldsymbol{k}_j^B \cdot \boldsymbol{r}_B) \\ &= |\phi_A(i)\rangle |\phi_B(j)\rangle \exp(\mathrm{i}\boldsymbol{k} \cdot \boldsymbol{r}) \exp(\mathrm{i}\boldsymbol{K} \cdot \boldsymbol{R}_{\rm cm}).\end{aligned} \tag{104}$$

The second equality follows from equation (103). Since the interaction potential V_q between A and B depends only upon the relative coordinates of $A - B$, the centre-of-mass momentum is conserved in the collision, allowing us to separate out the centre-of-mass motion and to describe the dynamics in the centre-of-mass coordinate system, i.e. in terms of $|\phi_A(i)\rangle|\phi_B(j)\rangle \exp(\mathrm{i}\boldsymbol{k}\cdot\boldsymbol{r})$. This state is, in fact, $\langle \boldsymbol{r}|E, q, \boldsymbol{m}; 0\rangle$, where the relative motion is in the coordinate representation.

Note that the scattering in equation (104) occurs at fixed value of the centre-of-mass momentum $\boldsymbol{K}$. Scattering may also occur from a state comprised of different $\boldsymbol{K}$ values. For example, the incident wavefunction may be of the form

$$|\psi_{\mathrm{in}}\rangle = \sum_{l\boldsymbol{m}} d_{l\boldsymbol{m}}|E, q, \boldsymbol{m}; 0\rangle|\boldsymbol{K}_l\rangle \qquad (\boldsymbol{K}_{l'} \neq \boldsymbol{K}_l). \tag{105}$$

Since the centre-of-mass momentum is conserved and can be measured, components of the wavefunction with different values of $|\boldsymbol{K}_l\rangle$ contribute independently to the reaction cross-section and do not interfere with one another. That is, the cross-section for scattering into $|E, q', \boldsymbol{n}; 0\rangle$ in this case is given by

$$\sigma_E(\boldsymbol{n}, q'; \{d_{l\boldsymbol{m}}\}, q) = \sum_l \left| \langle E, q', n^-|V_q \sum_{\boldsymbol{m}} d_{l\boldsymbol{m}}|E, q, \boldsymbol{m}; 0\rangle \right|^2. \tag{106}$$

Consider now preparation of the generalized superposition states (equation (100)) where for simplicity we limit consideration to a superposition of two states. To do so we examine the scattering of A and B, each in a previously prepared in the laboratory in a superposition state. The wavefunctions of A and B in the laboratory frame, ψ_A and ψ_B, are of the general form:

$$|\psi_A\rangle = a_1|\phi_A(1)\rangle \exp(\mathrm{i}\boldsymbol{k}_1^A \cdot \boldsymbol{r}_A) + a_2|\phi_A(2)\rangle \exp(\mathrm{i}\boldsymbol{k}_2^A \cdot \boldsymbol{r}_A), \tag{107}$$

$$|\psi_B\rangle = b_1|\phi_B(1)\rangle \exp(\mathrm{i}\boldsymbol{k}_1^B \cdot \boldsymbol{r}_B) + b_2|\phi_B(2)\rangle \exp(\mathrm{i}\boldsymbol{k}_2^B \cdot \boldsymbol{r}_B). \tag{108}$$

The incident wavefunction is then the product

$$\begin{aligned} |\psi_{\mathrm{in}}\rangle = |\psi_A\rangle|\psi_B\rangle &= [a_1|\phi_A(1)\rangle \exp(\mathrm{i}\boldsymbol{k}_1^A \cdot \boldsymbol{r}_A) + a_2|\phi_A(2)\rangle \exp(\mathrm{i}\boldsymbol{k}_2^A \cdot \boldsymbol{r}_A)] \\ &\quad \times [b_1|\phi_B(1)\rangle \exp(\mathrm{i}\boldsymbol{k}_1^B \cdot \boldsymbol{r}_B) + b_2|\phi_B(2)\rangle \exp(\mathrm{i}\boldsymbol{k}_2^B \cdot \boldsymbol{r}_B)] \\ &= \sum_{i,j=1}^{2} A_{ij} \exp(\mathrm{i}\boldsymbol{k}_{ij} \cdot \boldsymbol{r}) \exp(\mathrm{i}\boldsymbol{K}_{ij} \cdot \boldsymbol{R}_{\mathrm{cm}}), \end{aligned} \tag{109}$$

where

$$A_{ij} = a_i b_j|\phi_A(i)\rangle|\phi_B(j)\rangle, \qquad \boldsymbol{k}_{ij} = \frac{(M_B\boldsymbol{k}_i^A - M_A\boldsymbol{k}_j^B)}{(M_A + M_B)}$$

and

$$\boldsymbol{K}_{ij} = \boldsymbol{k}_i^A + \boldsymbol{k}_j^B.$$

As constructed, equation (109) is composed of four independent non-interfering incident states since each has a different centre-of-mass wavevector $\boldsymbol{K}_{ij}$. However, we can set conditions so that interference, and hence control, is allowed. That is, we can require the equality of the centre-of-mass motion of two components, plus energy degeneracy:

$$\begin{aligned} &\boldsymbol{K}_{12} = \boldsymbol{K}_{21} \\ &\frac{\hbar^2 k_{12}^2}{2\mu} + e_A(1) + e_B(2) = \frac{\hbar^2 k_{21}^2}{2\mu} + e_A(2) + e_B(1), \end{aligned} \tag{110}$$

with $\mu = M_A M_B/(M_A + M_B)$. Equation (109) then becomes

$$\psi_{\rm in} = [A_{12}\exp(\mathrm{i}\boldsymbol{k}_{12}\cdot\boldsymbol{r}) + A_{21}\exp(\mathrm{i}\boldsymbol{k}_{21}\cdot\boldsymbol{r})]\exp(\mathrm{i}\boldsymbol{K}_{12}\cdot\boldsymbol{R}_{\rm cm}) + A_{11}\exp(\mathrm{i}\boldsymbol{k}_{11}\cdot\boldsymbol{r})\exp(\mathrm{i}\boldsymbol{K}_{11}\cdot\boldsymbol{R}_{\rm cm}) + A_{22}\exp(\mathrm{i}\boldsymbol{k}_{22}\cdot\boldsymbol{r})\exp(\boldsymbol{K}_{22}\cdot\boldsymbol{R}_{\rm cm}), \quad (111)$$

where the term in the first bracket, due to equation (110), is a linear superposition of two degenerate states. We therefore expect that the scattering cross-section will be composed of non-interfering contributions from three components with differing $\boldsymbol{K}_{ij}$, but where the first term allows for control via the interference between the A_{12} and A_{21} terms. The two remaining terms, proportional to A_{11} and A_{22}, are uncontrolled satellite contributions.

For example, if we design the experiment so that $\boldsymbol{k}_1^A = -\boldsymbol{k}_2^B$ and $\boldsymbol{k}_2^A = -\boldsymbol{k}_1^B$ then $\boldsymbol{K}_{12} = \boldsymbol{K}_{21} = 0$, and $\boldsymbol{k}_{12} = \boldsymbol{k}_1^A$, $\boldsymbol{k}_{21} = -\boldsymbol{k}_1^B$, so that the degeneracy requirement (equation (110)) becomes

$$\frac{\hbar^2(k_1^A)^2}{2\mu} + e_A(1) + e_B(2) = \frac{\hbar^2(k_1^B)^2}{2\mu} + e_A(2) + e_B(1). \quad (112)$$

Note also that we can implement equation (112) for the case of atom-diatomic-molecule scattering by setting $|\phi_A(1)\rangle = |\phi_A(2)\rangle = |\phi_A(g)\rangle$, where $|\phi_A(g)\rangle$ is the, e.g. ground electronic state of atom A. In this case, the degeneracy condition (equation (112)) is

$$\frac{\hbar^2}{2\mu}[(k_1^A)^2 - (k_2^A)^2] = [e_B(1) - e_B(2)]. \quad (113)$$

In general, these conditions demand a method of preparing $|\psi_A\rangle$ and $|\psi_B\rangle$ that correlate the internal states $|\phi_A(i)\rangle$ and $|\phi_B(i)\rangle$ with their associated momenta $\boldsymbol{k}_i^A, \boldsymbol{k}_i^B$ so as to obtain equation (112). Since the overall phase of the wavefunction is irrelevant to the state of the system, the dynamics is not sensitive to the overall phase of $|\psi_A\rangle|\psi_B\rangle$. However, the phases of the interference term must be well defined, or the control will average to zero.

Specifically, CC of collisional processes requires the production of states (equation (108)) where the translational and internal states are entangled, i.e. composed of components in which two or more translational and internal states are correlated. Although such states result from photodissociation processes (see, e.g. equation (38)) they are not necessarily suitable for our purposes. Below we provide three tentative suggestions for producing these states whose realization would require an extension of current laboratory techniques.

For example, entangled states which might be useful for collisional control have been prepared in atoms in a relatively straightforward way [99]. Consider, for example, a system with two levels $|E_1\rangle$, $|E_2\rangle$, initially in the lower state $|E_1\rangle$ and moving with kinetic energy $E_t(1)$. Passing the system through a spatially dependent field with off-resonant frequency $\omega = (E_2 - E_1)/\hbar - \delta$ results in excitation to the state $|E_2\rangle$ with kinetic energy $E_t(2)$. Conservation of energy requires, however, that

$$E_1 + E_t(1) + \hbar\omega = E_2 + E_t(2) \quad (114)$$

or $E_t(2) = E_t(1) - \hbar\delta$. That is, the created superposition state has two internal states correlated with two different translational energy states, precisely as required for the CC of collisions. Tuning δ above or below the resonance results in an increase, or decrease, of kinetic energy upon excitation. The extension of this technique to most cases of interest to us will, however, be difficult since the $\hbar\delta$ required is far larger than that in the atomic case.

Similarly, the momentum transfer associated with a collision of photons with atoms is used regularly to cool atoms (see [100] for a review), i.e. to alter the translational energy of an atom. Indeed, the momentum of large numbers of photons (over 140 photon momenta) have been successfully transferred coherently to atoms [101]. This suggests the possibility

of preparing an initial superposition of internal states of a molecule, followed by the state-specific absorption of photon momenta of one of the internal states in order to form the required entangled superposition of the translational and internal states.

Finally, we note that a number of experiments have shown that it is possible to accelerate or decelerate molecules using time varying electric fields (see [102] and references therein). In this case, the molecule is passed through an array of synchronously pulsed electric field stages that interact with the molecular dipole. Since the dipole is a function of the state of the system it may be possible to prepare a superposition of internal states and then selectively accelerate one of the two internal states to produce the desired superposition.

8.2. Identical particle collisions

A number of computations ([91–94], [95][5], [96–98]) have been carried out, on systems such as $H + H_2$ and $F + HD$, that demonstrate the degree of control afforded by this approach to atom–diatom scattering. However, in this review we call attention to applications to identical particle scattering which provide a simplified means of satisfying the conditions above and are of interest to studies of entangled states and cold collisions.

Consider then the case of identical particle collisions, i.e. when $B = A$. Specifically, consider

$$A + A' \rightarrow C + D \tag{115}$$

with $\boldsymbol{k}_i^A = \boldsymbol{k}_i^{A'}$. Here, we have used A' to denote the molecule A, but in a superposition state that is not necessarily the same as A. If we prepare each of the two initial A and A' superposition states from the same molecular bound states, e.g. $|\phi_A(1)\rangle = |\phi_{A'}(1)\rangle$ and $|\phi_A(2)\rangle = |\phi_{A'}(2)\rangle$ then the requirement for conservation of energy in the centre-of-mass (equation (110)) becomes

$$k_{12}^2 = k_{21}^2. \tag{116}$$

For the case of $A + A'$ collisions, this condition is always satisfied.

This scenario opens up a wide range of possible experimental studies of control of collisional processes. Specifically, we need only prepare A and A' in a controlled superposition of two-states (e.g. by resonant laser excitation of $|\phi_A(1)\rangle$) to produce a superposition with $|\phi_A(2)\rangle$, direct them antiparallel in the laboratory and vary the coefficients in the superposition to affect the reaction probabilities. Control originates in quantum interference between two degenerate states associated with the contributions of $|\phi_A(1)\rangle|\phi_{A'}(2)\rangle$ and $|\phi_A(2)\rangle|\phi_{A'}(1)\rangle$. This is accompanied by two uncontrolled scattering contributions corresponding to the contributions of $|\phi_A(1)\rangle|\phi_{A'}(1)\rangle$ and $|\phi_A(2)\rangle|\phi_{A'}(2)\rangle$. Control is achieved by varying the four coefficients $a_i, b_i, i = 1, 2$.

The control approach described above can be generalized to a superposition of N levels in each of the two A and A' reactants. Specifically, choosing all $\boldsymbol{k}_i^A = \boldsymbol{k}^A$ and with $\boldsymbol{k}_i^{A'} = -\boldsymbol{k}^A$ we have

$$\begin{aligned} |\psi_A\rangle &= \exp(\mathrm{i}\boldsymbol{k}^A \cdot \boldsymbol{r}_A)\left[\sum_{i=1}^{N} a_i|\phi_A(i)\rangle\right], \\ |\psi_{A'}\rangle &= \exp(-\mathrm{i}\boldsymbol{k}^A \cdot \boldsymbol{r}_{A'})\left[\sum_{j=1}^{N} b_j|\phi_{A'}(j)\rangle\right]. \end{aligned} \tag{117}$$

The scattering wavefunction is then

$$|\psi_{\mathrm{in}}\rangle = |\psi_A\rangle|\psi_{A'}\rangle = \exp(\mathrm{i}\boldsymbol{k} \cdot \boldsymbol{r})\left[\sum_{i=1}^{N} a_i|\phi_A(i)\rangle\right]\left[\sum_{j=1}^{N} b_j|\phi_{A'}(j)\rangle\right]. \tag{118}$$

Since $M_A = M_{A'}$, $\boldsymbol{k} = (\boldsymbol{k}^A - \boldsymbol{k}^{A'})/2 = \boldsymbol{k}^A$. The kinetic energy $k^2/2\mu$ is the same for each term in equation (118) so that degenerate states in the centre-of-mass frame correspond to states $|\phi_A(i)\rangle|\phi_{A'}(j)\rangle$ in equation (118) which are of equal internal energy $e_A(i) + e_{A'}(j)$. Expanding the product in equation (118) gives N^2 terms, N terms of which are of differing energy $2e_A(i)$, $i = 1, \ldots, N$ and $(N^2 - N)$ states of energy $e_A(i) + e_{A'}(j)$, $i \neq j$. Of the latter terms, each is accompanied by another term of equal energy (i.e. $e_A(i) + e_{A'}(j) = e_A(j) + e_{A'}(i)$). Hence, the N^2 terms are comprised of N direct terms plus $(N^2 - N)/2$ degenerate pairs which are a source of interference, and hence control. Here control is achieved by altering the $2N$ coefficients a_i, b_i in the initially prepared state (equation (118)), e.g. by shaped pulsed laser excitation of A and A'.

Computational examples of this approach have been restricted to control over rotational excitation in H_2 + H_2, a consequence of limitations on the ability to perform quantum computations on $AB + AB$ scattering. A careful analysis of the scattering [103] requires consideration both of the interference effects as well as the nature of the identical particle scattering. Typical results are shown in figure 19 for various low energy scattering cases. Specifically, we show the differential cross-section into scattering angles θ and final states $j_1' = j_2' = 2$, arising from scattering of para H_2 + para H_2, where each H_2 is in an initial superposition, with either a plus or minus sign, of $j_1 = 4$ and $j_2 = 0$. The cross term contributing to the scattering in these cases is

$$|\psi^{\pm}_{j_1 j_2}\rangle = \frac{1}{\sqrt{2}}[|j_1\rangle|j_2\rangle \pm |j_2\rangle|j_1\rangle]|m_1 = 0, v_1 = 0\rangle|m_2 = 0, v_2 = 0\rangle, \qquad (119)$$

where v_i, m_i denote the vibrational state and angular momentum projection along the z-axis. Note that results for $m_i = m_2$ are essentially independent of the value of m_i.

The results of this computation (figure 19—note the logarithmic ordinate scale) clearly show that the phase of the j_1, j_2 superposition has a significant effect on the differential cross-section. This translates into considerable control over the total inelastic cross-section, i.e. the integral of the differential cross-section over θ. For example, in panel (c) of figure 19, the total inelastic cross-section is 0.057 for $|\psi^{+}_{j_1 j_2}\rangle$ and 0.032 for $|\psi^{-}_{j_1 j_2}\rangle$. A careful analysis [103] shows that the control contribution is due to the presence of entangled states between the two reactant molecules.

Results on more complex scattering, e.g. reactive scattering, await further computational (or experimental) developments.

9. Decoherence and loss of control

Thus, far we have dealt with idealized isolated molecules that are neither subject to external collisions nor display spontaneous emission. Further, we have assumed that the molecule is initially in a pure state and that the externally imposed electric field is coherent, i.e. that the field is described by a well defined function of time. Under these circumstances the molecule is in a pure state before and after laser excitation, and remains so throughout its evolution. However, if the molecule is initially in a mixed state (e.g. due to prior collisional relaxation), or if the incident radiation field is not fully coherent (e.g. due to random fluctuations of the laser phase or of the laser amplitude), or if collisions cause the loss of quantum phase after excitation, then phase information is degraded, interference phenomena are muted and laser control is jeopardized.

Loss of quantum information (either of the phase or of the amplitude of a state) due to the interaction of a system with its environment is termed decoherence. Examples include the

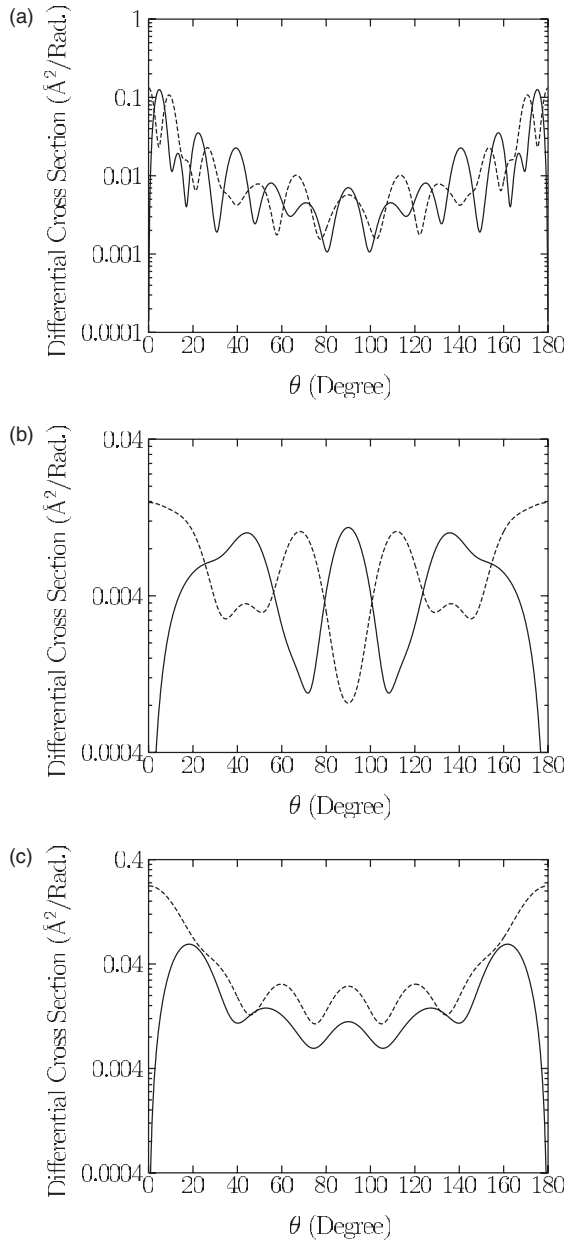

Figure 19. Inelastic differential cross-section for para H_2 + para H_2, where the collision energy is (*a*) 400 cm^{-1}, (*b*) 40 cm^{-1}, and (*c*) 4 cm^{-1}. Dashed and solid lines are for the incoming free entangled states $|\psi^{+}_{j_1 j_2}\rangle$ and $|\psi^{-}_{j_1 j_2}\rangle$. Here, $j_1 = 4$, $j_2 = 0$, $j_1' = j_2' = 2$. From figure 2, [103].

obvious case where a system is actually embedded in an external environment, e.g. a molecule in solution, or more subtle cases, e.g. where the system is chosen as the centre-of-mass of a body and the environment is the 10^{23} variables associated with the motion of the atoms that comprise the system.

The current view is that certain forms of decoherence can cause the loss of quantum interference in just such a way that the resultant system then obeys classical mechanics [104].

This view does not obviate the possibility that classical mechanics is, in fact, the limit of quantum mechanics when $\hbar \to 0$, (i.e. when the system action becomes very large) [82]. Rather, it proposes an alternate route to classical mechanics for systems in interaction with their environment. Clearly, decoherence effects that change the dynamics from quantum to classical mechanics will destroy quantum phases and hence destroy CC. Indeed, most decoherence effects work towards the loss of quantum phase and have deleterious effects on control.

Consider then a system s interacting with an environment. The total Hamiltonian $H_{\rm tot}$ is of the form

$$H_{\rm tot} = H_s + H_{\rm env} + H_{\rm int}, \tag{120}$$

where H_s is the system Hamiltonian, $H_{\rm env}$ is the Hamiltonian of the environment, and $H_{\rm int}$ is the interaction between them. Ultimately, we intend to focus solely on the properties of the system, i.e. the quantities of interest. To do so we have to deal with mixed states and hence we have to invoke the density matrix formulation of quantum mechanics [105]. That is, the system plus environment is described by a density operator $\rho_{\rm tot}(t)$ whose dynamics is given by the quantum Liouville–von Neumann equation;

$$\mathrm{i}\hbar \frac{\partial \rho_{\rm tot}(t)}{\partial t} = [H_{\rm tot}, \rho_{\rm tot}(t)]. \tag{121}$$

Since it is the dynamics of the system that is of interest, it would be convenient to pre-average over the environment variables and obtain an equation of motion for $\rho_s(t)$, the system component of the density matrix. Formal work of this kind [106, 107] yields the so-called generalized master equation. Deriving the generalized master equation and extracting the various approximations utilized goes well astray of the central focus of this review, but many reviews of this topic are available [106, 107].

If the correlation time of the environment is much shorter than the typical timescale for the variation of the system then the generalized master equation is of the form

$$\frac{\partial \rho_s(t)}{\partial t} = -\mathrm{i}\hbar^{-1}[H_s, \rho_s(t)] + F(\rho_s), \tag{122}$$

where $F(\rho_s)$ is a functional of ρ_s. Its functional form depends upon the nature of the environment and on the coupling $H_{\rm int}$. A variety of approximations to these generally complicated equations are available, and are utilized below.

9.1. Sample computational results on decoherence

To demonstrate the effect of decoherence we consider computational results [108] using a model, due to Caldeira–Leggett and Zurek [109], that is widely regarded as a paradigm for studies of decoherence. Here, the system interacts with a bath comprising harmonic oscillators in the weak coupling and high temperature limit. The harmonic bath thus serves as the source of the decoherence experienced by the system. As a concrete example, we consider the vibrational motion of a model molecule with two degrees of freedom coupled to an harmonic bath.

In doing so it proves convenient to carry out the computations in the Wigner representation. Recall that the Wigner representation ρ^W of the density operator ρ is defined, for an N degree of freedom system, by

$$\rho^W \equiv \rho^W(\boldsymbol{q}, \boldsymbol{p}) = (\pi\hbar)^N \int \mathrm{d}\boldsymbol{v}\, \mathrm{e}^{-2\mathrm{i}\boldsymbol{p}\cdot\boldsymbol{v}/\hbar} \langle \boldsymbol{p} - \boldsymbol{v}|\rho|\boldsymbol{q} + \boldsymbol{v}\rangle \tag{123}$$

and the Wigner representation of any operator A, denoted by the superscript W, is given by

$$\boldsymbol{A}^W = 2^N \int \mathrm{e}^{-2\mathrm{i}\boldsymbol{p}\cdot\boldsymbol{v}/\hbar} \langle \boldsymbol{q} - \boldsymbol{v}|A|\boldsymbol{q} + \boldsymbol{v}\rangle. \tag{124}$$

The Caldeira–Leggett and Zurek models for a two degree of freedom oscillator system with Hamiltonian H_s in contact with a bath is given by [108]

$$\frac{\partial \rho_s^W(t)}{\partial t} = -\mathrm{i}\hbar^{-1}[H_s, \rho_s(t)]^W + F_{\mathrm{CL}}^W(\rho_s)$$
$$\equiv \left[\{H_s, \rho_s^W\} + \sum_{(l_1+l_2)\ \mathrm{odd}} \frac{(\hbar/2i)^{(l_1+l_2-1)}}{l_1!l_2!} \frac{\partial^{(l_1+l_2)} V(x,y)}{\partial x^{l_1} \partial y^{l_2}} \frac{\partial^{(l_1+l_2)} \rho_s^W}{\partial p_x^{l_1} \partial p_y^{l_2}} \right] + F_{\mathrm{CL}}^W(\rho_s). \tag{125}$$

Here,

$$F_{\mathrm{CL}}^W(\rho_s) = D\left(\frac{\partial^2 \rho_s^W}{\partial p_x^2} + \frac{\partial^2 \rho_s^W}{\partial p_y^2}\right)$$

denotes the Caldeira–Leggett form of $F(\rho_s)$ in the Wigner representation. The term in square brackets in equation (125) is the Wigner representation $[H_s, \rho_s(t)]^W$ of $[H_s, \rho_s(t)]$. Here (p_x, p_y, x, y) are the system momenta and coordinates, $V(x, y)$ is the potential contribution to the Hamiltonian H and $\rho_s^W = \rho_s^W(p_x, p_y, x, y; t)$. The first term

$$\{H_s, \rho_s^W\} = \frac{\partial H_s}{\partial x}\frac{\partial \rho_s^W}{\partial p_x} - \frac{\partial H_s}{\partial p_x}\frac{\partial \rho_s^W}{\partial x} + \frac{\partial H_s}{\partial y}\frac{\partial \rho_s^W}{\partial p_y} - \frac{\partial H_s}{\partial p_y}\frac{\partial \rho_s^W}{\partial y}$$

on the right-hand side of equation (125) is the classical Poisson bracket that generates classical dynamics, the second term is responsible for the difference between quantum and classical mechanics, and the third term induces decoherence.

Numerical calculations on equation (125) can be compared to classical mechanics by computing the classical phase space density $\rho_{\mathrm{cl}}(x, y, p_x, p_y)$, which is obtained as the solution to the Fokker–Planck equation:

$$\frac{\partial}{\partial t}\rho_{\mathrm{cl}}(x, y, p_x, p_y) = \{H_s, \rho_{\mathrm{cl}}(x, y, p_x, p_y)\}$$
$$+D\left(\frac{\partial^2}{\partial p_x^2}\rho_{\mathrm{cl}}(x, y, p_x, p_y) + \frac{\partial^2}{\partial p_y^2}\rho_{\mathrm{cl}}(x, y, p_x, p_y)\right). \tag{126}$$

The extent to which quantum effects are diminished in the presence of decoherence is demonstrated in the figures that follow for the specific case of the non-linear oscillator Hamiltonian (see, e.g. [111])

$$H_s = \frac{1}{2}(p_x^2 + p_y^2 + \alpha x^2 y^2) + \frac{\beta}{4}(x^4 + y^4) \tag{127}$$

with parameters that can be related to typical molecules: $\beta = 0.01, \alpha = 1.0$. Figure 20 shows the classical and quantum expectation values, in the absence of decoherence (i.e. $D = 0$ in equations (125) and (126)) for four moments associated with y. All figures show qualitatively similar behaviour, i.e. after an initial period of classical/quantum agreement the quantum results continue to oscillate while the classical results show smooth relaxation (see [112][6]). Note in particular that the quantum results do not always simply oscillate about the classical (e.g. see results for $\langle y^2 \rangle$) and that the quantum fluctuations about the mean are substantial (e.g. 30% in the case of $\langle E_y \rangle$).

Results for the same moments, after introducing decoherence, are shown in figure 21. A comparison of figures 20 and 21 shows substantially improved classical-quantum correspondence upon introducing decoherence. Remarkably, this is true even for $\langle y^2 \rangle$, where the long term quantum average in the closed system deviated significantly from the long term classical average. Qualitatively similar results have been obtained for reactive scattering [113].

[6] Analogous results were observed previously for the stadium billiard.

These computational results demonstrate the way in which decoherence tends to eliminate quantum effects in the system. As a consequence, quantum control processes must be effectively shielded from decoherence effects in order to survive.

Below we consider a number of approaches to combating decoherence in solutions and other media where collisions are present. An alternative approach, which we do not address, is the method of 'decoherence free subspaces' [114]. In this approach, one deals with the explicit design of systems where a particular subspace is free from decoherence effects. These approaches are of particular interest to the development of subspaces in which to carry out quantum computation, an approach in which the computational machinery follows the laws of quantum mechanics [115]. By contrast, we deal below with the need to curb decoherence effects in traditional pre-existent systems.

9.2. Condensed phases: the optical Bloch equation

Recent experimental studies on interference effects in solution, and on collisional vibrational energy transfer between molecules in solution provides some insight into the timescales for these relaxation events. For example [116], the timescale for transfer of population to the vibrational modes in liquid CH_3OH is on the order of 5–15 ps [117]. Further, studies of the preparation of coherent superpositions of states in solution show that phase coherences of

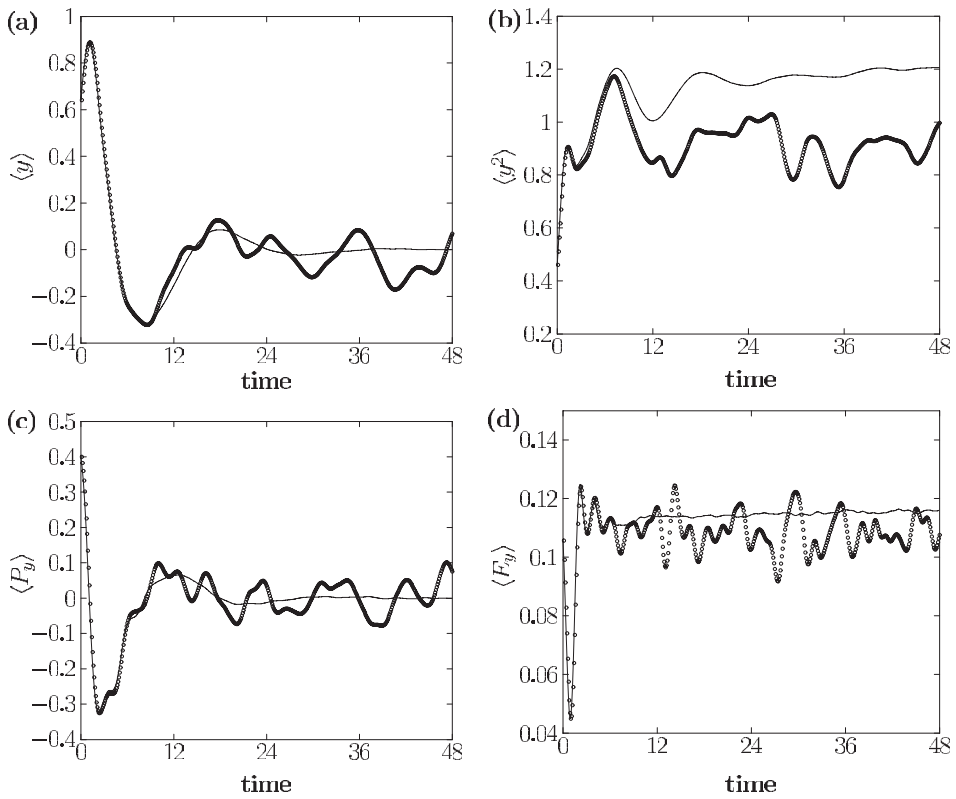

Figure 20. Time dependence of four statistical moments ($\langle y\rangle$, $\langle y^2\rangle$, $\langle P_y\rangle$ and $\langle E_y\rangle$) for the system in the absence of decoherence. Dark dots denote quantum results, thin solid lines are classical results. From figure 1, [108].

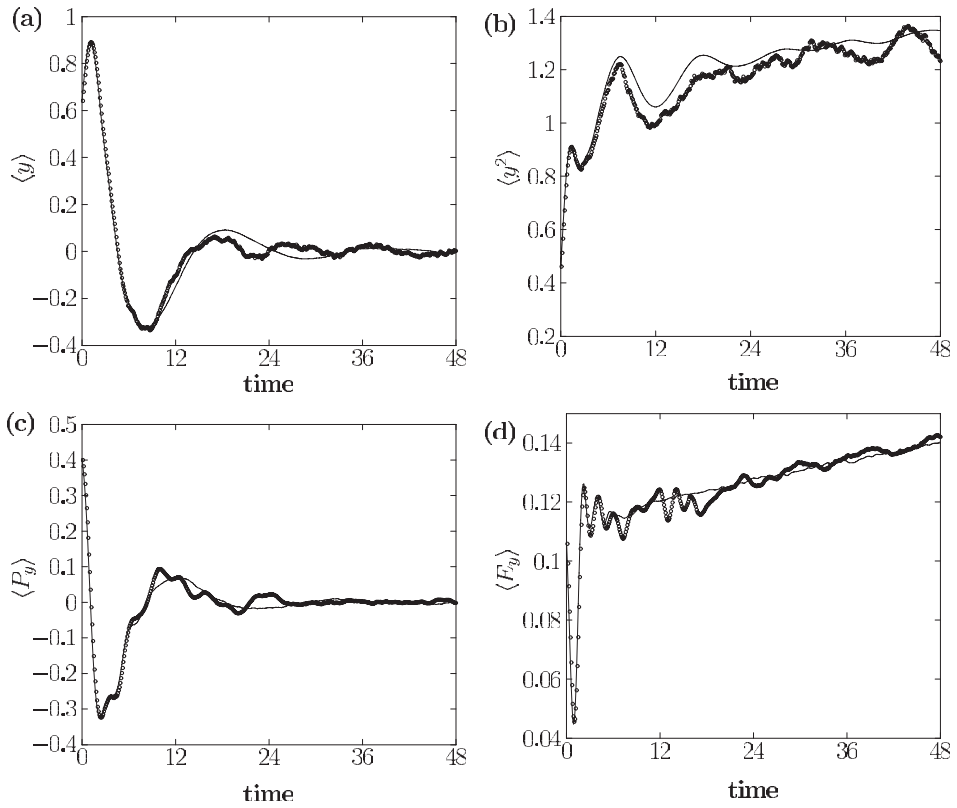

Figure 21. As in the previous figure, but in the presence of decoherence. From figure 2, [108].

molecules exist in solution for timescales greater than 100 fs [118, 119]. However, coherence is expected to be lost over longer timescales.

Consider then CC as it would apply to liquid phase chemistry. Here, molecules of species B in solution would be subjected to laser irradiation. Since we are ultimately interested in the fate of the B molecules, B is the system and the remaining molecules in the solution, and the laser, are the environment. Decoherence effects can then arise from the collisions of the solvent with the molecule of interest, or from incoherence properties of the laser that cause some loss of quantum phase information. Countering these decoherence effects is discussed below.

We consider the simplest of models, the optical Bloch equation for relaxation and concomitant decoherence in the energy representation, and examine scenarios to counter collisional effects. With $|E_i\rangle$ denoting the eigenstates of the system Hamiltonian, we define $\rho_{i,j}(t) = \langle E_i|\rho_s(t)|E_j\rangle$ as the matrix (energy) representation of the density operator. The equation of motion for $\rho_s(t)$ is then

$$\frac{\partial \rho_{i,j}(t)}{\partial t} = -\mathrm{i}\hbar^{-1}[H_s, \rho_s(t)]_{i,j} - \frac{1}{T_{i,j}}\rho_{i,j}(t) \tag{128}$$

with $T_{i,i} = T_1$ and $T_{i,j} = T_2$ for $i \neq j$. Here, T_1 and T_2 are phenomenological relaxation times. In this model, where $F(\rho)_{i,j} = -\rho_{i,j}(t)/T_{i,j}$, the coherent terms $\rho_{i,j}(t)$, $i \neq j$ decay with a rate $1/T_2$ and populations $\rho_{i,i}(t)$ decay with rate $1/T_1$. If the system is in the presence of a radiation field, then H_s in equation (128) is augmented by the dipole–electric field interaction.

The simplest optical Bloch equations result from a system comprised of two eigenstates $|E_1\rangle$, $|E_2\rangle$ of the molecule Hamiltonian H_M that experience the electric field-dipole interaction

$$H_{\mathrm{MR}} = -\mathcal{E}\hat{\epsilon}\cdot\boldsymbol{d}\cos(\omega t+\phi). \tag{129}$$

The Hamiltonian H_s in equation (128) is $H_s = H_M + H_{\mathrm{MR}}$. Equation (128) then becomes (where we suppress the t dependence of $\rho(t)$):

$$\frac{\partial\rho_{i,j}}{\partial t} = -\mathrm{i}\hbar^{-1}\sum_k [H_{i,k}\rho_{k,j} - \rho_{i,k}H_{k,j}] - \frac{1}{T_{i,j}}\rho_{i,j}, \tag{130}$$

where

$$H_{i,k} = E_i\delta_{i,k} - \mathcal{E}\cos(\omega t+\phi)\mathrm{d}_{i,k}(1-\delta_{i,k}) \tag{131}$$

and $\mathrm{d}_{i,k} = \langle E_i|\hat{\epsilon}\cdot\boldsymbol{d}|E_k\rangle$. Noting that $\rho_{i,j} = \rho^*_{j,i}$, we define

$$\begin{aligned} R_1 &= 2\mathrm{Im}(\rho_{1,2}) = \mathrm{Im}(\rho_{1,2}-\rho_{2,1}),\\ R_2 &= 2\mathrm{Re}(\rho_{1,2}) = \mathrm{Re}(\rho_{1,2}+\rho_{2,1}),\\ R_3 &= \rho_{11}-\rho_{22}. \end{aligned} \tag{132}$$

Then, with $H_{1,2} = H_{2,1}$ for bound states subjected to equations (129) and (130) becomes

$$\begin{aligned} \frac{\mathrm{d}R_1}{\mathrm{d}t} &= \Delta R_2 - \frac{1}{T_2}R_1 + 2H_{1,2}\frac{R_3}{\hbar},\\ \frac{\mathrm{d}R_2}{\mathrm{d}t} &= -\Delta R_1 - \frac{1}{T_2}R_2,\\ \frac{\mathrm{d}R_3}{\mathrm{d}t} &= -\frac{1}{T_1}R_3 - 2H_{1,2}\frac{R_1}{\hbar}. \end{aligned} \tag{133}$$

Here, $\Delta \equiv (E_2-E_1)/\hbar - \omega \equiv \omega_{2,1}-\omega$, i.e. the detuning of ω from the $|E_1\rangle$ to $|E_2\rangle$ transition.

Equation (133) constitutes the standard form of the two level optical Bloch equation.

9.2.1. Countering collisional effects. Consider now a scenario that is capable of maintaining CC in the presence of collisions for systems that are described by the optical Bloch equations. In particular, we reconsider the bichromatic control scenario discussed in chapter 3.2, assuming, however, that the molecules are in solution at temperature T. Further, we irradiate the system so as to saturate the $|E_1\rangle$ to $|E_2\rangle$ transition and simultaneously photodissociate the system.

The initial-state, prior to dissociation, is a mixed state described, in the energy representation, by a 2×2 density matrix with elements $\rho_{i,j}$, $(i,j=1,2)$. Photodissociation of this mixed state can be written as a generalization [120] of equation (48). In equation (48), we assumed an initial-state of the form of $\sum_{j=1}^{2} a_j|E_j\rangle\exp(-\mathrm{i}E_jt/\hbar)$ so that the corresponding density matrix would be $\rho_{m,k} = a_k a^*_m$. That is, equation (48) could be rewritten as

$$P_q(E) = \left(\frac{2\pi}{\hbar}\right)^2 \sum_{i,j=1}^{N} [\rho_{i,j}\bar{\epsilon}(\omega_{E,i})\bar{\epsilon}^*(\omega_{E,j})]\mathrm{d}_q(ji). \tag{134}$$

Equation (134) is, in fact, the correct generalization to the case where the initial-state is mixed and is represented by $\rho_{i,j}$. Below we neglect the z dependence in $\bar{\epsilon}$, replacing it by ϵ.

To utilize equation (134) we determine $\rho_{i,j}$ for the case where two levels $|E_1\rangle$ and $|E_2\rangle$ are continuously subjected to radiation and to collisions, using the optical Bloch approach. We note that if, as in the bichromatic control cases discussed above (section 3.2), $|E_1\rangle$ and $|E_2\rangle$ have the same parity, a one-photon absorption cannot couple these states. We must therefore consider saturating this transition using two-photon absorption through an off-resonant intermediate

bound state $|E_0\rangle$ with dipole matrix elements $\mathrm{d}_{0j} = \langle E_0 \mid \boldsymbol{d}\cdot\hat{\varepsilon} \mid E_j\rangle$, and with $E_2 > E_0 > E_1$. For simplicity, we assume that $2\omega = (E_2 - E_1)/\hbar$, so that the transition is two-photon resonant, and we sketch the extension [121] of equation (133) to two-photon absorption[7]. To carry out this extension, we write the Bloch equations (equation (130)) for the three level $|E_0\rangle$, $|E_1\rangle$ and $|E_2\rangle$, and adopt the adiabatic approximation for off-resonant transitions to level $|E_0\rangle$. This approximation is equivalent [121] to setting $\mathrm{d}\rho_{2,0}/\mathrm{d}t = \mathrm{d}\rho_{1,0}/\mathrm{d}t = 0$. Substituting the result into the remaining equations gives the set of equations for $\mathrm{d}\rho_{i,j}/\mathrm{d}t$, with $i, j = 1, 2$. This set can be rewritten, with the help of a modified version of equation (132), where $\rho_{1,2}$ is replaced by $\rho_{1,2}\exp(-2i\phi)$, as

$$\begin{aligned}
\frac{\mathrm{d}R_1}{\mathrm{d}t} &= -\frac{D_{2,1}R_3}{2} - \frac{R_1}{T_2},\\
\frac{\mathrm{d}R_2}{\mathrm{d}t} &= -\frac{R_2}{T_2},\\
\frac{\mathrm{d}R_3}{\mathrm{d}t} &= \frac{D_{2,1}R_1}{2} - \frac{(R_3 - R_3^e)}{T_1},
\end{aligned} \tag{135}$$

where

$$D_{2,1} = \frac{\mathcal{E}^2 \mathrm{d}_{2,0}\mathrm{d}_{0,1}}{[2\hbar^2(\omega - \omega_{01})]}. \tag{136}$$

Here, we have recognized that the quantity R_3 relaxes to the thermodynamic population difference R_3^e at temperature T, with:

$$R_3^e = \frac{[1 - \exp(-\hbar\omega_{2,1}/k_B T)]}{[1 + \exp(-\hbar\omega_{2,1}/k_B T)]}. \tag{137}$$

At long times ($t \gg T_2, T_1$) the system saturates, i.e. $\mathrm{d}R_3/\mathrm{d}t = 0$ and equation (135) implies that $\mathrm{d}R_1/\mathrm{d}t = 0$. The equations for R_i can then be readily solved and, in conjunction with equation (132), gives $\rho_{1,2}$ at saturation:

$$\begin{aligned}
\rho_{1,2} &= \frac{R_3^e T_2 D_{2,1}\exp[\mathrm{i}(2\phi - \pi/2)]}{(4 + D_{2,1}^2 T_1 T_2)},\\
\rho_{1,1} &= 0.5\left[1 + \frac{R_3^e}{(1 + D_{2,1}^2 T_1 T_2/4)}\right],\\
\rho_{2,2} &= 0.5\left[1 - \frac{R_3^e}{(1 + D_{2,1}^2 T_1 T_2/4)}\right].
\end{aligned} \tag{138}$$

Consider then excitation of this mixed state with a Gaussian pulse, within the rotating-wave approximation. The pulse is of the form

$$\varepsilon(t) = \mathcal{E}\mathrm{e}^{-\mathrm{i}(\omega_L t + \delta)}\mathrm{e}^{-(t-t_0)^2/\tau^2} \tag{139}$$

with Fourier transform

$$\epsilon(\omega) = \left(\frac{\mathcal{E}\tau}{\sqrt{\pi}}\right)\mathrm{e}^{-\tau^2(\omega_L - \omega)^2/4}\mathrm{e}^{-\mathrm{i}(\omega_L - \omega)t_0}\mathrm{e}^{-\mathrm{i}\delta} \equiv \epsilon_\omega \mathrm{e}^{-\mathrm{i}(\omega_L - \omega)t_0}\mathrm{e}^{-\mathrm{i}\delta}. \tag{140}$$

Note that this control arrangement differs from that in section 3.2 insofar as the two frequencies $\omega_1 = (E - E_1)/\hbar$ and $\omega_2 = (E - E_2)/\hbar$ that dissociate the system are components of a single pulse. The temporal width of the pulse is such that $\tau \gg T_1, T_2$.

[7] For the case of $\phi = 0$, and $T_1 = T_2 = \infty$, see [121]. Note, however, that there are serious misprints in equation (3.6) of this reference.

Inserting the long-time $\rho_{i,j}$ into equation (134) gives (denoting $\epsilon_{\omega_{qi}}$ by ϵ_i) the probability $P_q(E)$ of forming product in channel q at energy E as

$$P_q(E) = \left(\frac{\pi}{\hbar}\right)^2 [P_{1,1}(E,q) + P_{2,2}(E,q) + P_{1,2}(E,q)], \tag{141}$$

where

$$P_{1,1}(E,q) = \rho_{1,1}\epsilon_1^2 \mathrm{d}_q(11) = 0.5\left[1 + \frac{R_3^e}{(1 + D_{2,1}^2 T_1 T_2/4)}\right]\epsilon_1^2 \mathrm{d}_q(11),$$

$$P_{2,2}(E,q) = \rho_{2,2}\epsilon_2^2 \mathrm{d}_q(22) = 0.5\left[1 - \frac{R_3^e}{(1 + D_{2,1}^2 T_1 T_2/4)}\right]\epsilon_2^2 \mathrm{d}_q(22)$$

and

$$P_{1,2}(E,q) = 2 \mid \rho_{1,2} \mid\mid \mathrm{d}_q(12) \mid \epsilon_1\epsilon_2 \cos\left(\alpha_q(12) + \omega_{2,1}t_0 + 2\phi - \frac{\pi}{2}\right)$$
$$= \frac{0.5 T_2 D_{2,1} R_3^e}{(1 + D_{2,1}^2 T_1 T_2/4)\epsilon_1\epsilon_2 |\mathrm{d}_q(12)| \cos(\alpha_q(12) + \omega_{2,1}t_0 + 2\phi - \frac{\pi}{2})}, \tag{142}$$

where $\alpha_q(12)$ is the phase of $\mathrm{d}_q(12)$ (see equation (54)). From these equations, it is evident that CC can be achieved in solution by, for example, varying τ to alter the quantum interference term.

A number of simple qualitative observations are evident. First, $P_q(E)$ depends upon the parameters associated with the saturation through the combinations $D_{2,1}T_1$ and $D_{2,1}T_2$ (or their ratio and product T_1/T_2 and $D_{2,1}^2 T_1 T_2$ used below). Control vanishes if $P_{1,2}(E,q) = 0$, which occurs if either the temperature $T \to \infty$ (i.e. $R_3^e \to 0$) or $D_{2,1}T_2 \to 0$. Both these limits correspond to complete loss of coherence. Examination of equation (142) shows that this is not the case, however, for $D_{2,1}T_1 \to 0$, consistent with the fact that T_1 relates to population, rather than phase, relaxation. Physically [122], however, in collisional environment, $T_1 \gg T_2$ so that the limit $T_1 \to 0$ also implies loss of control. Note also that control vanishes under extremely large pumping rates, $D_{2,1} \to \infty$ for which $\rho_{1,1} = \rho_{2,2}$ and $\rho_{1,2} \to 0$.

Sample computational results are shown in figures 22 and 23 for the case of the photodissociation of CH_3I into $CH_3 + I$ vs $CH_3 + I^*$. In particular, we show control over the ratio $I^*/(I + I^*)$ for the collision-free case in figure 22, and at temperature $T = 0.2\hbar\omega_{2,1}/k_B$ in the subsequent figure. The abscissa is $S = \epsilon_1^2/(\epsilon_1^2 + \epsilon_2^2)$ and the ordinate is the angle $\chi_{1,2} = \omega_{2,1}t_0 + 2\phi - \pi/2$. The results clearly show control persisting for $T = 0.2\hbar\omega_{2,1}/k_B$. Additional studies [120] show less control at $T = \hbar\omega_{2,1}/k_B$, with control being lost at somewhat higher temperatures.

Thus, we see that, although collisional effects do reduce the degree of control relative to the collision-free case, saturation pumping of superposition in the bichromatic control scenario can be used to overcome collisional effects up to some reasonable temperature.

Additional theoretical studies, several using optimal or pulse control, have been carried out to study control in the presence of solvent and decoherence effects. These include work in the Wilson group on a two level oscillator model coupled to a background bath [123] and on electronic population transfer in a molecule in solution [124]. This, and more recent related work [116, 125] have generally concluded that some degree of control is indeed possible in solution, depending upon the extent of the coupling between system and solvent, and the degree to which one can manipulate the incident pulses. No quantitative rules have yet emerged on the extent to which control is, in fact, possible.

In addition to model systems, there exists [126] one fully converged computation on control in the presence of decoherence. This computation deals with controlled proton transfer between the keto and enol forms of 2-(2′-hydroxyphenyl)-oxazole (see figure 24), computed

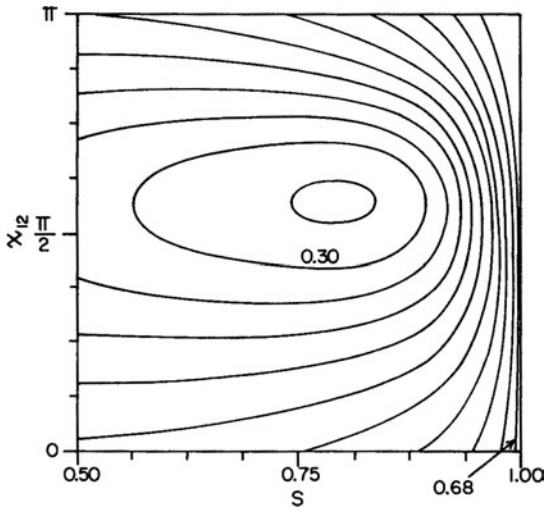

Figure 22. Contour plot of the I^* yield $[I^*/(I + I^*)]$ for two colour photodissociation of a pure CH_3I superposition state composed of bound states with vibrational and rotational quantum numbers $(v, J) = (0, 2)$ and $(1, 2)$ excited with frequencies $\omega_1 = 41\,579\,\mathrm{cm}^{-1}$ and $\omega_2 = 41\,163\,\mathrm{cm}^{-1}$. Contours increase, in increments of 0.04 from the 'centre well'. Taken from figure 1, [120].

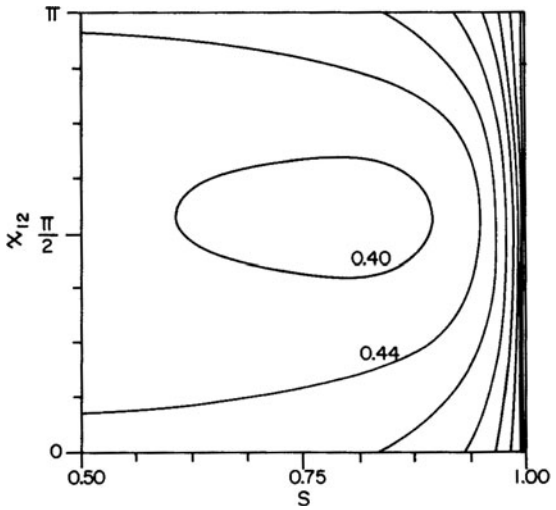

Figure 23. As in figure 22, but at $k_B T = 0.2\hbar\omega_{2,1}$. Taken from figure 2, [120].

using semiclassical mechanics (see [127] and references therein, [128]). Here, the proton is 'the system' and the remaining molecule, comprising 35 coupled degrees of freedom plus 16 out-of-plane vibrational modes, serves as the environment. The results show that despite extensive dephasing, the proton transfer dynamics is easily controlled using the bichromatic control scenario. For example, consider the case where the initial superposition state involves the ground vibrational state of the oxazole-hydroxyphenyl in-the-plane bending mode, i.e. bending motion of the $C_1C_2C_7$ angle, and the first excited state associated with such vibrational mode. Figure 25 shows a contour plot of the percentage yield of the reactant at 200 fs after excitation of the system. Here, the degree of yield control is maximum in the $0.2 < s < 0.8$

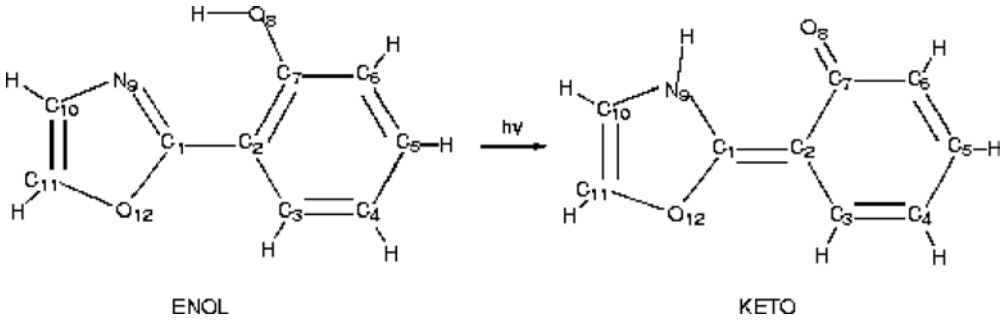

Figure 24. Keto and enol forms of 2-(2′-hydroxyphenyl)-oxazole. From figure 1, [126].

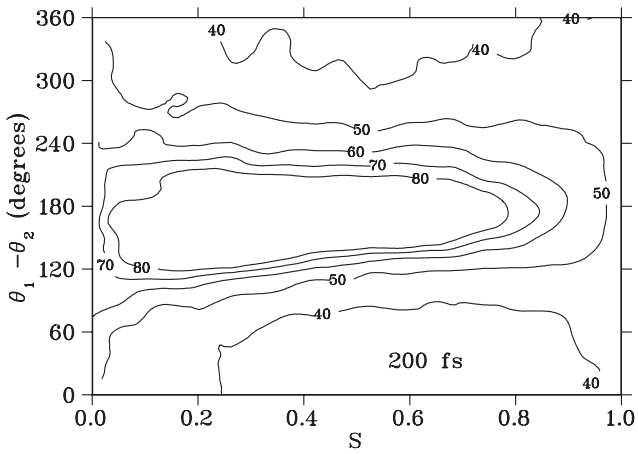

Figure 25. Contour plot of the percent reactant for bichromatic CC at 200 fs after photoexcitation of 2-(2′-hydroxyphenyl)-oxazole. Here, $\theta_i \equiv \phi(\omega_i)$, where $\phi(\omega_i)$ is the phase of the electric field, of frequency ω_i incident on the system. From figure 3, [126].

range, where the amount of the reactant can be reduced from more 80% to less than 40% by changing the relative phase of the two incident lasers from 120° to 180° to 0°.

The extent to which these results are significant is associated with the advent of intrinsic decoherence experienced by the proton during the course of the dynamics. That is, if there is little decoherence then the system is effectively a small molecule. To this end it is necessary to introduce a quantitative measure of decoherence. One such popular measure [129, 130] is $\mathrm{Tr}[\rho_s^2(t)]$ where $\rho_s(t)$ is the system density matrix. In this case, ρ_s would correspond to the density matrix of the proton. If the initial-state is chosen to be a pure state then $\rho_s^2(0) = \rho_s(0)$ and $\mathrm{Tr}[\rho_s^2(0)] = 1$. As the dynamics proceeds, and decoherence sets in, $\mathrm{Tr}[\rho_s^2(t)]$ decays. A computation on $\mathrm{Tr}[\rho_s^2(t)]$ on this system shows decay to $\mathrm{Tr}[\rho_s^2(t)] = 0.38$ by 200 fs. Hence decoherence is rapid and effective during the timescale of the control shown above.

Finally, we note studies of control in solution [131,132] indicate that control in the presence of collisional effects is indeed possible. For example, CC of the dynamics of I_3^- in ethanol and acetonitrile has been demonstrated. Specifically, I_3^- was excited with 30 fs UV laser pulse to the first excited state. The resultant wavefunction was comprised of a localized wavefunction on the ground electronic state and a corresponding depletion of wavefunction density, i.e. a 'hole', on the ground electronic state. In this instance, the target of the control was the nature

of the spectrum associated with the coherences associated with the symmetric stretch. By manipulating various attributes of the exciting pulse (intensity, frequency and chirp of the excitation pulse) aspects of the spectrum were controlled, despite the decoherence associated with collision effects.

9.3. Overcoming partial laser coherence

An alternate source of decoherence in CC experiments is in the nature of the laser used to irradiate the system. Specifically, if the laser has random components then it inputs a degree of randomness into the system, reducing the phase information content and hence decohering the system. Methods for dealing with such decoherence effects are described elsewhere ([1, 133, 134] and see [135] and references therein). One of these approaches, incoherent interference control is, however, worth noting. Specifically, figure 26 shows a level scheme where a cw field with frequency ω_1 excites the level $|E_i\rangle$ to the photodissociative continuum. Simultaneously, a stronger cw laser field of frequency ω_2 couples the continuum to the initially empty state $|E_j\rangle$. The phases associated with these two fields are ϕ_1 and ϕ_2, respectively. The effect of the strong field is to cause Rabi cycling of population between $|E_j\rangle$ and the continuum. Thus, in this arrangement, population can be transferred from $|E_i\rangle$ to the continuum by a variety of routes, as shown in figure 27. The method is the multi-channel generalization of 'laser induced continuum structure' (LICS) [136–140].

From the qualitative perturbation theory viewpoint, this scenario contains an infinite number of contributions, some of which are shown in figure 27. The first panel of figure 27 shows the bichromatic control scenario. The second panel in figure 27 shows the simplest path to the continuum, consisting of one-photon absorption of ω_1. The subsequent panels show the

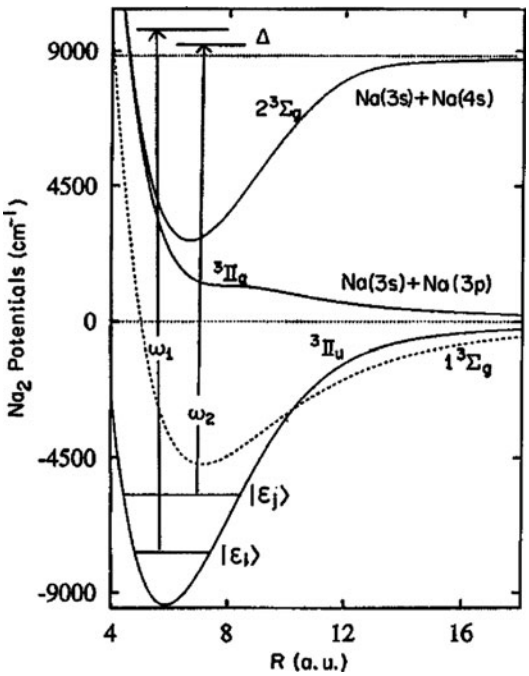

Figure 26. Sample scenario for the incoherent interference control of the photodissociation of Na_2. Taken from figure 1, [134].

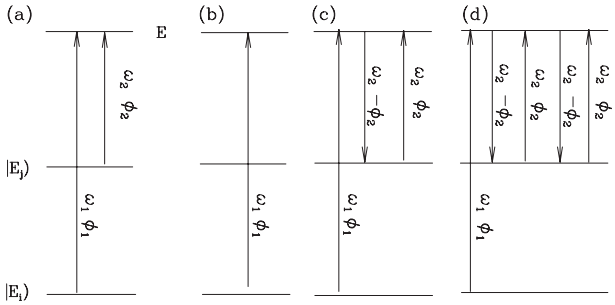

Figure 27. Interfering pathways from $|E_i\rangle$ to the continuum associated with the scenario in the previous figure. The frequency and phase of the lasers are ω_i and ϕ_i. (*a*) Bichromatic control. (*b*) One-photon absorption. (*c*) A three-photon process in which the initially unpopulated state $|E_j\rangle$ is coupled to the continuum at energy E and interferes with the one-photon absorption from state $|E_i\rangle$. (*d*) The same as in (*c*) for a five-photon process. Notice that in the processes depicted in (*c*) and (*d*) the phase ϕ_2 gets cancelled at the completion of each stimulated-emission-followed-by-absorption cycle.

three-photon process to the continuum (absorption of ω_1 followed by stimulated-emission and re-absorption of ω_2, etc), and a five-photon process (absorption of ω_1 followed by stimulated-emission and re-absorption of ω_2, twice). This series goes on ad-infinitum, resulting in an infinite number of interfering pathways.

In accord with standard perturbation theory, the phase imparted to the continuum state by the first route in figure 27 is ϕ_1, and by the second is $\phi_1 - \phi_2 + \phi_2$. The $-\phi_2$ contribution to the latter phase is due to the stimulated-emission-step, and the following $+\phi_2$ is due to the absorption. Hence, both routes impart the overall phase ϕ_1 to the continuum state. It is clear that this is also the case for all additional routes to the continuum, since they must contain an equal number of stimulated-emission and absorption steps.

Examination of all previous described scenarios makes clear, however, that it is the relative phase imparted to the routes which affects control. In the case described here, the relative phase of the routes is $\phi_1 - \phi_1 = 0$, so that control is independent of the laser phase. As a consequence, even lasers with extreme laser jitter and drift can be used in this scenario. Note, however, the additional consequence that in this scenario, control is achieved by varying the frequencies ω_1 and ω_2.

An experimental realization with the pulsed laser version of this approach has also been demonstrated [135].

10. CC of the synthesis and purification of chiral molecules

One challenging application of CC is to the issue of separating mixtures of chiral molecules. A molecule is said to be 'chiral' if it does not coincide, or cannot be made to coincide using a simple rotation, with its mirror image. In such cases, the molecule and its mirror image are called 'enantiomers', with one enantiomer being 'right-handed' and the other enantiomer being 'left-handed'. A sufficient (though not necessary) condition for chirality is for the molecule to have at least one 'asymmetric' carbon atom, i.e. a carbon atom bonded to four different groups of atoms. Two enantiomers can be distinguished experimentally, for example, by their ability to rotate linearly polarized light in opposite directions. A mixture of the two enantiomers is called a 'racemic' mixture or a 'racemate'.

The existence of enantiomers is one of the fundamental broken symmetries in nature [141–144]. In this section, we explain how to use CC techniques to perform asymmetric

synthesis ([145–149], [150], [155]) using the strong electric dipole–electric field interaction. This is in sharp contrast with previous techniques ([141] and see, e.g. [149]) where efforts were made to use the far weaker magnetic dipole interaction terms.

10.1. Principles of electric dipole-allowed enantiomeric control

We begin by establishing the general conditions under which the electric–dipole electromagnetic field interaction can be used to attain selective control over the population of a desired enantiomer. Consider a molecule, described by the total Hamiltonian (including electrons and nuclei) $H_{\rm MT}$. $H_{\rm MT}$ is assumed to have eigenstates describing the L and D enantiomers, denoted $|L_i\rangle$ and $|D_i\rangle$ ($i = 1, 2, 3, \ldots,$) that satisfy

$$\mathcal{I}|L_i\rangle = -|D_i\rangle, \qquad \mathcal{I}|D_i\rangle = -|L_i\rangle, \tag{143}$$

where $\mathcal{I}$ is the operator that inverts all space fixed coordinates through the origin. Note that the choice of phase (here minus one) in equation (143) is arbitrary, and that neither $|L_i\rangle$ nor $|D_i\rangle$ have well defined parity since they are not eigenstates of $\mathcal{I}$.

The dipole interaction of this molecule with an incident time dependent electric field $\boldsymbol{E}(t)$ is described by the Hamiltonian:

$$H(\boldsymbol{E}) = H_{\rm MT} - \boldsymbol{d}\cdot\boldsymbol{E}. \tag{144}$$

Here, $\boldsymbol{d}$ is the total dipole operator, including both electron and nuclear contributions, and we have explicitly indicated the dependence of the Hamiltonian on the electric field. Consider now the effect of inversion on H. Noting that $\mathcal{I}$ operates on the coordinates of the molecule, that $\mathcal{I}^\dagger = \mathcal{I}$ and that $[H_{\rm MT}, \mathcal{I}] = 0$, we have [152] that

$$\mathcal{I}H(\boldsymbol{E})\mathcal{I} = H(-\boldsymbol{E}), \tag{145}$$

where $H(-\boldsymbol{E}) = H_{\rm MT} + \boldsymbol{d}\cdot\boldsymbol{E}$. Further, if we define $U(\boldsymbol{E})$ and $U(-\boldsymbol{E})$ as the propagators corresponding to dynamics under $H(\boldsymbol{E})$ and $H(-\boldsymbol{E})$, respectively, then

$$U(\boldsymbol{E})\mathcal{I} = \mathcal{I}U(-\boldsymbol{E}). \tag{146}$$

Consider now irradiating a racemic mixture of D and L in its ground electronic state with an electric field $\boldsymbol{E}$ and examine the difference δ between the amount of D and L formed. We consider first the coherent process using transform limited light in the absence of collisions. Then, the difference δ is given by

$$\delta = \sum_i P_i \sum_j [|\langle D_j|U(\boldsymbol{E})|D_i\rangle|^2 + |\langle D_j|U(\boldsymbol{E})|L_i\rangle|^2] - [|\langle L_j|U(\boldsymbol{E})|D_i\rangle|^2 + |\langle L_j|U(\boldsymbol{E})|L_i\rangle|^2], \tag{147}$$

where P_i is the probability of state $|L_i\rangle$ and $|D_i\rangle$ in the initial mixed state. (If the initial-state is a racemic mixture, the states $|L_i\rangle$ and $|D_i\rangle$ appear with equal probability.)

To determine the conditions under which δ is non-zero, we rewrite equation (147) as

$$\delta = \sum_i P_i \sum_j [|\langle D_j|U(\boldsymbol{E})|D_i\rangle|^2 - |\langle L_j|U(\boldsymbol{E})|L_i\rangle|^2] + [|\langle D_j|U(\boldsymbol{E})|L_i\rangle|^2 - |\langle L_j U|(\boldsymbol{E})|D_i\rangle|^2] \tag{148}$$

and recast the second and third terms using:

$$\begin{aligned} |\langle L_j|U(\boldsymbol{E})|L_i\rangle|^2 &= |\langle D_j|\mathcal{I}^\dagger U(\boldsymbol{E})\mathcal{I}|D_i\rangle|^2 = |\langle D_j|U(-\boldsymbol{E})|D_i\rangle|^2 \\ |\langle D_j|U(\boldsymbol{E})|L_i\rangle|^2 &= |\langle D_j|U(\boldsymbol{E})\mathcal{I}|D_i\rangle|^2 = |\langle D_j|\mathcal{I}U(-\boldsymbol{E})|D_i\rangle|^2 = |\langle L_j|U(-\boldsymbol{E})|D_i\rangle|^2 \end{aligned} \tag{149}$$

giving

$$\delta = \sum_i P_i \sum_k [|\langle D_k|U(\boldsymbol{E})|D_i\rangle|^2 - |\langle D_k|U(-\boldsymbol{E})|D_i\rangle|^2] + [|\langle L_k|U(-\boldsymbol{E})|D_i\rangle|^2 - |\langle L_k|U(\boldsymbol{E})|D_i\rangle|^2]. \quad (150)$$

Equation (150) provides the general condition under which electric fields, assuming a dipole interaction, can break the right/left symmetry of the initial-state, and result in enhanced production of a desired enantiomer. Specifically, the difference between the amount of D and L formed is seen to depend entirely on the difference between the molecular dynamics when irradiated by $\boldsymbol{E}$ and by $-\boldsymbol{E}$. Hence, we can state that a necessary condition for non-zero enantiomeric excess, and the breaking of the left–right symmetry, is that the dynamics depend on the sign of the electric field. Note that the fact that molecular dynamics can, as discussed in previous sections, depend on the phase of the incident electric field is well substantiated [153, 154], but its utility for asymmetric synthesis is only evident from this result. Finally, note that the result is completely consistent with symmetry based arguments that can usefully provide conditions under which δ must equal zero. For example, a racemic mixture of thermally equilibrated molecules is rotationally invariant. Hence, any rotation that converts $\boldsymbol{E}$ to $-\boldsymbol{E}$ could not, in this case, result in enantiomeric control. In particular, in this case the sum over M_J (where M_J is the component of the reactant's total angular momentum along the direction of laser polarization) implicit in the sum over P_i in equation (150) would result in $\delta = 0$. By contrast, as discussed below, a racemic mixture of M_J polarized molecules irradiated with linearly polarized light [155] gives non-zero δ. New $\delta \neq 0$ examples emanating from equation (150) are also expected to display similar non-traditional characteristics.

Both qualitative and quantitative applications of equation (150) are possible. Qualitatively, for example, a traditional scheme where the ground electronic state of L and D are incoherently excited to bound levels of an excited state, gives $\delta = 0$. This is because all processes connecting the initial and final $|L_i\rangle$ and $|D_i\rangle$ states, i.e. contributions to the matrix elements in equation (150), are even in the power of the electric field. Hence, propagation under $\boldsymbol{E}$ and $-\boldsymbol{E}$ are identical. By contrast, consider the four level model scheme of figure 28 that is

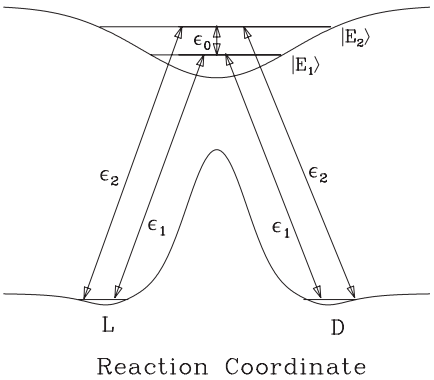

Figure 28. The 'laser distillation' control scenario discussed in detail in section 10.3. Two lasers, with pulse envelopes $\varepsilon_1(t)$ and $\varepsilon_2(t)$ couple, by virtue of the dipole operator, the states of the D and L enantiomers to two vib-rotational states $|1\rangle$ and $|2\rangle$ (denoted $|E_1\rangle$ and $|E_2\rangle$ in the text) in the excited electronic manifold. A third laser pulse with envelope $\varepsilon_0(t)$ couples the excited $|E_1\rangle$ and $|E_2\rangle$ states to one another. The system is allowed to absorb a photon and relax back to the ground state. After many such 'excitation–relaxation' cycles, a significant enantiomeric excess is obtained, as explained in section 10.3.

discussed in detail in section 10.3. When $\varepsilon_0(t) \neq 0$ there exist processes connecting the initial and final $|L\rangle$ and $|D\rangle$ states that are of the form $|L\rangle \rightarrow |1\rangle \rightarrow |2\rangle \rightarrow |D\rangle$ and hence there are terms in equation (150) that are odd in the power of the electric field. One therefore anticipates the possibility of altering the enantiomeric excess using this combination of pulses, providing the basis for the control results reported later. Further, if $\varepsilon_0 = 0$ then the situation reverts to the case discussed above, where only processes even in the electric field contribute to transitions between the initial $|D\rangle$, $|L\rangle$ and final $|D\rangle$, $|L\rangle$ transitions, and hence control over the enantiomeric excess is lost. For this reason, the $\varepsilon_0(t)$ coupling laser is crucial to enantiomeric control. This qualitative picture is substantiated quantitatively, later (section 10.3).

10.2. Symmetry breaking in the two-photon dissociation of pure states

Consider a molecule of the type BAB' where B and B' are enantiomers. This molecule possesses a hyper-plane of symmetry σ defined as the set of all configurations in which the $B - A$ distance is equal to the $A - B'$ distance. The operator corresponding to reflection across this hyper-plane is denoted σ_h. In order to coherently control the dissociation of this system, we take advantage of the existence of degenerate continuum states that do not possess this reflection symmetry. That is, the BAB' molecules possess degenerate continuum states $|E, \boldsymbol{n}, D^-\rangle$ and $|E, \boldsymbol{n}, L^-\rangle$ that correlate asymptotically with the dissociation of the right B' group and left B group, respectively. The collective quantum index $\boldsymbol{n}$ in the states $|E, \boldsymbol{n}, D^-\rangle$ and $|E, \boldsymbol{n}, L^-\rangle$ includes M_J, the magnetic quantum number of the B or B' fragment. These states are neither symmetric nor anti-symmetric with respect to the reflection operator σ_h, although linear combinations of these states might possess this symmetry.

We now consider using the pump-dump scenario described in section 6 above, for BAB' photodissociation. The application of this scenario to the chiral synthesis case is depicted schematically in figure 29. Our aim is to control the relative yield of two product arrangement channels. That is, we consider $P_{q,\boldsymbol{n}}(E)$, with q labelling either the right ($q = D$) or left ($q = L$) handed product. As in section 6, the product ratio $R_{DL;\boldsymbol{n}} = P_{D,\boldsymbol{n}}(E)/P_{L,\boldsymbol{n}}(E)$ is a

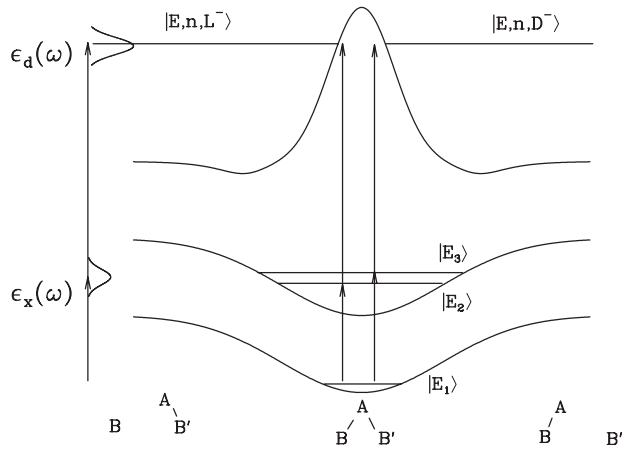

Figure 29. A schematic showing the controlled dissociation of the molecule $B - A - B'$ to yield the $B - A + B'$ or the $B + A - B'$ products, where B and B' are two enantiomers. The molecule is excited from an initial-state $|E_1\rangle$ to a superposition of antisymmetric ($|E_2\rangle$) and symmetric ($|E_3\rangle$) vibrational states belonging to an excited electronic state, by an excitation pulse $\varepsilon_x(t)$. After an appropriate delay time the molecule is dissociated by a second pulse $\varepsilon_d(t)$, to the $|E, \boldsymbol{n}, D^-\rangle$ or $|E, \boldsymbol{n}, L^-\rangle$ continuum state.

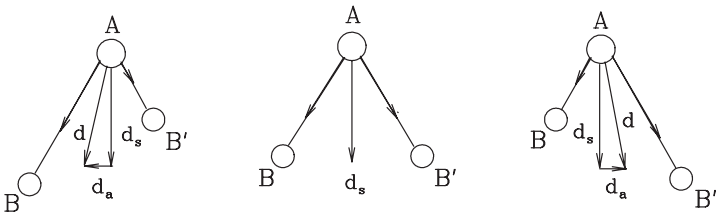

Figure 30. The emergence of an antisymmetric dipole component $\boldsymbol{d}_a$ in addition to the symmetric component $\boldsymbol{d}_s$ in a bent BAB' triatomic molecule as a result of an asymmetric stretching vibration, assuming that the dipole is a vectorial sum of bond dipoles that are proportional to the bond lengths.

function of the delay time $\Delta_d = (t_d - t_x)$ between pulses and the ratio $x = |c_2/c_3|$, the latter by varying the energy of the initial excitation pulse. Active control over the products $B + AB'$ vs $B' + AB$, i.e. a variation of $R_{DL;\boldsymbol{n}}$ with Δ_d and x, and hence control over left- vs right-handed products, will result only if $P_{D,\boldsymbol{n}}(E)$ and $P_{L,\boldsymbol{n}}(E)$ have different functional dependences on the control parameters x and Δ_d.

To show that $P_{D,\boldsymbol{n}}(E)$ may differ from $P_{L,\boldsymbol{n}}(E)$ for the $B'AB$ case, note first that this molecule belongs to the C_s point group. This group possesses only one symmetry element that is the σ_h reflection in the σ hyper-plane. Furthermore, we focus upon transitions between electronic states of the same representations, e.g. A' to A' or A'' to A'' (where A' denotes the symmetric representation and A'' the antisymmetric representation of the C_s group). We further assume that the ground vibronic state belongs to the A' representation.

To obtain control, we choose the intermediate state $|E_3\rangle$ to be symmetric, and the intermediate state $|E_2\rangle$ to be antisymmetric, with respect to σ_h. Hence, we must first demonstrate that it is possible to optically excite, simultaneously, both the symmetric $|E_3\rangle$ and antisymmetric $|E_2\rangle$ states from the ground state $|E_1\rangle$. Using equation (83) we see that this requires the existence of both a symmetric dipole component, denoted $\boldsymbol{d}_s$, and an antisymmetric component, denoted $\boldsymbol{d}_a$, with respect to σ_h, because, by the symmetry properties of $|E_3\rangle$ and $|E_2\rangle$,

$$\langle E_3|\boldsymbol{d}\cdot\hat{\varepsilon}|E_1\rangle = \langle E_3|\boldsymbol{d}_s\cdot\hat{\varepsilon}|E_1\rangle, \qquad \langle E_2|\boldsymbol{d}\cdot\hat{\varepsilon}|E_1\rangle = \langle E_2|\boldsymbol{d}_a\cdot\hat{\varepsilon}|E_1\rangle. \quad (151)$$

Since the σ plane rotates with the molecule, the σ_h operation is said to be 'body-fixed' (or 'molecule-fixed'). Both the body-fixed symmetric $\boldsymbol{d}_s$ and the body-fixed antisymmetric $\boldsymbol{d}_a$ dipole-moment components do occur in $A' \rightarrow A'$ electronic transitions whenever the bent $B' - A - B$ molecule deviates considerably from the σ hyper-plane where $\boldsymbol{d}_a = 0$ (see figure 30). The deviation of $\boldsymbol{d}_a$ from zero on the σ plane necessitates going beyond the Franck–Condon approximation, which assumes that the electronic dipole moment does not change as the molecule vibrates. (In the terminology of the theory of vibronic-transitions both symmetric and antisymmetric components can be non-zero due to a Herzberg–Teller intensity borrowing [156] mechanism.)

Note also that the dipole-moment operator, being a vector, must invert its sign under inversion $\mathcal{I}$. Hence, with respect to $\mathcal{I}$, the dipole-moment is always antisymmetric. Thus, for the integrals in equation (151) to be non-zero also requires that $|E_3\rangle$ and $|E_1\rangle$ be of opposite symmetry with respect to inversion. Given the extant conditions on the behaviour of $|E_3\rangle$ and $|E_1\rangle$ with respect to the reflection σ_h, the symmetry requirements with respect to $\mathcal{I}$ are most easily accommodated through the rotational components of the $|E_3\rangle$ and $|E_1\rangle$ states.

Thus, the excitation pulse can create a superposition of $|E_2\rangle$, $|E_3\rangle$ consisting of two-states of different reflection symmetry. The resultant superposition possesses no symmetry properties with respect to reflection (see also [157][8]).

[8] On the preparation and measurement of a superposition of chiral states see also [157].

We now show that the non-symmetry created by this excitation of non-degenerate bound states translates into a non-symmetry in the probability of populating the degenerate $|E, \boldsymbol{n}, D^-\rangle$, $|E, \boldsymbol{n}, L^-\rangle$ continuum states upon subsequent excitation. To do so, we examine the properties of the bound-free transition matrix elements $\langle E, \boldsymbol{n}, q^-|\mathrm{d}_{e,g}|E_k\rangle$ that enter into the probability of dissociation (equation (85)). Note first that although the continuum states $|E, \boldsymbol{n}, q^-\rangle$ are non-symmetric with respect to reflection, we can define symmetric and antisymmetric continuum eigenfunctions $|E, \boldsymbol{n}, s^-\rangle$ and $|E, \boldsymbol{n}, a^-\rangle$ via the relations

$$|E, \boldsymbol{n}, D^-\rangle \equiv \frac{[|E, \boldsymbol{n}, s^-\rangle + |E, \boldsymbol{n}, a^-\rangle]}{\sqrt{2}}, \tag{152}$$

$$|E, \boldsymbol{n}, L^-\rangle \equiv \frac{[|E, \boldsymbol{n}, s^-\rangle - |E, \boldsymbol{n}, a^-\rangle]}{\sqrt{2}}, \tag{153}$$

using the fact that $\sigma_h|E, \boldsymbol{n}, D^-\rangle = |E, \boldsymbol{n}, L^-\rangle$.

Consider first the nature of the $\mathrm{d}_q(ij)$ that enter equation (87), prior to averaging over product scattering angles, and denoted $\mathrm{d}_q(ij; \hat{\boldsymbol{k}})$, where $\hat{\boldsymbol{k}}$ is the scattering direction. Since $|E_3\rangle$ is symmetric and $|E_2\rangle$ is antisymmetric, and adopting the notation $A_{s2} \equiv \langle E, \boldsymbol{n}, s^-|\mathrm{d}_a|E_2\rangle$, $S_{a3} \equiv \langle E, \boldsymbol{n}, a^-|\mathrm{d}_s|E_3\rangle$, etc we have (see equation (87))

$$\begin{aligned}
\mathrm{d}_q(33; \hat{\boldsymbol{k}}) &= \sum{}'' [|S_{s3}|^2 + |A_{a3}|^2 \pm 2\mathrm{Re}(A_{a3}S^*_{s3})], \\
\mathrm{d}_q(22; \hat{\boldsymbol{k}}) &= \sum{}'' [|A_{s2}|^2 + |S_{a2}|^2 \pm 2\mathrm{Re}(A_{s2}S^*_{a2})], \\
\mathrm{d}_q(32; \hat{\boldsymbol{k}}) &= \sum{}'' [S_{s3}A^*_{s2} + A_{a3}S^*_{a2} \pm S_{s3}S^*_{a2} \pm A_{a3}A^*_{s2}],
\end{aligned} \tag{154}$$

where the plus sign applies for $q = D$, the minus sign applies for $q = L$, and $\mathrm{d}_q(23; \hat{\boldsymbol{k}}) = \mathrm{d}^*_q(32; \hat{\boldsymbol{k}})$. The double prime on the sum denotes a summation over all $q, \boldsymbol{n}$ other than the scattering angles and the product M_J, where M_J denotes the projection of the product angular momentum along the axis of laser polarization.

Equation (154) takes on a simpler form after angular averaging. The reason for this is that the overall parity of a state with respect to the inversion operation, $\mathcal{I}$, must change upon photon absorption since a photon has odd parity. As a result, if we have a single photon absorption process in which the parity of a vibrational state is unchanged, then the parity of the rotational states must change, and vice versa. Close examination of equation (154) reveals that the S^*_{s3} term does not involve a change in the parity of the vibrational state, whereas the A_{a3} term does. As a result, the rotational wavefunctions associated with each term must have opposing parities and the angular integral of the product must vanish. The same goes for the $A_{s2}S^*_{a2}$ term. In a similar manner the $S_{s3}A^*_{s2} + A_{a3}S^*_{a2}$ term vanishes in the $\mathrm{d}_q(32)$ interference term. By contrast, the $\pm S_{s3}S^*_{a2} \pm A_{a3}A^*_{s2}$ terms do not vanish upon angular integration since they correspond to final rotational states that have the same parity.

As a consequence, the net result is that, after angular averaging, equation (154) becomes

$$\begin{aligned}
\mathrm{d}_q(33) &= \sum{}' [|S_{s3}|^2 + |A_{a3}|^2], \\
\mathrm{d}_q(22) &= \sum{}' [|A_{s2}|^2 + |S_{a2}|^2], \\
\mathrm{d}_q(32) &= \sum{}' \pm [S_{s3}S^*_{a2} + A_{a3}A^*_{s2}],
\end{aligned} \tag{155}$$

where single prime on the sum indicates that the sum over product M_J is not carried out.

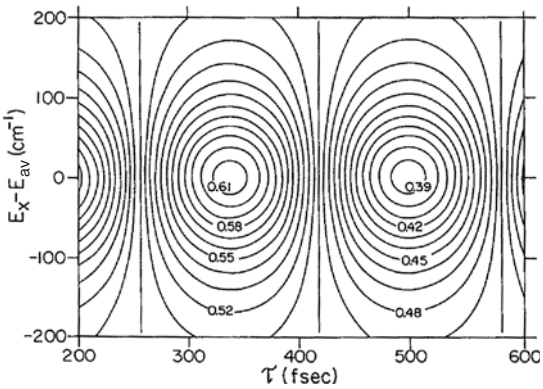

Figure 31. Contour plot of percent HO + H (as distinct from HO + H) in HOH photodissociation. Ordinate is the detuning from $E_{\rm av} = (E_3 - E_2)/2$ and the abscissa is the time delay between pulses. Taken from figure 9, [14].

These equations display two noteworthy features:

(1) $\mathrm{d}_L(jj) = \mathrm{d}_D(jj)$, $j = 2, 3$, i.e. lacking interference, no discrimination between the left- and right-handed products is possible.
(2) $\mathrm{d}_L(23) \neq \mathrm{d}_D(23)$, i.e. laser controlled symmetry breaking, which depends upon $\mathrm{d}_q(23)$ in accordance with equation (86), is possible. As noted below, this type of discrimination is possible only if we select of the direction of the angular momentum of the products (M_J-polarization).

To demonstrate the extent of expected control, as well as the effect of M_J summation, we considered a model of enantiomer selectivity, i.e. HOH photodissociation in three dimensions, where the two hydrogens are assumed distinguishable,

$$\mathrm{H}_a\mathrm{O} + \mathrm{H}_b \leftarrow \mathrm{H}_a\mathrm{OH}_b \rightarrow \mathrm{H}_a + \mathrm{OH}_b.$$

A computation of the R_{DL} ratio of the HO + H (as distinct from the HO + H) product in a fixed M_J state, was performed using the formulation and methodology of [158, 159]. Specifically, figure 31 shows the result of first exciting the superposition of symmetric plus asymmetric vibrational modes [(1, 0, 0) + (0, 0, 1)] with $J_i = J_k = 0$ in the ground electronic state, followed by dissociation at 70 700 cm^{-1} to the B state using a pulse width of 200 cm^{-1}. The results show that varying the time delay between pulses allows for controlled variation of P_D from 61% to 39%. This variation is significant since it reveals the symmetry breaking arising within this scenario.

10.3. Purification of racemic mixtures by 'laser distillation'

In section 10.2, we dealt with chiral discrimination given an initial pure achiral state. However, in practice, the initial-state is in general a (racemic) mixture of the two enantiomers. If we were to use the scenario of section 10.2 to attempt chiral discrimination of a racemic mixture one would have to first prepare the BAB' adduct in a pure state. Since the preparation of BAB', and especially its separation from the BAB and $B'AB'$ adducts that would inevitably accompany it, is not a trivial task, it is preferable to find control methods that can separate the B and B' racemic mixture directly. In this section, we outline a method that can achieve this much more ambitious task. The essential principles of this method remain the same as

in section 10.2, i.e. excitation of a superposition of symmetric and antisymmetric states with respect to σ_h, the reflection operation.

Consider then a molecular system composed of a pair of stable nuclear configurations, denoted L and D, with L being the (distinguishable) mirror image of D. Note that the electronic Hamiltonian H_e commutes with σ_h, hence, the potential energy surfaces, which are the eigenvalues of the electronic Schrödinger equation at all nuclear configurations, must be symmetric with respect to σ_h. Since L and D are assumed stable, it follows that the ground potential energy surface must possess a sufficiently high barrier at nuclear coordinates separating L and D such that the rate of interconversion between them by tunnelling is negligible. By contrast, L and D need not be stable on an excited potential energy surface. To this end, we assume that there is at least one excited potential surface, denoted G, which possesses a potential well midway between the L and the D geometries (see figure 28). (A number of molecules expected to be of this type are tabulated in [144] and a number of examples are discussed below). Hence, the interconversion between L and D on the excited surface G is expected to be very facile.

A direct consequence of the potential well midway between the L and the D geometries is the existence of stable vibrational eigenstates on the excited surface. Because of the symmetry of G, the vibrational eigenstates must be either symmetric or antisymmetric with respect to σ_h.

The procedure that we propose in order to enhance the concentration of a particular enantiomer when starting with a racemic mixture, i.e. to 'purify' the mixture, is as follows. The racemic mixture of L and D is irradiated with a specific sequence of three coherent laser pulses, as described below. These pulses excite a coherent superposition of symmetric and antisymmetric vibrational states of G. After each pulse the excited system is allowed to relax back to the ground electronic state by spontaneous emission or by a non-radiative process. By allowing the system to go through many irradiation and relaxation cycles, we show below that the concentration of the selected enantiomer L or D can be enhanced, depending on the laser characteristics. We call this scenario 'laser distillation' of chiral enantiomers.

We note at the outset that detailed angular momentum considerations show that if the three incident lasers are of the same polarization then control results only if we do not average over M_J, the projection of the total angular momentum of the reactant along the z-axis (chosen as the direction of laser polarization). In particular, enantiomeric enhancement of one enantiomer from molecules in state M_J is exactly counterbalanced by enantiomeric enhancement of the other enantiomer by molecules in state $-|M_J|$. Hence, enantiomeric control in this scenario requires prior M_J selection of the molecules. This scenario is discussed below, but results are also provided for the case of three lasers of perpendicular polarization, where M_J averaging is non-destructive.

Consider then a molecule with Hamiltonian H_M, in the presence of a series of laser pulses. (In general, we may deal with lasers that are not fully coherent, but for simplicity we focus here on transform limited pulses of linearly polarized light.) The treatment is in accord with section 2, equation (3), where the interaction between the molecule and radiation is given by

$$H_{\mathrm{MR}}(t) = -\boldsymbol{d}\cdot\boldsymbol{E}(t) = -2\boldsymbol{d}\cdot\sum_k \mathrm{Re}[\hat{\varepsilon}_k\varepsilon_k(t)\exp(-\mathrm{i}\omega_k t)]. \tag{156}$$

Here, $\varepsilon_k(t)$ is the pulse envelope, ω_k is the central laser frequency and $\hat{\epsilon}_k$ is the polarization direction. Expanding $|\Psi(t)\rangle$ in eigenstates $|E_j\rangle$ of the molecular Hamiltonian we obtain the coupled first order differential equations of equation (7).

We now specialize the treatment to a four state model, composed of the D and L molecules in their ground electronic states and in vib-rotational states $|E_D\rangle$ and $|E_L\rangle$, of energy $E_D = E_L$, being excited by two light fields to two eigenstates $|E_1\rangle$ and $|E_2\rangle$ of the electronically excited

potential surface G. The states $|E_1\rangle$ and $|E_2\rangle$ are also coupled by an additional laser field (see figure 28). Specifically, we choose $\boldsymbol{E}(t)$ to be composed of three linearly polarized light pulses (all of the same polarization),

$$\boldsymbol{E}(t) = \sum_{k=0,1,2} 2\mathrm{Re}[\varepsilon_k(t)\exp(-\mathrm{i}\omega_k t)]\hat{\varepsilon}_k \tag{157}$$

with ω_0 in near-resonance with $\omega_{2,1} \equiv (E_2 - E_1)/\hbar$, ω_1 is chosen to be near resonant with $\omega_{1,D} \equiv (E_1 - E_D)/\hbar$, and ω_2 near resonant with $\omega_{2,D} \equiv (E_2 - E_D)/\hbar$ (see figure 28). In this case, only four molecular states are relevant and the wavefunction can be expanded as:

$$\begin{aligned}|\Psi\rangle = {} & b_D(t)\exp\left(-\frac{\mathrm{i}E_D t}{\hbar}\right)|E_D\rangle + b_L(t)\exp\left(-\frac{\mathrm{i}E_L t}{\hbar}\right)|E_L\rangle + b_1(t)\exp\left(-\frac{\mathrm{i}E_1 t}{\hbar}\right)|E_1\rangle \\ & + b_2(t)\exp\left(-\frac{\mathrm{i}E_2 t}{\hbar}\right)|E_2\rangle.\end{aligned} \tag{158}$$

Inserting this expansion into the time dependent Schrödinger equation, and invoking the rotating-wave approximation, gives us the following set of equation for the coefficients:

$$\begin{aligned}\dot{b}_1 &= \mathrm{i}\exp(\mathrm{i}\Delta_1 t)[\Omega^*_{D,1}b_D + \Omega^*_{L,1}b_L] + \mathrm{i}\exp(-\mathrm{i}\Delta_0 t)\Omega^*_0 b_2, \\ \dot{b}_2 &= \mathrm{i}\exp(\mathrm{i}\Delta_2 t)[\Omega^*_{D,2}b_D + \Omega^*_{L,2}b_L] + \mathrm{i}\exp(\mathrm{i}\Delta_0 t)\Omega_0 b_1, \\ \dot{b}_D &= \mathrm{i}\exp(-\mathrm{i}\Delta_1 t)\Omega_{D,1}b_1 + \mathrm{i}\exp(-\mathrm{i}\Delta_2 t)\Omega_{D,2}b_2, \\ \dot{b}_L &= \mathrm{i}\exp(-\mathrm{i}\Delta_1 t)\Omega_{L,1}b_1 + \mathrm{i}\exp(-\mathrm{i}\Delta_2 t)\Omega_{L,2}b_2,\end{aligned} \tag{159}$$

where $\Omega_{i,j}(t) \equiv d^{(j)}_{i,j}\varepsilon_1(t)/\hbar$, $\Omega_0 \equiv d^{(0)}_{2,1}\varepsilon_0(t)/\hbar$, $\Delta_j \equiv \omega_{j,D} - \omega_1$, $\Delta_0 \equiv \omega_{2,1} - \omega_0$, where $d^{(k)}_{i,j} \equiv \langle E_i|\boldsymbol{d}\cdot\hat{\varepsilon}_k|E_j\rangle$, with $i = D, L$; $k = 0, 1, 2$ and $j = 1, 2$.

The essence of the laser distillation process lies in choosing the laser of central frequency ω_1 so that it excites the system to a state $|E_1\rangle$ that is symmetric with respect to the reflection operation σ_h, and to a state $|E_2\rangle$ that is antisymmetric with respect to σ_h. By contrast, $|E_D\rangle$ and $|E_L\rangle$ do not share these symmetries but are related to one another through reflection (i.e. $\sigma_h|E_D\rangle = |E_L\rangle$, $\sigma_h|E_L\rangle = |E_D\rangle$ whereas $\sigma_h|E_1\rangle = |E_1\rangle$, $\sigma_h|E_2\rangle = -|E_2\rangle$).

To consider the nature of the 'Rabi frequencies' Ω in equation (159) we rewrite $|E_D\rangle$ and $|E_L\rangle$ in terms of a symmetric state $|S\rangle$ and an antisymmetric state $|A\rangle$:

$$\begin{aligned}|E_D\rangle &= |A\rangle + |S\rangle, \\ |E_L\rangle &= |A\rangle - |S\rangle.\end{aligned} \tag{160}$$

In addition to their symmetry properties with respect to σ_h, we choose the $|S\rangle$ and $|A\rangle$ states to be, respectively, symmetric and antisymmetric under the inversion operation $\mathcal{I}$. Coupled with the fact that the dipole operator must be antisymmetric with respect to $\mathcal{I}$, the relevant matrix elements satisfy the following relations:

$$\begin{aligned}\langle 1|d^{(1)}|D\rangle &= \langle 1|d^{(1)}|A+S\rangle = \langle 1|d^{(1)}|A\rangle, \\ \langle 1|d^{(1)}|L\rangle &= \langle 1|d^{(1)}|A-S\rangle = \langle 1|d^{(1)}|A\rangle, \\ \langle 2|d^{(2)}|D\rangle &= \langle 2|d^{(2)}|A+S\rangle = \langle 2|d^{(2)}|S\rangle, \\ \langle 2|d^{(2)}|L\rangle &= \langle 2|d^{(2)}|A-S\rangle = -\langle 2|d^{(2)}|S\rangle.\end{aligned} \tag{161}$$

That is,

$$\Omega_{D,1} = \Omega_{L,1}, \qquad \Omega_{D,2} = -\Omega_{L,2}. \tag{162}$$

Given equations (162) and (159) becomes

$$\begin{aligned}
\dot{b}_1 &= \mathrm{i}\exp(\mathrm{i}\Delta_1 t)\Omega^*_{D,1}[b_D + b_L] + \mathrm{i}\exp(-\mathrm{i}\Delta_0 t)\Omega^*_0 b_2,\\
\dot{b}_2 &= \mathrm{i}\exp(\mathrm{i}\Delta_2 t)\Omega^*_{D,2}[b_D - b_L] + \mathrm{i}\exp(\mathrm{i}\Delta_0 t)\Omega_0 b_1,\\
\dot{b}_D &= \mathrm{i}\exp(-\mathrm{i}\Delta_1 t)\Omega_{D,1} b_1 + \mathrm{i}\exp(-\mathrm{i}\Delta_2 t)\Omega_{D,2} b_2,\\
\dot{b}_L &= \mathrm{i}\exp(-\mathrm{i}\Delta_1 t)\Omega_{D,1} b_1 - \mathrm{i}\exp(-\mathrm{i}\Delta_2 t)\Omega_{D,2} b_2.
\end{aligned} \tag{163}$$

The essence of optically controlled enantioselectivity in this scenario lies in equation (162) and the effect of these relationships on the dynamical equations for the level populations (equation (163)). Note specifically that the equation for $\dot{b}_D(t)$ is different than the equation for $\dot{b}_L(t)$, due to the sign difference in the last term in equation (163). Although not sufficient to ensure enantiomeric selectivity, the ultimate consequence of this difference is that populations of $|E_D\rangle$ and $|E_L\rangle$ after laser excitation are different when there is radiative coupling between levels $|E_1\rangle$ and $|E_2\rangle$.

Note, in accord with section 10.1, the behaviour of equation (163) under the transformation $\boldsymbol{E} \to -\boldsymbol{E}$. Specifically, changing $\boldsymbol{E}$ to $-\boldsymbol{E}$ means changing all $\varepsilon_j(t)$ to $-\varepsilon_j(t)$. Doing so, and defining $b'_1 = -b_1$ and $b'_2 = -b_2$ converts equation (163) into

$$\begin{aligned}
\dot{b}'_1 &= \mathrm{i}\exp(\mathrm{i}\Delta_1 t)\Omega^*_{D,1}[b_D + b_L] - \mathrm{i}\exp(\mathrm{i}\Delta_0 t)\Omega^*_0 b'_2,\\
\dot{b}'_2 &= \mathrm{i}\exp(\mathrm{i}\Delta_2 t)\Omega^*_{D,2}[b_D - b_L] - \mathrm{i}\exp(-\mathrm{i}\Delta_0 t)\Omega_0 b'_1,\\
\dot{b}_D &= \mathrm{i}\exp(-\mathrm{i}\Delta_1 t)\Omega_{D,1} b'_1 + \mathrm{i}\exp(-\mathrm{i}\Delta_2 t)\Omega_{D,2} b'_2,\\
\dot{b}_L &= \mathrm{i}\exp(-\mathrm{i}\Delta_1 t)\Omega_{D,1} b'_1 - \mathrm{i}\exp(-\mathrm{i}\Delta_2 t)\Omega_{D,2} b'_2.
\end{aligned} \tag{164}$$

Clearly, equation (164) is the same as equation (163) barring the change of sign in the Ω_0 terms. Thus, the solution to equation (163) depends on the sign of $\boldsymbol{E}$ when $\varepsilon_0 \neq 0$. Hence, by the argument in section 10.1, this scenario allows for chirality control when $\varepsilon_0(t) \neq 0$. For $\varepsilon_0(t) = 0$ the equation (164) is the same as equation (163) so that enantiomer control is not possible.

To obtain quantitative estimates for the extent of obtainable control we consider results for model cases assuming Gaussian pulses

$$\varepsilon_k(t) = \mathcal{E}_k \exp\left[-\left(\frac{(t - t_k)}{\alpha_k}\right)^2\right] \qquad k = 0, 1, 2 \tag{165}$$

and system parameters $\langle 1|d^{(1)}|D\rangle = \langle 1|d^{(1)}|L\rangle = \langle 2|d^{(2)}|L\rangle = -\langle 2|d^{(2)}|D\rangle = 1$ a.u., $\langle 1|d^{(0)}|2\rangle = 1$ a.u., $\omega_{2,1} = 100\,\mathrm{cm}^{-1}$ and $\Delta_0 = 0$. Figure 32 displays the final probabilities $P_D = |b_D(\infty)|^2$, $P_L = |b_L(\infty)|^2$ of population in $|E_D\rangle$ and $|E_L\rangle$, after a single pulse, for a variety of pulse parameters. Results are shown for various values of Δ_1 at various different pulse powers assuming that one starts solely with D, solely with L, or with a racemic mixture of both enantiomers. Clearly, for particular parameters, one can significantly enhance the population of one chiral enantiomer over the other. For example, for $\Delta_1 = -115\,\mathrm{cm}^{-1}$, $\mathcal{E}_0 = \mathcal{E}_1 = 4.5 \times 10^{-4}$, a racemic mixture of D and L can be converted, after a single pulse, to a enantiomerically enriched mixture with predominantly D.

Control is strongly affected by the relative phase θ of the ε_1 and ε_0 fields, as shown in figure 33. Here, it is clear that changing θ by π interchanges the dynamical evolution of the L and D enantiomers.

Although not immediately obvious, this control scenario relies entirely upon quantum interference effects. To see this note that in the absence of an $\varepsilon_0(t)$ pulse, excitation from $|D\rangle$ or $|L\rangle$ to level $|E_i\rangle$, for example, occurs via one-photon excitation with $\varepsilon_i(t)$, $i = 1, 2$. In this case, as noted above, there is no chiral control. By contrast, with non-zero $\varepsilon_0(t)$, there is

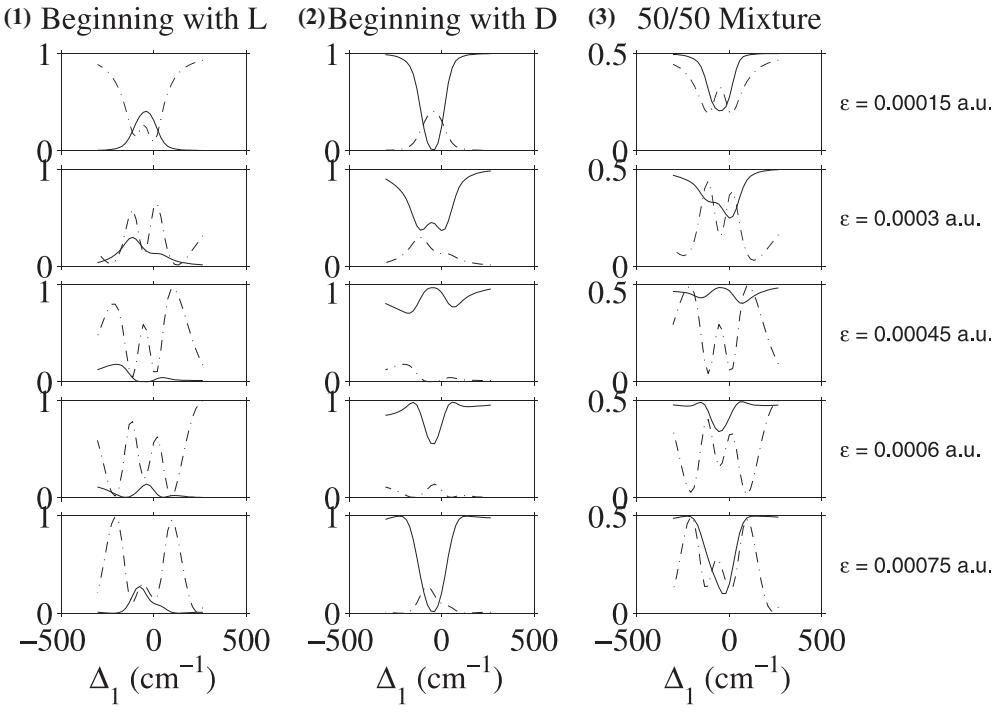

Figure 32. Probabilities of populating the $|E_D\rangle$ (——) and $|E_L\rangle$ (— · —) after laser excitation, but prior to relaxation, as a function of the detuning Δ_1. Three different cases are shown, corresponding to three different initial conditions: (1) only state $|E_L\rangle$ is initially populated; (2) only state $|E_D\rangle$ is initially populated; (3) a statistical mixture made up of equal shares of the $|E_D\rangle$ and $|E_L\rangle$ states is initially populated. Results are shown for five different $\mathcal{E}_1 = \mathcal{E}_0 \equiv \mathcal{E}$ laser peak electric fields, where Gaussian pulses are assumed with $\alpha_0 = \alpha_1 = 0.15$ ps, and $t_0 = t_1$.

an additional (interfering) route to $|E_i\rangle$, i.e. a two-photon route using $\varepsilon_j(t)$ excitation to level $|E_j\rangle$, $j \neq i$, followed by an $\varepsilon_0(t)$ induced transition from $|E_j\rangle$ to $|E_i\rangle$. The one and two-photon routes interfere and, as implied in section 5.2, allow for symmetry breaking transitions.

The computation, that results in figure 32, which gives the result of a single pulse, provides input into a calculation of the overall result. In the overall process, we begin with an incoherent mixture of N_D molecules of type D and N_L molecules of type L. In the first step the system is excited, as above, with a laser pulse sequence. In the second step, the system collisionally and radiatively relaxes so that all the population returns to the ground state to produce an incoherent mixture of $|E_L\rangle$ and $|E_D\rangle$. This pair of steps is then repeated until the populations of $|E_L\rangle$ and $|E_D\rangle$ reach convergence.

To obtain the result computationally note that the population after laser excitation, but before relaxation, consists of the weighted sum of the results of two computations: N_D times the results of laser excitation starting solely with molecules in $|E_D\rangle$, plus N_L times the results of laser excitation starting solely with molecules in $|E_L\rangle$. If $P_{D\leftarrow D}$ and $P_{L\leftarrow D}$ denote the probabilities of $|E_D\rangle$ and $|E_L\rangle$ resulting from laser excitation assuming the first of these initial conditions, and $P_{D\leftarrow L}$ and $P_{L\leftarrow L}$ for the results of excitation following from the second of these initial conditions, then the populations of $|E_D\rangle$ and $|E_L\rangle$ after laser excitation of the mixture are $N_D P_{D\leftarrow D} + N_L P_{D\leftarrow L}$ and $N_D P_{L\leftarrow D} + N_L P_{L\leftarrow L}$, respectively. The remainder of the population, $N_D\,[1 - P_{D\leftarrow D} - P_{L\leftarrow D}] + N_L\,[1 - P_{D\leftarrow L} - P_{L\leftarrow L}]$, is in the upper two

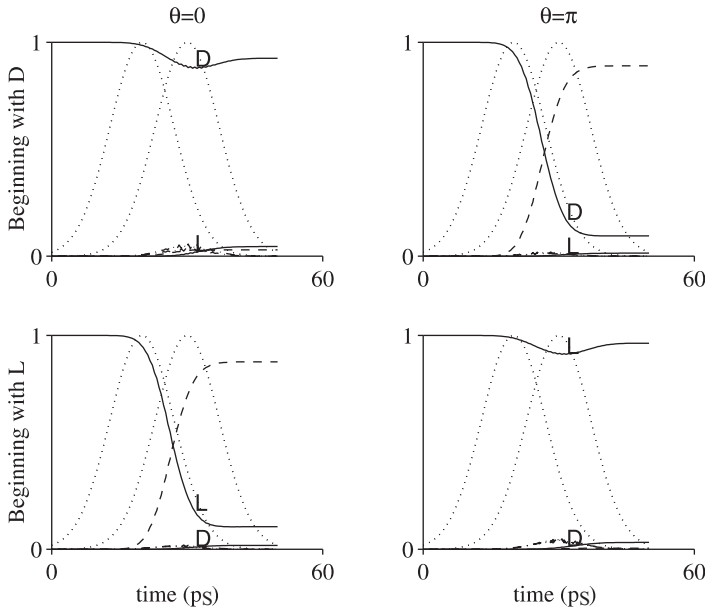

Figure 33. The time evolution of the enantiomeric populations for two different relative phases θ between the ε_1 and ε_0 beams. (——) population in the D or L enantiomer; (· · · · · ·) the $\varepsilon_1(t)$ and $\varepsilon_0(t)$ laser pulses; (- - - -) excited state population in levels $|E_1\rangle + |E_2\rangle$.

levels $|E_1\rangle$ and $|E_2\rangle$. Relaxation from levels $|E_1\rangle$ and $|E_2\rangle$ then follows, with the excited population dividing itself equally between $|E_D\rangle$ and $|E_L\rangle$. The resultant populations $\mathcal{N}_D$ and $\mathcal{N}_L$ in ground state $|E_D\rangle$ and $|E_L\rangle$ is then:

$$\begin{aligned}\mathcal{N}_D &= 0.5N_D[1 + P_{D\leftarrow D} - P_{L\leftarrow D}] + 0.5N_L[1 + P_{D\leftarrow L} - P_{L\leftarrow L}],\\ \mathcal{N}_L &= 0.5N_D[1 + P_{L\leftarrow D} - P_{D\leftarrow D}] + 0.5N_L[1 + P_{L\leftarrow L} - P_{D\leftarrow L}].\end{aligned} \tag{166}$$

The sequence of laser excitation followed by collisional relaxation and radiative emission is then iterated to convergence. In the second step, for example, the populations in equation (166) are taken as the initial populations for two independent computations, one assuming a population of $\mathcal{N}_D$ in $|E_D\rangle$, with $|E_L\rangle$ unpopulated, and the second assuming a population of $\mathcal{N}_L$ in $|E_L\rangle$, with $|E_D\rangle$ unpopulated.

Clearly, convergence is obtained when the populations, post-relaxation, are the same as those prior to laser excitation, i.e. when $\mathcal{N}_D = N_D$, and $\mathcal{N}_L = N_L$. These conditions reduce to

$$N_D(1 - P_{D\leftarrow D} + P_{L\leftarrow D}) = N_L(1 + P_{D\leftarrow L} - P_{L\leftarrow L}). \tag{167}$$

If the total population is chosen to be normalized ($N_D + N_L = 1$), then the final probabilities $\mathcal{P}_D, \mathcal{P}_L$ of populating states $|E_D\rangle$ and $|E_L\rangle$ are

$$\begin{aligned}\mathcal{P}_D &= \frac{1 + P_{D\leftarrow L} - P_{L\leftarrow L}}{2 - P_{D\leftarrow D} + P_{L\leftarrow D} + P_{D\leftarrow L} - P_{L\leftarrow L}},\\ \mathcal{P}_L &= \frac{1 - P_{D\leftarrow D} + P_{L\leftarrow D}}{2 - P_{D\leftarrow D} + P_{L\leftarrow D} + P_{D\leftarrow D} - P_{L\leftarrow L}}\end{aligned} \tag{168}$$

and the equilibrium enantiomeric branching ratio is simply,

$$R_{D,L} \equiv \frac{\mathcal{P}_D}{\mathcal{P}_L} = \frac{1 + P_{D\leftarrow L} - P_{L\leftarrow L}}{1 - P_{D\leftarrow D} + P_{L\leftarrow D}}. \tag{169}$$

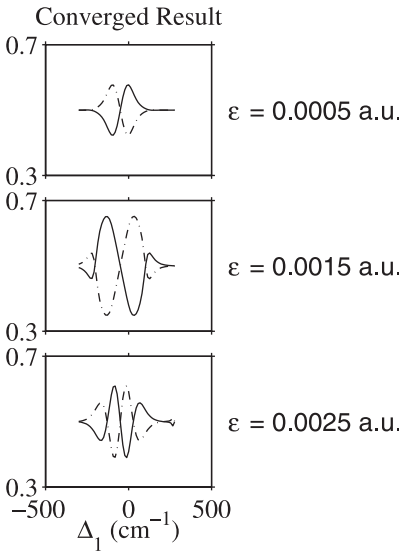

Figure 34. Results for laser distillation after a convergent series of steps comprised of radiative excitation, followed by collisional and radiative relaxation. Shown are the results at three different field strengths.

Results for the converged probabilities for the cases depicted in figure 32, are shown in figure 34. The results clearly show substantially enhanced enantiomeric ratios at various choices of control parameters. For example, at $\mathcal{E}_0 = \mathcal{E}_1 = 1.5 \times 10^{-3}$, tuning Δ_1 to $50\,\mathrm{cm}^{-1}$ gives a preponderance of L whereas tuning to the $\Delta_1 = -125\,\mathrm{cm}^{-1}$ gives more D.

Numerous other parameters in this system, such as the pulse shape, time delay between pulses, pulse frequencies and pulse powers, etc. can be varied to affect the final L to D ratio [146] resulting in a very versatile approach to asymmetric synthesis.

Finally, note that although we have only included two ground state levels, the method applies equally well when a large number of ground state levels are included. In this case, relaxation will be amongst all of these ground state levels, but the proposed scenario, tuned to the above set of transitions, will 'bleed' population from one M_J level of the desired enantiomer. As relaxation refills this level it will continue to be pumped over to the other enantiomer, with the overall effect that the major amount of the population will be transferred from one enantiomer to the other.

As a realization of the above scheme we now examine [160] the case of enantiomer control in dimethylallene, a molecule shown in figure 35. Note that, at equilibrium in the ground state, the H–C–CH_3 groups at both ends of the molecule lie on planes that are perpendicular to one another, resulting a molecule that is chiral. By contrast, in the excited state, the C=C double bond breaks, allowing for rotation of one plane relative to the other. Cuts through the ground and first two excited state potential energy surfaces for this molecule along the α and θ coordinates (see figure 35) are shown in figure 36. The potentials show the features required for control in this scenario, i.e. a minimum in the excited state potential surface at the geometry corresponding to the potential energy maximum on the ground state potential.

The results of a computation [147] on the control of L vs D 1,3-dimethylallene are shown in figure 37. Outstanding enantiomeric control over the dimethylallene enantiomers is evident for a wide variety of powers. For example, a most impressive result is achieved for $\Delta_1 = 0.0986\,\mathrm{cm}^{-1}$ and $\mathcal{E}_0 = 1.5 \times 10^{-4}$ a.u., $\mathcal{E}_1 = \mathcal{E}_2 = 4.31 \times 10^{-5}$ a.u., corresponding

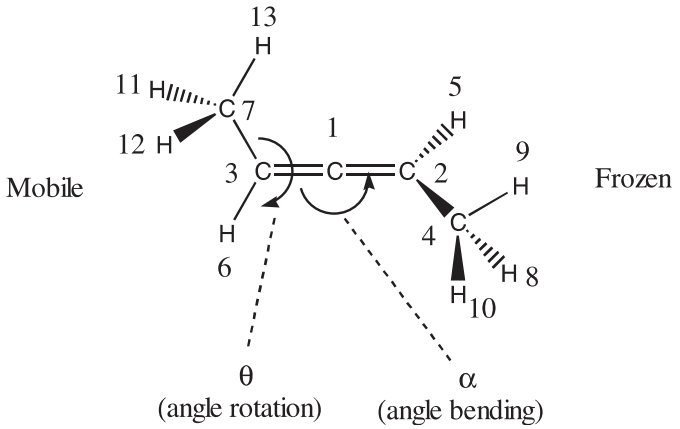

Figure 35. The geometry of the 1,3-dimethylallene and the two angles θ and α that were varied to scan the potential energy surface. Here θ is the dihedral angle between the H_3C–C=C and the C=C–CH_3 planes and α is the C–C–C bending angle, here shown by an arrow that brings the H_3C–C–H out of the plane of paper. From figure 2, [160].

to laser powers of $7.90 \times 10^8\,\mathrm{W\,cm^{-2}}$ and $6.52 \times 10^7\,\mathrm{W\,cm^{-2}}$, respectively. Here, a racemic mixture of dimethylallene in a specific J, M_J, λ state can be converted, after a series of pulses, to a mixture of dimethylallene, containing 92.7% of the D-dimethylallene in this state. (Here λ is the projection of the total angular momentum J along an axis fixed in the molecule.) Similarly, detuning to $\Delta_1 = -0.0986\,\mathrm{cm^{-1}}$ results in a similar enhancement of L-dimethylallene. Slightly lower extremes of control are seen to be achievable for the two other laser powers shown. Further, control was achievable to field strengths down to $10^4\,\mathrm{W\,cm^{-2}}$. Note, however, that this computation neglects the competitive process of internal conversion, discussed later.

It is of some interest to note the character of the eigenstates $|E_1\rangle$ and $|E_2\rangle$ that contribute to these results; they are shown in figure 38. Clearly, they are states with considerable vibrational energy, so that they are broad enough in configuration space to overlap the ground electronic state, ground vibrational state wavefunctions. If this is not the case then the dipole matrix elements are too small to allow control at reasonable laser intensities.

The primary experimental difficulty associated with this scenario is the requirement to isolate a particular subset of M_J levels, in order to avoid cancellation of M_J and $-|M_J|$ control. That is, from the viewpoint of the M_J structure, this scenario is associated with the level structure shown in figure 39.

To remove this restriction, we introduced another scenario [155] where all of the three laser polarizations, $\hat{\varepsilon}_0$, $\hat{\varepsilon}_1$ and $\hat{\varepsilon}_2$, are perpendicular to one another. This laser arrangement now allows for transitions between different M_J levels. The first few of these levels is shown in figure 40. Under these circumstances, control survives averaging over M_J levels [155].

Sample results for the three laser case with perpendicular polarizations are shown in figure 41, first row, where extensive control is evident. Here, even with M_J averaging, one can choose to convert the racemic mixture to over 90% of the L enantiomer, or of the D enantiomer, depending on the detuning. In this case, the 1,3-dimethylallene was treated as an asymmetric top and averaging was carried out over all M_J levels.

A realistic model of dimethylallene control must also recognize the possibility of internal conversion to the ground state. In this process, the electronically excited molecule undergoes a radiationless transition to the ground electronic state, leaving a highly vibrationally excited

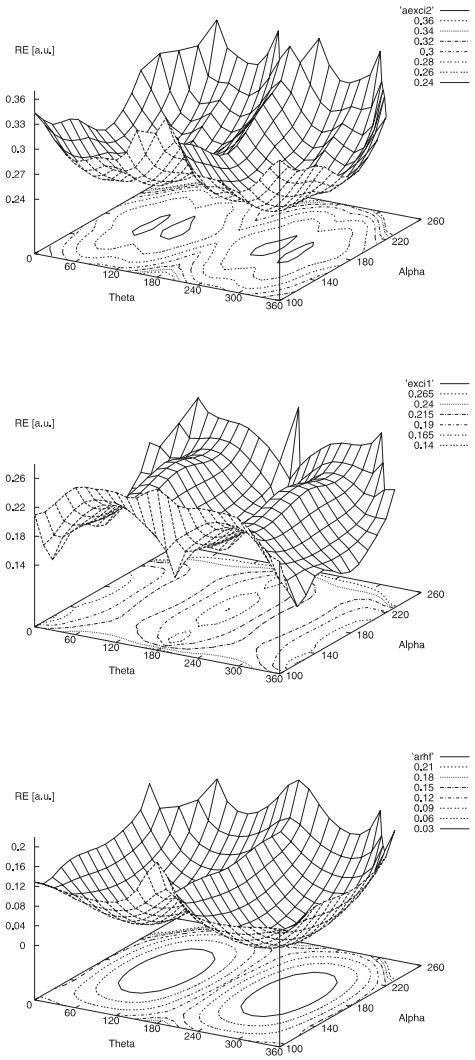

Second excited state surface.

First excited state surface.

Ground state surface.

Figure 36. Potential energy surfaces for 1,3-dimethylallene. Here, we show in-plane surfaces for the ground and first two excited electronic states. From figure 4, [160].

species. Only a few estimates or measurements of the internal conversion timescales for molecules are available [161, 162] and dimethylallene has not been explored. Further, after internal conversion one expects, in the dimethylallene case, that the excited molecule subsequently dissociates, leaving molecular fragments that no longer participate in the control scenario. Hence, the process of internal conversion serves as a decoherence mechanism that can reduce control. Further decoherence effects, but on a slower timescale, would arise, for example, if the control was carried out in solution.

The second row in figure 41 shows control with similar parameters as in the first row, but in the presence of a T_2 associated with decoherence chosen arbitrarily as 10 ps. Clearly, almost all of the control is lost. However, if the laser parameters are changed to those shown on the right-hand side of the figure, bottom-most column, then significant control is restored once again. In this case, however, the process occurs with the loss of considerable reactant population to

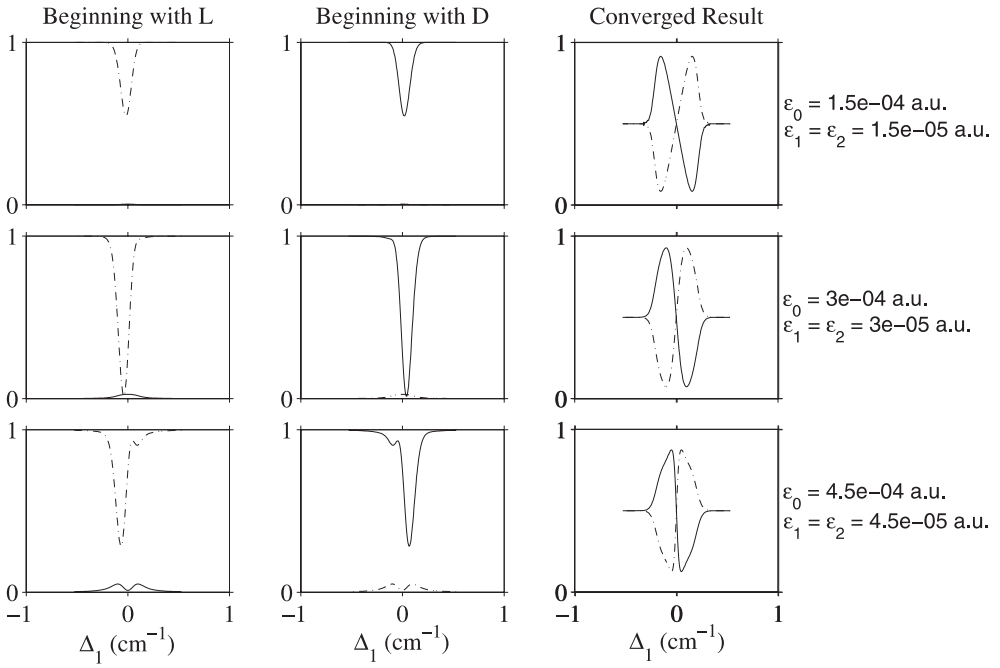

Figure 37. Control over dimethylallene enantiomer populations as a function of the detuning Δ_1 for various laser powers. The first column corresponds to probabilities of L (— · —) and D (——) after a single laser pulse, assuming that the initial-state is all L. The second column is similar, but for an initial-state that is all D. The rightmost column corresponds to the probabilities L and D after repeated excitation–relaxation cycles, as describe in the text. This is a corrected version of figure 2, [147].

dissociated dimethylallene. Additional studies designed to establish the relationship between the laser requirements for control, and the internal conversion rates, is in progress at the time of writing [163]. The possibility of alternate substituents to replace the hydrogens is also of interest, as is the effect of changes to molecular structure to alter the radiative lifetime, the internal conversion rates, etc.

Enantiomeric control is more difficult if the excited molecular potential energy surfaces do not posses an appropriate minimum at the σ_h hyper-plane configurations (see figure 28). In this case, the method introduced in this subsection is not applicable. One may however be able to apply the laser distillation procedure by adding a molecule B to the initial L, D mixture to form weakly bound $L - B$ and $B - D$, which are themselves right- and left-handed enantiomeric pairs [164]. The molecule B is chosen so that electronic excitation of $B - D$ and $L - B$ forms an excited species G that has stationary ro-vibrational states that are either symmetric or antisymmetric with respect to reflection through σ_h. The species $L-B$ and $B-D$ now serve as the L and D enantiomers in the general scenario above and the laser distillation procedure described above then applies. Further, the molecule B serves as a catalyst that may be removed from the final product by traditional chemical means.

For example, L and D might be the left- and right-handed enantiomers of a chiral alcohol, and B is the ketone derived from this alcohol (see figure 42). In this case, studies [164] of the electronic structure of the alcohol–ketone system show that there are weakly bound chiral alcohol–ketone minima in the ground electronic state, as desired. The particular advantage of

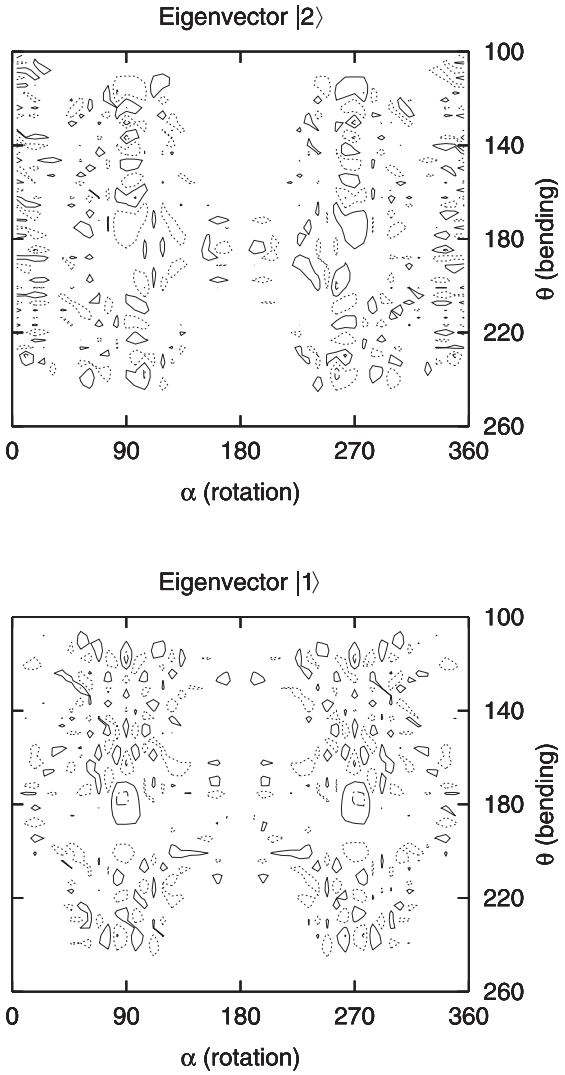

Figure 38. Contour plots of $|E_1\rangle$ and $|E_2\rangle$ where dash-dash lines $= 0.012$ a.u., dot-dot lines $= 0.0004$ a.u., solid lines $= -0.004$ a.u. and dot-dash lines $= -0.012$ a.u. Note that $|E_1\rangle$ is symmetric with respect to reflection and $|E_2\rangle$ is antisymmetric. Reflection here corresponds to changing $(\alpha - 180^\circ)$ to $(\alpha + 180^\circ)$. From figure 1, [147].

using the ketone–alcohol complex is that the ketone, which is 'recycled' after the conversion of one enantiomer to another, serves as a catalyst for the process.

The results in this section make clear that a chiral outcome, the enhancement of a particular enantiomer, can arise by coherently encoding quantum interference information in the excitation of a racemic mixture. The fact that the initial-state displays a broken symmetry and that the excited state has states that are either symmetric or antisymmetric with respect to σ_h allows for the creation of a superposition state that does not have these transformation properties. Radiatively coupling the states in the superposition then allows for the transition probabilities from L and D to differ, allowing for depletion of the desired enantiomer.

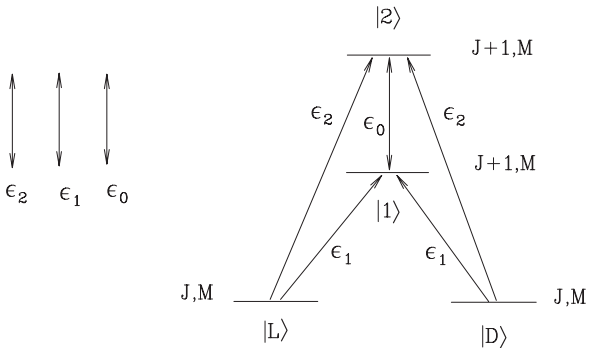

Figure 39. Schematic level diagram emphasizing the $M \equiv M_J$ features of the four level scheme in figure 28.

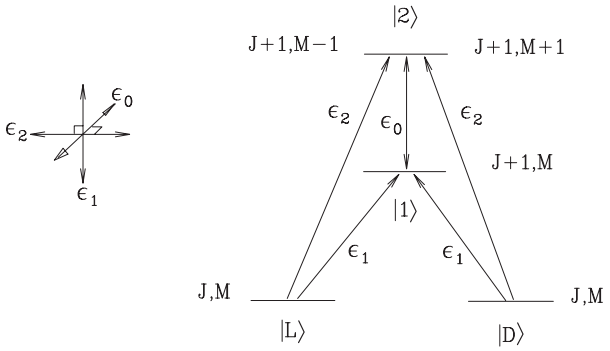

Figure 40. Schematic level diagram emphasizing the $M \equiv M_J$ coupling where three lasers of perpendicular polarization irradiate the D and L enantiomers. Only the first five levels that are coupled by these lasers are shown.

11. Adiabatic following and the non-degenerate quantum control problem

The most general 'quantum control' problem can be phrased as the problem of finding ways to completely transfer population from an arbitrary initial-state to a desired 'target' state, under the guidance of external fields (e.g. laser pulses). The general solution of this problem can only be attained using 'brute-force' numerical optimization schemes. However, there is a more restricted problem, namely achieving population transfer between superpositions of non-degenerate energy eigenstates, which we term the 'non-degenerate quantum control problem'. We show below that this problem can be solved analytically using the concept of 'trapped-states'. This solution does not help in the control of chemical reactions and photodissociation, dealt with in previous sections, because in those cases the continuum is characterized by exact degeneracies. It is nevertheless useful when we encounter a non-degenerate manifold composed of bound (vibrational) states. This problem has also received much attention (see, e.g. [165–168]) and has usually been solved numerically. Here [169] we present an analytic solution of the problem that generalizes the three level stimulated Raman adiabatic passage (STIRAP) (see [170] for a review) to the multi-level case.

Consider population transfer between an arbitrary initial-state $|\Psi^s\rangle = \sum_k c_k^s \mathrm{e}^{-\mathrm{i}E_k t/\hbar}|k\rangle$ to an arbitrary target state $|\Psi^e\rangle = \sum_l c_l^e \mathrm{e}^{-\mathrm{i}E_l t/\hbar}|l\rangle$, where both spectra E_k and E_l are non-degenerate and differ from one another.

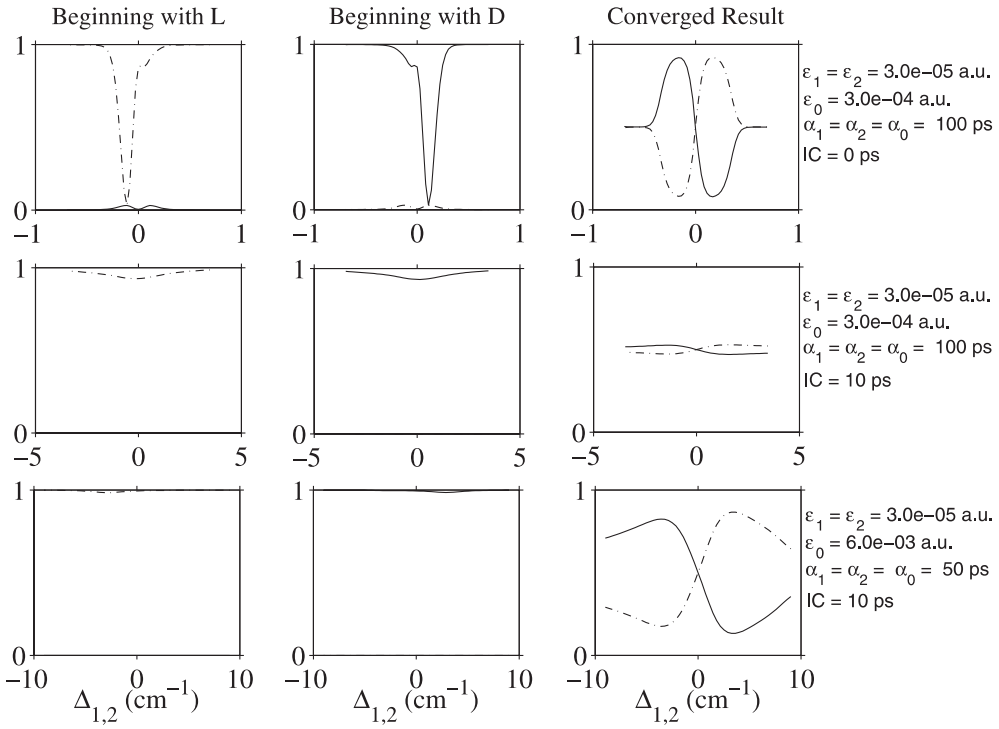

Figure 41. Control over dimethylallene enantiomer populations as a function of the detuning Δ_1 for various laser powers. The first column corresponds to probabilities of L (— · —) and D (——) after a single laser pulse, assuming that the initial-state is all L. The second column is similar, but for an initial-state that is all D. The rightmost column corresponds to the probabilities L and D after repeated excitation–relaxation cycles, as describe in the text. The first row corresponds to control using the laser parameters on the extreme right, in which there is no internal conversion; the second row uses the same laser parameters as does the first row, but with an internal conversion time of 10 ps; the bottom row shows results for an internal conversion time of 10 ps, but with the modified laser parameters shown.

Figure 43 illustrates the proposed method. The transfer process is induced by two pulses, represented by a multi-mode electric field:

$$\mathcal{E}(t) = \mathrm{Re}\sum_{k=1}^{n+m} \mathcal{E}_{0,k}(t)\mathrm{e}^{-\mathrm{i}\omega_{0,k}t}, \tag{170}$$

where $\omega_{i,j} \equiv (E_i - E_j)/\hbar$, and $\mathcal{E}_{0,k}(t)$ are the slowly varying amplitudes of each $\omega_{0,k}$ mode. By choosing a different time dependence for the $\mathcal{E}_{0,k}(t)$ amplitudes of the 'dump' process, connecting the $|k\rangle = |n+1\rangle, |n+2\rangle, \ldots, |n+m\rangle$ states to the $|0\rangle$ state, and of the 'pump' process, connecting the $|0\rangle$ state to the $|k\rangle = |1\rangle, |2\rangle, \ldots, |n\rangle$ states, we in effect construct two temporally distinct ('dump' and 'pump') pulses. The intensity and phase of each $\mathcal{E}_{0,k}(t)$ amplitude is adjusted, as explained below, to yield the desired transfer. In the so-called 'counter-intuitive' order [170], the pump pulse with the $\mathcal{E}_{1,0}, \ldots, \mathcal{E}_{n,0}$ components follows the dump pulse with the $\mathcal{E}_{n+1,0}, \ldots, \mathcal{E}_{n+m,0}$ components.

We solve for $\underline{c}(t)$ the column vector of the $c_k(t)$ expansion coefficients, $\underline{c}(t) = (c_0, c_1, \ldots, c_n, c_{n+1}, \ldots, c_{n+m})$, of the system wavefunction, $|\Psi(t)\rangle = \sum_{k=0}^{n+m} c_k(t)\,\mathrm{e}^{-\mathrm{i}E_k t/\hbar}|k\rangle$, in the rotating-wave approximation. One convenient way to do so is to write the Hamiltonian

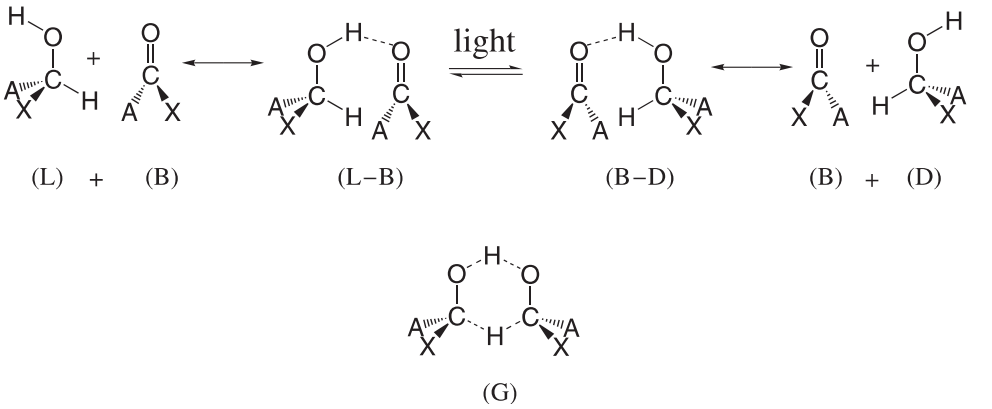

Figure 42. Sample scenario for enhanced enantiomeric selectivity in a racemic mixture of two chiral alcohols related by inversion. An alcohol and ketone exchange two hydrogen atoms so as to produce the ketone, but with an alcohol of reverse handedness. Here, A and X are distinct organic groups and dashes denote, in the upper panel, hydrogen bonds. The electronically excited species G, which is formed upon excitation with light, is postulated to be given by the structure at the bottom of the figure. In this case, the top-most and bottom-most hydrogens are attached to the oxygens and carbons, respectively, by 'half-bonds'. From figure 4, [146].

directly in this approximation, and neglect off-resonance terms. This corresponds to a molecule–field interaction of

$$H_{\mathrm{MR}} = \hbar \sum_{k=1}^{n+m} [\Omega_{0,k}(t) \mathrm{e}^{-\mathrm{i}\omega_{0,k}t} |0\rangle\langle k| + \Omega_{k,0}(t) \mathrm{e}^{\mathrm{i}\omega_{0,k}t} |k\rangle\langle 0|]. \tag{171}$$

Here, $\Omega_{i,j}(t)$, the time dependent Rabi frequencies, are given by

$$\Omega_{i,j}(t) \equiv \mathcal{O}_{i,j}\, f_{D(P)}(t) \equiv \frac{\hat{\varepsilon} \cdot \boldsymbol{d}_{i,j} \mathcal{E}_{i,j}(t)}{\hbar}, \tag{172}$$

where $\hat{\varepsilon} \cdot \boldsymbol{d}_{0,k}$ are the electric-dipole matrix-elements, projected along the field polarization and $0 < f_D(t) < 1$ and $0 < f_P(t) < 1$ describe the pulse envelopes of the dump and the pump pulses, respectively.

Inserting $\Psi(t)$ into the time dependent Schrödinger equation and using equation (171) gives

$$\dot{\underline{c}}(t) = -\mathrm{i}\underline{\underline{H}}(\mathrm{t}) \cdot \underline{c}(\mathrm{t}), \tag{173}$$

where the effective Hamiltonian matrix is

$$\underline{\underline{H}}(t) = \begin{bmatrix} 0 & \Omega_{0,1} & \cdots & \Omega_{0,n} & \Omega_{0,n+1} & \cdots & \Omega_{0,n+m} \\ \Omega_{1,0} & 0 & \cdots & 0 & 0 & \cdots & 0 \\ \cdots & \cdots & \cdots & \cdots & \cdots & \cdots & \cdots \\ \Omega_{n,0} & 0 & \cdots & 0 & 0 & \cdots & 0 \\ \Omega_{n+1,0} & 0 & \cdots & 0 & 0 & \cdots & 0 \\ \cdots & \cdots & \cdots & \cdots & \cdots & \cdots & \cdots \\ \Omega_{n+m,0} & 0 & \cdots & 0 & 0 & \cdots & 0 \end{bmatrix}.$$

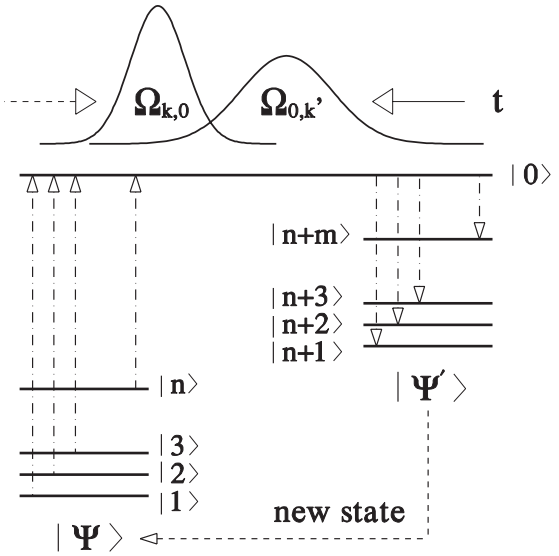

Figure 43. A transfer scheme between the states $|\Psi\rangle \to |0\rangle \to |\Psi^e\rangle$. The first (dump) laser pulse, with Rabi frequencies $\Omega_{0,k'}(t)$, couples all the $|k'\rangle$ final (empty) states to state $|0\rangle$, while the second (pump) pulse, with Rabi frequency $\Omega_{k,0}(t)$, couples state $|0\rangle$ to the initial (populated) states $|k\rangle$. Taken from figure 1, [169].

Of the $n+m+1$ eigenvalues of $\underline{\underline{H}}(t)$, $n+m-1$ are zero and two are non-zero:

$$\lambda_{1,2,\ldots,n+m-1} = 0,$$
$$\lambda_{n+m} = -\lambda_{n+m+1} = \left(\sum_{k=1}^{n+m} |\Omega_{0,k}(t)|^2\right)^{1/2}. \tag{174}$$

Corresponding to the zero eigenvalues of H_{MR} are nm ('trapped') eigenvectors of the type

$$|D_{kl}\rangle = \Omega_{0,l}\,|k\rangle \mathrm{e}^{-\mathrm{i}E_k t/\hbar} - \Omega_{0,k}|l\rangle \mathrm{e}^{-\mathrm{i}E_l t/\hbar}, \qquad (k = 1,\ldots,n;\, l = n+1,\ldots,n+m). \tag{175}$$

Clearly, only $n+m-1$ of these states are linearly independent. We can use the above trapped eigenvectors to obtain a state that correlates (in the 'counter-intuitive' pulse ordering scheme) at $t = t_s$ with the initial-state $|\Psi^s\rangle = \sum_k c_k^s |k\rangle$, and at $t = t_e$ with the final state $|\Psi^e\rangle = \sum_l c_l^e |l\rangle \mathrm{e}^{-\mathrm{i}E_l t_e/\hbar}$. The particular combination that satisfies these asymptotic conditions is

$$|D\rangle = \sum_{k,l} t_{kl}|D_{kl}\rangle = \sum_{k=1}^{n} |k\rangle \mathrm{e}^{-\mathrm{i}E_k t/\hbar} \sum_{l=n+1}^{n+m} t_{kl}\Omega_{0,l} - \sum_{l=n+1}^{n+m} |l\rangle \mathrm{e}^{-\mathrm{i}E_l t/\hbar} \sum_{k=1}^{n} t_{kl}\Omega_{0,k}, \tag{176}$$

where the t_{kl} coefficients are chosen such that

$$\sum_{l=n+1}^{n+m} t_{kl}\Omega_{0,l} = c_k^s, \qquad \sum_{k=1}^{n} t_{kl}\Omega_{0,k} = c_l^e. \tag{177}$$

Equations (177) can be satisfied by choosing a 'counter-intuitive' pulse ordering in which the $\mathcal{E}_{0,l}$, $l = n+1,\ldots,n+m$ components exist at $t = t_s$ and the $\mathcal{E}_{0,k}$, $k = 1,\ldots,n$ components exist at $t = t_e$, and choosing t_{kl} and $\Omega_{k,0}(t) \equiv \mathcal{O}_{k,0} f_P(t)$ such that

$$t_{kl} \propto \mathcal{O}_{k,0}\mathcal{O}_{l,0}, \qquad \text{and} \qquad \mathcal{O}_{k,0} = \mathcal{C}c_k^s, \qquad \mathcal{O}_{l,0} = \mathcal{C}c_l^e, \tag{178}$$

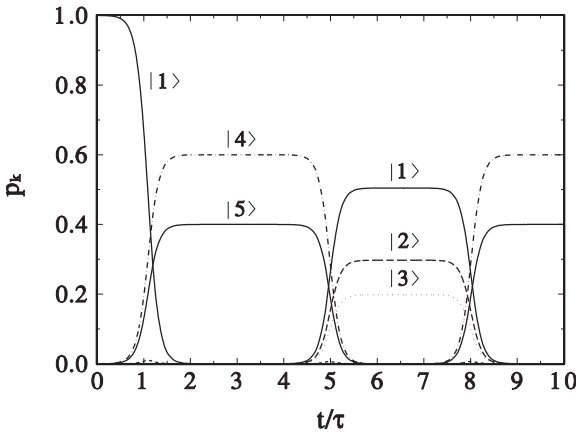

Figure 44. Complete population transfer between various superpositions of the $|k\rangle$ $k = 1 - 5$ states. The lines are denoted by the symbols $|k\rangle$ for the respective populations p_k. Taken from figure 2, [169].

where $\mathcal{C}$ is an arbitrary complex number. The only limitation on the choice of $\mathcal{C}$ is that the (slowly varying) Rabi frequencies should be strong enough to guarantee the adiabaticity of the transfer process. Other than that, the process is quite robust against changes in $\mathcal{C}$.

The approach is demonstrated in figure 44 for a population transfer chain. This is composed of the transfer from state $|1\rangle$ to a linear combination of states $|4\rangle$ and $|5\rangle$, followed by the transfer from this superposition state to a superposition of the $|1\rangle$, $|2\rangle$ and $|3\rangle$ states, and back to the $|4\rangle$ plus $|5\rangle$ superposition. This transfer chain is carried out using Gaussian pulses for which the Rabi frequencies are given as $\Omega_{0,k}(t) = \mathcal{O}_{0,k} \exp[-(t - t_0)^2/\tau^2]$ $(k = 1, \ldots, n)$ and $\Omega_{0,l}(t) = \mathcal{O}_{0,l} \exp[-t^2/\tau^2]$ $(l = n + 1, \ldots, n + m)$, with $t_0 = 2\tau$ being the delay between the pulses. The $\mathcal{C}$ coefficient of equation (178) is chosen to be $\mathcal{C} = 50/\tau$.

Thus, the above method provides a very simple and analytic pulse shaping recipe for achieving a complete population transfer between two arbitrary superposition states $|\Psi^s\rangle$ and $|\Psi^e\rangle$, composed of non-degenerate energy eigenstates.

12. Suppression of spontaneous emission

The possibility of suppressing spontaneous emission has been a source of great interest in recent years [171–179]. More recently [180, 181] we proposed a new method of completely suppressing spontaneous emission by utilizing the interference between resonances. The same method is applicable to any decay process, provided that it is governed by overlapping resonances.

The proposed approach relies on the fact that one can coherently excite a set of overlapping resonances such that their decay exhibits a step-like behaviour. That is, the system starts in a quiescent period in which no spontaneous emission occurs, followed by a 'photon-burst' in which spontaneous emission is greatly accelerated, followed by another quiescent period, etc. The quiescent period (and subsequent photon-bursts) are due to destructive and constructive interferences between overlapping resonances. The reason it is impossible to suppress the decay over all times in this fashion is that the phase and magnitude relations that guarantee the suppression of decay at a given time, change as the system evolves in time, until at a certain time-point the interference for decay becomes constructive and the system displays the 'photon-burst'.

In order to suppress decay at all times we suggest irradiating the system before it reaches the photon-burst phase with an external laser field that re-shuffles the phases of the coefficients of the superposition of overlapping resonances. For the two overlapping resonances case this pulse is simply a π pulse that inverts the populations between levels, thereby effectively sending the system 'backwards' in time into the quiescent period. Additional external pulses ('interruptions') must be applied periodically just before the system reaches the photon-burst phases as it moves backwards and forwards in time. In this way the system is forced to forever live on the quiescent period ledge.

As explained below, this approach is not limited to cases with pre-existing overlapping resonances. It is possible to suppress the decay of any system, even that of a single decaying resonance. This is achieved by (Autler–Townes) splitting [182] a given decaying state into two overlapping field-dressed resonances using an external cw field. Below we describe computational applications of this method to the suppression of the decay of a variety of realistic atomic (e.g. H($2p$) and Pb($6p7s^3P_1^0$)) and molecular (e.g. $Na_2(A\ ^1\Sigma_u^+)$) excited states.

12.1. The decay of overlapping resonances

The decay of, and interference between, overlapping resonances is best explained using 'partitioning' theory [184–187, 160]. Assuming that we have a situation in which bound states interact with a continuum of states, we define two projection operators Q and P, satisfying the equalities $QQ = Q$, $PP = P$, $PQ = QP = 0$, $P + Q = I$, where I is the identity operator. The Q and P operators are chosen to project out the subspaces spanned by bound states and continuum states, respectively.

The full scattering incoming states $|E, \boldsymbol{n}^-\rangle$, are eigenstates of the Schrödinger equation, written as,

$$[E - \mathrm{i}\epsilon - H]|E, \boldsymbol{n}^-\rangle = 0, \tag{179}$$

where the $-\mathrm{i}\epsilon$ serves to remind us of the incoming boundary conditions. Using the completeness and orthogonality of P and Q, we obtain two coupled equations from the Schrödinger equation,

$$\begin{aligned} [E - \mathrm{i}\epsilon - PHP]P|E, \boldsymbol{n}^-\rangle &= PHQ|E, \boldsymbol{n}^-\rangle, \\ [E - \mathrm{i}\epsilon - QHQ]Q|E, \boldsymbol{n}^-\rangle &= QHP|E, \boldsymbol{n}^-\rangle. \end{aligned} \tag{180}$$

We define two basis sets, $|E, \boldsymbol{n}\rangle$ and $|\alpha\rangle$, that are the solutions of the homogeneous (decoupled) parts of equations (180). That is

$$[E - \mathrm{i}\epsilon - PHP]|E, \boldsymbol{n}\rangle = 0, \tag{181}$$

$$[E_s - QHQ]|\alpha\rangle = 0. \tag{182}$$

Implicit in equations (181) and (182) is that $|E, \boldsymbol{n}\rangle \in P$ and $|\alpha\rangle \in Q$ and as such they are orthogonal to one another. We, in fact, assume that each basis set spans the entire subspace to which it belongs. Hence we can write an explicit representation of Q and P as,

$$Q = \sum_s |\alpha\rangle\langle\alpha|, \tag{183}$$

$$P = \sum_{\boldsymbol{n}} \int \mathrm{d}E |E, \boldsymbol{n}\rangle\langle E, \boldsymbol{n}|. \tag{184}$$

Following Fano [185] we can use equations (183) and (184) to write $|E, \boldsymbol{n}^-\rangle = [P + Q]|E, \boldsymbol{n}^-\rangle$ in terms of Q and P as

$$|E, \boldsymbol{n}^-\rangle = \sum_s |\alpha\rangle\langle\alpha|E, \boldsymbol{n}^-\rangle + \sum_{\boldsymbol{n}'} \int \mathrm{d}E'|E', \boldsymbol{n}'\rangle\langle E', \boldsymbol{n}'|E, \boldsymbol{n}^-\rangle. \tag{185}$$

We now solve for $P|E, \boldsymbol{n}^-\rangle$ by writing it as a sum of the homogeneous solution of equation (181) and a particular solution of the first of equation (180) obtained by inverting $[E - \mathrm{i}\epsilon - PHP]$,

$$P|E, \boldsymbol{n}^-\rangle = P|E, \boldsymbol{n}\rangle + [E - \mathrm{i}\epsilon - PHP]^{-1} PHQ|E, \boldsymbol{n}^-\rangle. \tag{186}$$

Substituting this solution into the second equation (180) we obtain

$$Q|E, \boldsymbol{n}^-\rangle = [E - \mathrm{i}\epsilon - Q\mathcal{H}(E)Q]^{-1} QHP|E, \boldsymbol{n}\rangle, \tag{187}$$

where

$$Q\mathcal{H}(E)Q \equiv QHQ + QHP[E - \mathrm{i}\epsilon - PHP]^{-1} PHQ. \tag{188}$$

We now consider the case of optically induced overlapping resonances. We consider therefore an isolated resonance $|a\rangle$ that acquires its width due to spontaneous emission to a manifold of lower lying states denoted as $|\gamma\rangle$. In order to create more resonances we (Autler–Townes [182]) split this resonance by coupling it to a lower lying state $|b\rangle$ using a monochromatic source of frequency ω_i. The situation is described in figure 45.

The total Hamiltonian then assumes the form,

$$H = H_M + H_R + H_{\mathrm{MR}}, \tag{189}$$

where H_M is the matter Hamiltonian, H_R is the radiative Hamiltonian, and H_{MR} is the matter-radiation interaction. For the two material levels $|a\rangle$ and $|b\rangle$ we write H_M as,

$$H_M = \tfrac{1}{2}\hbar\omega_{\alpha,b}\sigma_z, \tag{190}$$

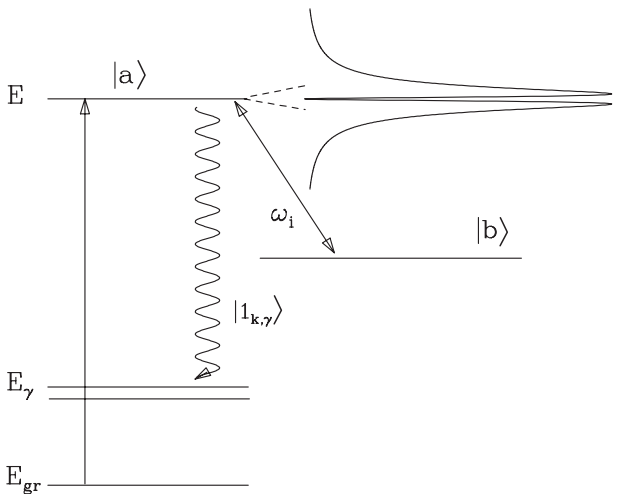

Figure 45. The energy levels and spontaneous emission pathways of an Autler–Townes split resonance. Shown is a resonance $|a\rangle$ of energy E_a, coupled by a monochromatic light of frequency ω_i to a lower lying state $|b\rangle$. As a result of this coupling, the resonance splits, displaying a hole at the centre of the absorption line at $E = E_a$. The wiggly line represents spontaneously emitted photons to lower lying states of energies E_γ. Also shown is the ground state of energy E_{gr} that is excited, using a shaped pulse, to form a superposition of the split components of $|a\rangle$ such that the decay is delayed.

where $\omega_{\alpha,b} \equiv (E_a - E_b)/\hbar$ and

$$\sigma_z|a\rangle = |a\rangle, \qquad \sigma_z|b\rangle = -|b\rangle. \tag{191}$$

The free radiative Hamiltonian is written as

$$H_R = \sum_{\boldsymbol{k}} \hbar\omega_k \left[a_{\boldsymbol{k}}^\dagger a_{\boldsymbol{k}} + \frac{1}{2} \right]. \tag{192}$$

The $|a\rangle|0,\ldots,0,n_i,0,\ldots,0\rangle$ state, denoted for simplicity as $|a,n_i,0\rangle$, and the $|b\rangle|0,\ldots,0,n_i+1,0,\ldots,0\rangle$ state, denoted for simplicity as $|b,n_i+1,0\rangle$, are eigenstates of H_0, the un-coupled Hamiltonian, defined as, $H_0 = H_M + H_R$. Fixing the zero of energy to be mid-way between E_a and E_b we have that

$$\begin{aligned} H_0|a,n_i,0\rangle &= \left(E_{n_i} + \tfrac{1}{2}\hbar\Delta\right)|a,n_i,0\rangle, \\ H_0|b,n_i+1,0\rangle &= \left(E_{n_i} - \tfrac{1}{2}\hbar\Delta\right)|b,n_i+1,0\rangle, \end{aligned} \tag{193}$$

where $E_{n_i} \equiv n_i\hbar\omega_i + \frac{1}{2}\hbar\omega_{\alpha,b} - \frac{1}{2}\hbar\Delta$ with $\Delta \equiv \omega_{\alpha,b} - \omega_i$, is the energy of these states relative to the vacuum energy.

The matter-radiation Hamiltonian within the dipole approximation is given by

$$H_{\mathrm{MR}} = -\boldsymbol{d}\cdot\boldsymbol{\varepsilon}, \tag{194}$$

where

$$\boldsymbol{d} = \boldsymbol{d}_{ab}(\sigma_+ + \sigma_-), \qquad \boldsymbol{\varepsilon} = \sqrt{\frac{\hbar\omega_i}{2\epsilon_0 V}}\hat{\boldsymbol{\varepsilon}}(a + a^\dagger). \tag{195}$$

Assuming the rotating-wave approximation, we obtain that

$$H_{\mathrm{MR}} = \hbar g_i(\sigma_+ a + a^\dagger\sigma_-). \tag{196}$$

Therefore,

$$\begin{aligned} H_{\mathrm{MR}}|a,n_i,0\rangle &= \hbar g_i\sqrt{n_i+1}|b,n_i+1,0\rangle, \\ H_{\mathrm{MR}}|b,n_i+1,0\rangle &= \hbar g_i\sqrt{n_i+1}|a,n_i,0\rangle, \end{aligned}$$

where

$$g_i = -\sqrt{\frac{\hbar\omega_i}{2\epsilon_0 V}}\frac{\hat{\boldsymbol{\varepsilon}}\cdot\boldsymbol{d}_{ab}}{\hbar}.$$

Taking the Q operator as

$$Q \equiv |a,n_i,0\rangle\langle a,n_i,0| + |b,n_i+1,0\rangle\langle b,n_i+1,0|, \tag{197}$$

we have (in matrix form) that,

$$\underline{\underline{QHQ}} = \begin{pmatrix} E_{n_i} + \frac{1}{2}\hbar\Delta & \hbar g_i\sqrt{n_i+1} \\ \hbar g_i\sqrt{n_i+1} & E_{n_i} - \frac{1}{2}\hbar\Delta \end{pmatrix}. \tag{198}$$

The eigenvalues of $\underline{\underline{QHQ}}$ are given as,

$$E_{n_i}^{\pm} = E_{n_i} \pm \tfrac{1}{2}\hbar\Omega_{n_i}, \tag{199}$$

where, $\Omega_{n_i}^2 = \Delta^2 + 4g_i^2(n_i+1)$. The ('dressed') eigenstates corresponding to these eigenvalues are given [187] by

$$\begin{aligned} |+n_i,0\rangle &= \sin\theta|b,n_i+1,0\rangle + \cos\theta|a,n_i,0\rangle, \\ |-n_i,0\rangle &= \cos\theta|b,n_i+1,0\rangle - \sin\theta|a,n_i,0\rangle, \end{aligned} \tag{200}$$

where

$$\tan 2\theta = -\frac{\Omega_i}{\Delta},$$

where

$$\hbar\Omega_i \equiv -\boldsymbol{d}_{ab} \cdot \mathcal{E}_i$$

and

$$\mathcal{E}_i \equiv 2\hat{\varepsilon}\sqrt{\frac{n_i\hbar\omega_i}{2\epsilon_0 V}}. \tag{201}$$

The two orthogonal states $|+n_i, 0\rangle$, $|-n_i, 0\rangle$ of the Q manifold and the states $|E, m_i, 1_\beta\rangle$ of the P manifold satisfy,

$$\langle\alpha', n_i, 0|QHQ|\alpha, n_i, 0\rangle = E_\alpha \delta_{n_i', n_i}\delta_{\alpha',\alpha} \qquad \text{where } \alpha, \alpha' = \pm, \tag{202}$$

$$\langle E', n_i, 1_{\beta'}|PHP|E, m_i, 1_\beta\rangle = (E + n_i\hbar\omega_i)\delta(E' - E)\delta_{n_i,m_i}\delta_{\beta'\beta}. \tag{203}$$

The $|1_\beta\rangle$ state of the above is a (spontaneously emitted) one-photon state in the β mode. The excited $|a, n_i, 0\rangle$ state emits a photon and decays into the P space, with the ω_i photons acting as spectators [188], which means that their number does not change in the process.

Assuming that the lower lying $|b, n_i + 1, 0\rangle$ state is a non-decaying (or a slowly decaying) state, and denoting the matter-radiation matrix elements as,

$$V^{(n)}(a, 0|E, 1_\beta) \equiv \langle a, n, 0|QHP|E, n, 1_\beta\rangle,$$

we have that,

$$\begin{aligned} V^{(n)}(+, 0|E, 1_\beta) &= \cos\theta V^{(n)}(a, 0|E, 1_\beta), \\ V^{(n)}(-, 0|E, 1_\beta) &= -\sin\theta V^{(n)}(a, 0|E, 1_\beta), \end{aligned} \tag{204}$$

where we have for brevity denoted n_i as n.

The fully interacting $|E, n, 1_\beta^-\rangle$ states, obtained from equation (185), form a complete basis set and can be used to expand $|\Psi(t)\rangle$, the full time dependent wavefunction. Assuming that initially (at $t = 0$) we populate a superposition of zero-photon states and a coherent state in the ω_i mode,

$$|\Psi(t = 0)\rangle = \sum_{\alpha,n} c_{\alpha,n}|\alpha, n, 0\rangle, \tag{205}$$

where $c_{\alpha,n_i} = c_\alpha c_n$, with $c_n = \sum_n(\alpha^n/n!)$, the wavefunction at time t is given by

$$|\Psi(t)\rangle = \sum_{\alpha,n,\beta} c_{\alpha,n}\int_{E_i}^{E_f} \mathrm{d}E\, \mathrm{e}^{-\mathrm{i}Et/\hbar}|E, n, 1_\beta^-\rangle\langle E, n, 1_\beta^-|\alpha, n, 0\rangle. \tag{206}$$

Applying equation (187) to the present case we obtain that $a_{\alpha,n,\beta,m}(E)$ the amplitude function is given as,

$$\begin{aligned} a_{\alpha,n,\beta,m}(E) &\equiv \langle\alpha, n, 0|E, n, 1_\beta^-\rangle \\ &= \sum_{\alpha'}\langle\alpha, n, 0|(E - \mathrm{i}\varepsilon - Q\mathcal{H}(E)Q)^{-1}|\alpha', n, 0\rangle\langle\alpha' n, 0|QHP|E, n, 1_\beta\rangle, \end{aligned} \tag{207}$$

where, $Q\mathcal{H}(E)Q$ is defined in equation (188). Using the well-known identity, $[E - \mathrm{i}\epsilon - PHP]^{-1} = \mathsf{P}_v[E - PHP]^{-1} + \mathrm{i}\pi\delta(E - PHP)$, with P_v denoting the Cauchy principal value integral, we can write the matrix elements of $Q\mathcal{H}(E)Q$ as,

$$\langle\alpha, n, 0|Q\mathcal{H}(E)Q|\alpha', n, 0\rangle = E_\alpha\delta_{\alpha\alpha'} + \hbar\Delta^{(n)}_{\alpha,\alpha'}(E) + \mathrm{i}\frac{\hbar}{2}\Gamma^{(n)}_{\alpha,\alpha'}(E), \tag{208}$$

where

$$\Gamma^{(n)}_{\alpha,\alpha'}(E) \equiv \frac{2\pi}{\hbar}\sum_{\beta} V^{(n)}(\alpha|E,\beta)V^{(n)}(E,\beta|\alpha'),$$
$$\Delta^{(n)}_{\alpha,\alpha'}(E) \equiv \frac{1}{2\pi}\mathsf{P}_v\int_{E_i}^{E_f} \mathrm{d}E' \frac{\Gamma^{(n)}_{\alpha,\alpha'}(E')}{(E-E')}. \tag{209}$$

The amplitudes of the $|\alpha', n, 0\rangle$ states at time t equal,

$$\begin{aligned}\langle \alpha, n, 0|\Psi(t)\rangle &= \sum_{\alpha} c_{\alpha,n}\int_{E_i}^{E_f} \mathrm{d}E\, \mathrm{e}^{-\mathrm{i}Et/\hbar}\sum_{\beta}\langle \alpha, n, 0|E, n, 1^-_\beta\rangle\langle E, n, 1^-_\beta|\alpha, n, 0\rangle \\ &= \sum_{\alpha} c_{\alpha,n} M^{(n)}_{\alpha',\alpha}(t),\end{aligned} \tag{210}$$

where

$$M^{(n)}_{\alpha',\alpha} = \sum_{\beta}\int_{E_i}^{E_f} \mathrm{d}E\, \mathrm{e}^{-\mathrm{i}Et/\hbar} a^{(n)}_{\alpha',\beta}(E) a^{(n)*}_{\alpha,\beta}(E). \tag{211}$$

The total population in the zero-photon material states with n spectator photons in the ith mode, at time t, $P^{(n)}(0, \boldsymbol{c}, t)$, is given by

$$P^{(n)}(0, \boldsymbol{c}, t) = \sum_{\alpha'} |\langle \alpha', n, 0|\Psi(t)\rangle|^2, \tag{212}$$

where $\boldsymbol{c} \equiv \{c_{\alpha,n}\}$.

In order to delay the decay we need to find the set of initial coefficients $\boldsymbol{c}$ that maximizes $P^{(n)}(0, \boldsymbol{c}, t)$ over a given time interval τ after preparation. Once such a set of coefficients is found, the overlapping resonances thus populated exhibit a step-like decay pattern [180, 181], a sample of which is shown in figure 49. Indeed, after a quiescent period in which a photon emitted by one resonance gets immediately re-absorbed by the other, the system undergoes a period of rapid decay in which a burst of photons escapes the atom. The 'photon-burst' phase is followed by another quiescent phase etc.

The delay in the emission afforded by the quiescent phase may itself be of great practical importance for many laser applications. However, we usually want to go one step further and suppress the emission at all times. It is possible to do so in the 2×2 case [180] by applying a π pulse at, or close to, the end of the quiescent period. The effect of the π pulse that transforms the system according to the transformation matrix, $\left(\begin{smallmatrix} 0 & i \\ i & 0 \end{smallmatrix}\right)$, is to interchange the populations between the two levels. Such an interchange of population in a two level system is known to effectively reverse the direction of time. As a result, after the application of the π pulse, the system moves away from the onset of the 'photon-burst' phase until it reaches the $-\tau$ time, at which point another photon-burst is about to be launched. We avoid such a burst by applying another π pulse that reverses the flow of time once again, sending the system back in the positive time sense. By continuing to apply the π pulse every 2τ interval we confine the system forever to the quiescent phase, making it shuttle back and forth between $-\tau$ and τ. As shown, e.g. in figure 49, to be discussed in greater detail below, spontaneous emission is thereby effectively blocked. The above analysis also applies to the $N_\alpha > 2$ case, where the transformation is slightly more complicated [180].

We now turn our attention to the application of the above strategy for the Autler–Townes split resonance case. The radiative couplings to the $\beta = \boldsymbol{k}, \gamma$ mode, where $\omega_\gamma = (E - E_\gamma)/\hbar$

are [189],

$$V(\alpha, 0|E, \gamma, 1_{k,\gamma}) = \begin{cases} ie\sqrt{\dfrac{\hbar\omega_k}{2\epsilon_0 V_0}}\hat{\varepsilon}_{k,j} \cdot \boldsymbol{D}_{\alpha,\gamma}, & E > E_\gamma, \\ 0, & \text{otherwise.} \end{cases} \tag{213}$$

Here, we have dropped the (n) superscript denoting the number of ω_i spectator photons because the dipole matrix elements for spontaneous emission do not depend on this number.

Integrating over the directions of emission of the photons and summing over the two possible photon polarization directions, we obtain that

$$\Gamma_{\alpha\alpha'}(E) = \frac{e^2}{3\pi\epsilon_0\hbar^4 c^3} \sum_{\{\gamma: E > E_\gamma\}} \boldsymbol{D}_{\alpha,\gamma} \cdot \boldsymbol{D}^*_{\alpha',\gamma}(E - E_\gamma)^3. \tag{214}$$

The level-shifts $\Delta_{\alpha\alpha'}(E)$ can be calculated from $\Gamma_{\alpha\alpha'}(E)$ using equation (209).

The decay matrix elements in the dressed state basis (dropping the energy argument for brevity) can be expressed in the $|a\rangle$, $|b\rangle$ basis as,

$$\begin{aligned} \Gamma_{++}(\theta) &= \sin^2\theta\,\Gamma_{bb} + \cos^2\theta\,\Gamma_{aa} + \sin 2\theta\,\mathrm{Re}[\Gamma_{ab}], \\ \Gamma_{--}(\theta) &= \cos^2\theta\,\Gamma_{bb} + \sin^2\theta\,\Gamma_{aa} - \sin 2\theta\,\mathrm{Re}[\Gamma_{ab}], \\ \Gamma_{+-}(\theta) &= \tfrac{1}{2}\sin 2\theta\,(\Gamma_{bb} - \Gamma_{aa}) + \cos 2\theta\,\mathrm{Re}[\Gamma_{ab}] - i\mathrm{Im}[\Gamma_{ab}]. \end{aligned} \tag{215}$$

Since the bare states $|a\rangle$ and $|b\rangle$ have opposite symmetries, they emit into different sets of levels, resulting in $\Gamma_{ab} = 0$. The above expressions can therefore be written as,

$$\begin{aligned} \Gamma_{++}(\theta) &= \bar{\Gamma} - \cos 2\theta\,\hat{\Gamma}, \\ \Gamma_{--}(\theta) &= \bar{\Gamma} + \cos 2\theta\,\hat{\Gamma}, \\ \Gamma_{+-}(E, \theta) &= \sin 2\theta\,\hat{\Gamma}(E), \end{aligned} \tag{216}$$

where $\bar{\Gamma} = \frac{1}{2}(\Gamma_{aa} + \Gamma_{bb})$ and $\hat{\Gamma} = \frac{1}{2}(\Gamma_{bb} - \Gamma_{aa})$.

The possibility of delaying the spontaneous emission is governed by the ratio,

$$f_1(E, \theta) \equiv \frac{|\Gamma_{+-}(E)|}{[\Gamma_{++}(E)\Gamma_{--}(E)]^{1/2}}, \tag{217}$$

which (due to the Schwartz inequality) can assume values between 0 and 1. The value of unity leads to maximal delay and the null value to the complete loss of control over spontaneous emission. The ratio reaches its maximum value when $\theta = \pi/4$, i.e. when the field is on-resonance. It then equals

$$f_1\left(\frac{\pi}{4}\right) = \frac{|\Gamma_{bb} - \Gamma_{aa}|}{\Gamma_{aa} + \Gamma_{bb}} = \left|\frac{\Gamma_{aa}}{\bar{\Gamma}} - 1\right|. \tag{218}$$

The maximal degree of delay of the spontaneous emission is attained when $\Gamma_{bb} \approx 0$, i.e. the $|b\rangle$ state is a meta-stable excited state; in that case $\Gamma_{++}(E) = \Gamma_{--}(E) = |\Gamma_{--}(E)| = \frac{1}{2}\Gamma_{aa}(E)$.

The ability to control the spontaneous emission resulting from the introduction of the cw field is demonstrated by a series of computations presented below. In all these computations we have assumed that the energy-dependence of the widths can be neglected over the integration range, which is of the order of magnitude of the width itself. In figure 46 we show Γ_{++}, Γ_{--}, $|\Gamma_{+-}|$ and f_1 that result from the introduction of a cw coupling field as a function of the mixing angle θ. The results are shown for several different values of $\Gamma_{bb}/\bar{\Gamma}$.

In figure 46(a), $\Gamma_{bb}/\bar{\Gamma} = 0.01$, which means that state $|b\rangle$ is a meta-stable state. The degree of delay of emission we achieve in this case reaches the maximum value it possibly can: $f_1(\theta) \approx 1$. This degree of control is maintained over a wide range of the mixing angle θ.

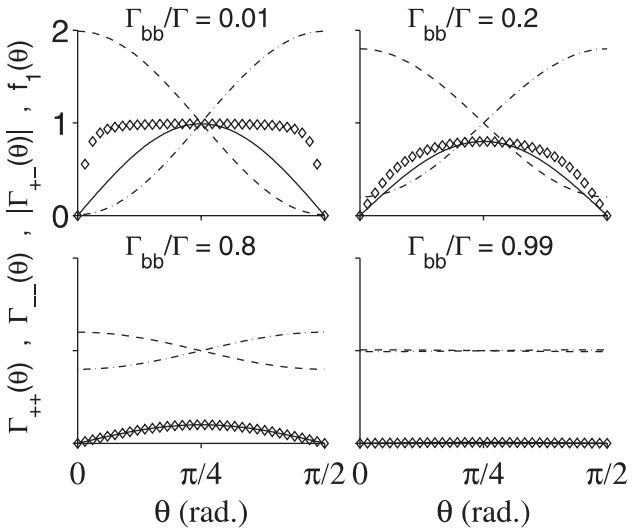

Figure 46. Γ_{++} (- - - -), Γ_{--} (— · —), $|\Gamma_{+-}|$ (——) and $f \equiv |\Gamma_{+-}|/(\Gamma{+}{+}\Gamma_{--})^{1/2}$ ($\Diamond$).

Essentially, control is degraded only when the detuning is very large, causing almost no mixing between the $|a\rangle$ and the $|b\rangle$ states ($\theta \approx 0$ or $\theta \approx \pi/2$).

In the next case, shown figure 46(b), $\Gamma_{bb}/\bar{\Gamma} = 0.2$. It shows slightly less control, with our ability to delay the decay now being more dependent on the field tuning. The optimal control is achieved, as discussed above, exactly on-resonance, where $f_1 = 0.8$ (see equation (218)). The possibility of control is being completely eliminated as the $\Gamma_{bb}/\bar{\Gamma}$ ratio is increased, as shown in the lower panel of figure 46.

Another important control variable is the ratio between Γ_{aa}, the resonance widths, and $\Delta E \equiv |E^+_{n_i} - E^-_{n_i}| = \hbar|\Omega_{n_i}|$, the energy spacings between Autler–Townes split resonances. According to equation (199), the Autler–Townes splitting enables the tuning of the energy spacings between the resonances by varying the Rabi frequency Ω_{n_i} of the 'spectator' cw field. Sample $a_{\alpha,n,\beta,m}(E)$ amplitudes for overlapping resonances with $\Delta E/(\hbar\Gamma)$ varying between 0.2 and 5 are shown in figure 47.

The signature of the interference is the appearance of a 'dark state' i.e. a continuum energy where the lineshape ($= |a_{\alpha,n,\beta,m}(E)|^2$) dips to zero, occurring at the peaks ($E^+_{n_i}$ or $E^-_{n_i}$) of the neighbouring resonance for each lineshape. These dark states, first discovered in [159], bring about the phenomenon of electromagnetically induced transparency' [190], midway between the resonances, shown in figure 45, for a particular linear combination of the resonances. In the optimized case studied here the $\sum_\beta |\sum_{\alpha=\pm} c_\alpha a_{\alpha,\beta}(E)|^2$ lineshapes shown in the figure 47(b) do not necessarily dip to zero.

12.2. Suppression of spontaneous emission in sample systems

12.2.1. The hydrogen atom. We first consider the suppression of the spontaneous emission of a hydrogen atom in the $|2P_0\rangle$ state, which can only decay to a single (the ground $|1S_0\rangle$) state. We do so by coupling the $|2P_0\rangle$ state, which is identified with state $|a\rangle$ of figure 45, with the $|3S\rangle$ state (identified with the $|b\rangle$ state of that figure) using a resonant cw field. In contrast to figure 45, here $E_b > E_a$, which means that $\Gamma_{bb} \neq 0$.

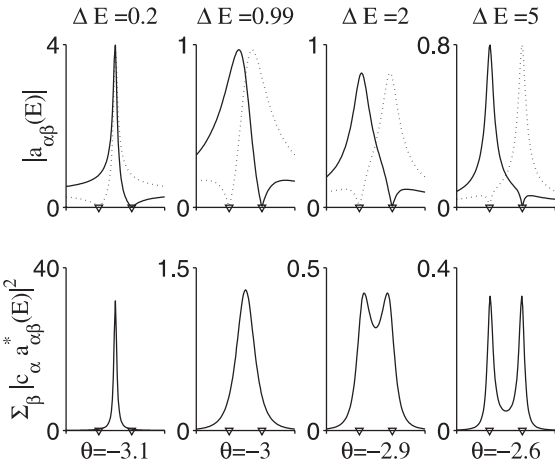

Figure 47. (*a*) The $|a_{\pm,\beta}(E)|$ amplitudes in the 2×2 case, for several values of the levels spacing ΔE for a constant Γ. The x-axis is scaled to encompass $3\Delta E$. The $|a_{+,\beta}(E)|$ is seen to dip to zero at $E^-_{n_i}$ and the $|a_{-,\beta}(E)|$ is seen to dip to zero at $E^+_{n_i}$. The $E^{\pm}_{n_i}$ positions are denoted by the triangles. Each amplitude is automatically normalized, i.e. they satisfy $\int \mathrm{d}E\, a_{\alpha\beta}(E)a_{\alpha'\beta}(E) = \delta_{\alpha,\alpha'}$. (*b*) The same as the upper panel for the $\sum_\beta |\sum_{\alpha=\pm} c_\alpha a_{\alpha,\beta}(E)|^2$ lineshapes.

All the parameters needed for this case are known analytically. Thus, the energy differences between the material states are,

$$E_{2P} - E_{1S} = \frac{3}{4}\frac{me^4}{2\hbar^2(4\pi\epsilon_0)^2} = \frac{3}{8}\,\text{a.u.},$$

and $E_{3S} - E_{2P} = \frac{5}{72}$ a.u. We obtain that,

$$\begin{aligned}\Gamma_{2P_0,2P_0}(E) &= \frac{2^{15}}{3^{11}}\frac{4\pi\epsilon_0}{m^2e^2c^3}(E - E_{1S} - (n_i+1)\hbar\omega_i)^3 = 626.8\,\mu\text{s}^{-1},\\ \Gamma_{3S,3S}(E) &= 3 \times \frac{2^{15}3^6}{5^{12}}\frac{4\pi\epsilon_0}{m^2e^2c^3}(E - E_{2P} - n_i\hbar\omega_i)^3 = 6.32\,\mu\text{s}^{-1}.\end{aligned} \tag{219}$$

The corresponding lifetimes are $\tau_{2P_0} = 1.586$ ns and $\tau_{3S} = 157.4$ ns. Using equation (216), we obtain for the on-resonance Autler–Townes split states, $|\pm, n\rangle = (|2P, n+1\rangle \pm |3S, n\rangle)/\sqrt{2}$, that $\Gamma_{++}(E) = \Gamma_{--}(E) = 316.6\ \mu\text{s}^{-1}$, and $|\Gamma_{+-}(E)| = 310.2\,\mu\text{s}^{-1}$.

Delaying the spontaneous emission is achieved by exciting the ground-state hydrogen atom with a light pulse (linearly polarized in the x direction) whose shape, determined according to the procedure outlined in the previous section, for an optimization time of 2.4 ns, is shown in figure 48.

The result of exciting with the optimized pulse of figure 48 is displayed in figure 49 for four different splittings (ΔE). We see a step-like decay: the system starts with a quiescent period that lasts longer and longer the smaller the Autler–Townes splitting (i.e. Ω_{n_i}) is. As mentioned above, the onset of the photon-burst can be avoided by exchanging the population between levels, thereby sending the time backwards until the next onset of the photon-burst phase at which point another exchange of population is executed. In [180], the application of a π pulse was suggested as a means of achieving this population exchange. However, because

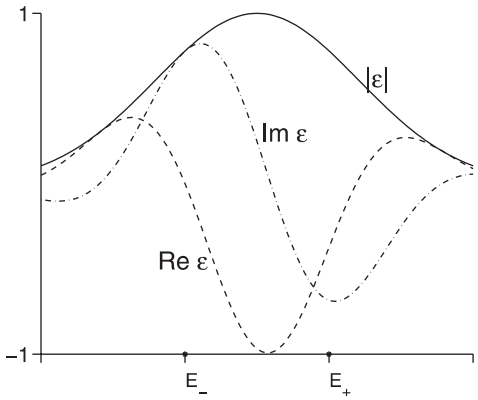

Figure 48. The light pulse (in frequency space) used to excite the Autler–Townes split $|2P_0\rangle$ state from the ground 1S state to produce the optimal c_α coefficients. This choice of coefficients is the one most effective in delaying the emission (in the absence of the interruptions) over the optimization time of 2.4 ns.

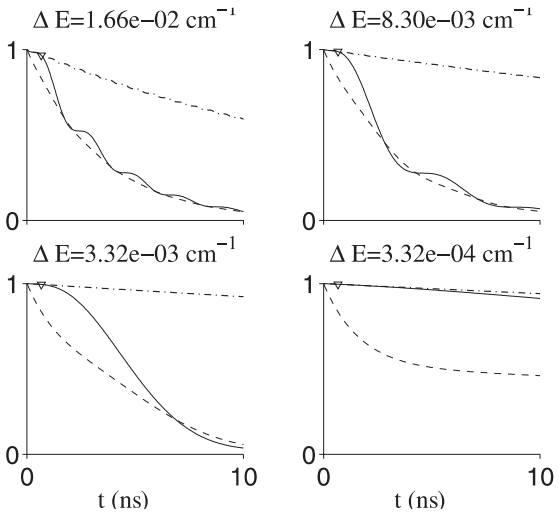

Figure 49. Suppression of the 2P–1S spontaneous emission in the hydrogen atom, for which the natural line-width is $\hbar\bar{\Gamma} = 1.66 \times 10^{-3}\,\mathrm{cm}^{-1}$. The solid lines display the decay of the optimized superposition of the Autler–Townes split levels with no interruptions. The dot-dashed lines are the decay curves of the same superposition states in the presence of interruptions. The dashed lines display the average decay of the two Autler–Townes split components. The optimization time τ ($\triangle$) is $0.2/\Gamma = 0.65$ ns, and the total time range displayed is 0 to $3/\Gamma = 10$ ns.

in atoms and homonuclear diatomic molecules the $|+n_i, 0\rangle$ and $|-n_i, 0\rangle$ states are not coupled optically to one another, the desired π pulse would have to arise from a two-photon (e.g. Raman) process. Rather, we can achieve the same reversal of time by switching the levels while keeping the population of the levels intact. According to equation (199), we can switch the order of the $E^{\pm}_{n_i}$ levels by adiabatically changing the sign of Ω_{n_i}. A schematic illustration as to the kind of interruption needed in the spectator cw field to achieve this is displayed in figure 50.

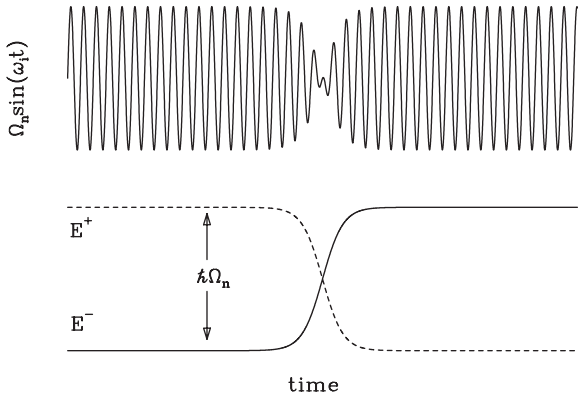

Figure 50. The train wave of the spectator cw field of frequency ω_i near an interruption that switches Ω_{n_i} to $-\Omega_{n_i}$, thereby exchanging the order of the $E^{\pm}_{n_i}$ levels, as shown in the lower panel.

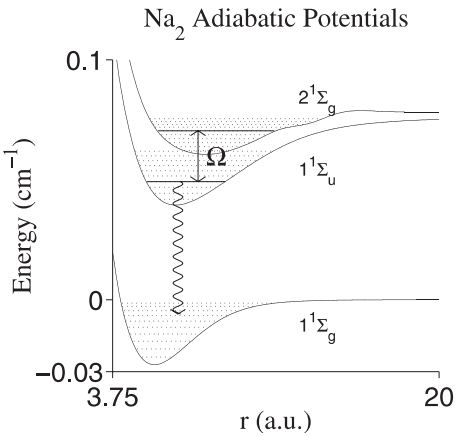

Figure 51. The three lowest singlet potential energy curves of Na_2: $1\,^1\Sigma_g$, $1\,^1\Sigma_u$, and $2\,^1\Sigma_g$. Every fifth vibrational level is marked with a dashed line. The $|a\rangle$ state is the $v = 20$ vibrational level of the second potential. The $|b\rangle$ state is the $v' = 30$ vibrational level of the third potential. Both are marked by solid lines. The Franck–Condon factor (= overlap integral) between these two-states is 0.118.

The decay curves resulting from the Autler–Townes split levels subject to the interruptions displayed in figure 50 is shown as the dot-dash curve of figure 49. We see that the spontaneous emission has been effectively suppressed, with the suppression becoming more effective, the smaller is the Autler–Townes splitting. Also shown in figure 49 (as the dashed line) are the natural decay curves, arising when we start with one of the eigenstates, i.e. $c_{\alpha'} = \delta_{\alpha\alpha'}$. As can be seen, this decay, which is non-exponential due to the interaction between the resonances, is still much faster than the suppressed decay aided by the interruptions.

12.3. Suppression of the $Na_2(A \rightarrow X)$ spontaneous emission

We now demonstrate that the suppression of spontaneous emission method works equally well for molecular systems. In a molecule there are usually a multitude of final states to which

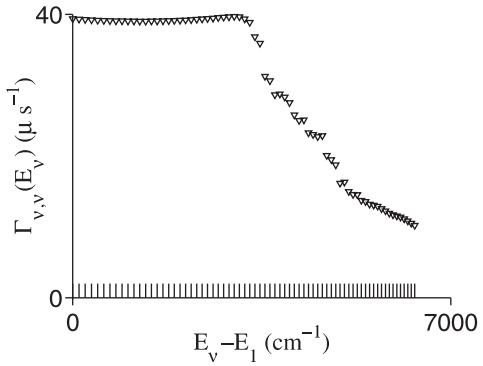

Figure 52. The decay rates $\Gamma_{vv}(E_v)$ of the 70 lowest vibrational states $|v\rangle$ of the $1\,^1\Sigma_u$ surface.

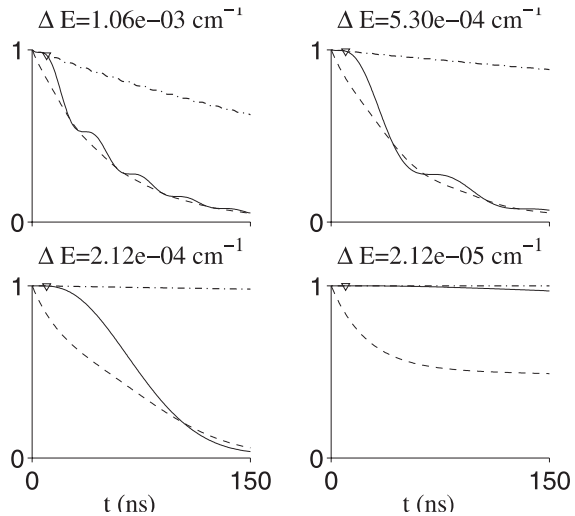

Figure 53. Suppression of the spontaneous emission of the sodium dimer. The optimization time τ ($\triangle$) is $0.2/\Gamma = 10$ ns, and the total time range displayed is 0 to $3/\Gamma = 150$ ns.

the system can emit. In this example, we consider suppressing the emission from a particular ($|a\rangle$) vibrational state belonging to the $1\,^1\Sigma_u$ (A) electronic manifold, aided by a particular vibrational ($|b\rangle$) state belonging to the $2\,^1\Sigma_g$ electronic manifold. The relevant potentials are displayed in figure 51.

Using an average electronic transition-dipole moment μ_e of 7 Debye ($= 2.756$ a.u.) between the $1\,^1\Sigma_u$ (A) and the ground $1\,^1\Sigma_g$ (X) states [192], we have calculated the dipole moment matrix elements within the Franck–Condon approximation, according to which

$$\boldsymbol{D}_{v,\gamma} \approx \mu_e \langle v|\gamma\rangle, \tag{220}$$

where $|v\rangle$ and $|\gamma\rangle$ signify vibrational states.

The vibrational wavefunctions needed for this calculation were derived from the potential energy curves of Schmidt and Meyer [193][9]. In the present initial study only the vibrational states (without the rotational sub-levels) were included in the calculations; the inclusion of rotation is not expected to qualitatively change the conclusions drawn here.

[9] The Na–Na potential curves and the relevant electronic dipole moments are from [193].

The lineshape for the vibrational levels (and specifically that of $v = 20$) of the excited surface $1\,^1\Sigma_u$ are much narrower than the energy level spacing, therefore all the resonances are isolated, as in the atomic cases discussed above.

Assuming that the decay rates of the vibrational levels belonging to the $2\,^1\Sigma_g$ manifold (which can decay to the $1\,^1\Sigma_u$ manifold) are negligible compared to those of the $1\,^1\Sigma_u$ surface, we can write $\Gamma_{vv}(E)$ as,

$$\Gamma_{vv}(E) = \frac{e^2}{3\pi\epsilon_0\hbar^4c^3} \sum_{\{\gamma:E>E_\gamma\}} |\boldsymbol{D}_{v,\gamma}|^2(E - E_\gamma)^3, \tag{221}$$

where γ includes only the vibrational levels in the ground electronic manifold. We obtain that for $0 \leqslant v \leqslant 30$, $\Gamma_{vv}(E_v) \approx 40\,\mu s^{-1}$ or $\hbar\Gamma_{vv} = 2.12 \times 10^{-4}\,cm^{-1}$. The change of $\Gamma_{vv}(E)$ with energy may be neglected, since the relevant integration range around E_v, $\pm\hbar\Gamma = \pm 2.1 \times 10^{-4}\,cm^{-1}$, is much smaller than $E_v - E_\gamma$ for all $|\gamma\rangle$ ground states considered.

Figure 52 displays the decay widths $\Gamma_{vv}(E_v)$ for the 70 lowest vibrational states $|v\rangle$ of the $1\,^1\Sigma_u$ surface. Also displayed are the energy levels E_v.

The decay curves resulting from coupling the $|a\rangle = |v = 20\rangle$ with the $|b\rangle = |v' = 30\rangle$ are shown in figure 53. Again the method is very successful in completely suppressing the decay.

Acknowledgments

This work was supported by the US Office of Naval Research, by the Minerva Foundation, Germany, by the German Israel Fund, and by the EU IHP program HPRN-CT-1999-00129.

References

[1] Shapiro M and Brumer P 2003 *Principles of the Quantum Control of Molecular Processes* (New York: Wiley) at press
[2] Rice S A and Zhao M 2000 *Optical Control of Molecular Dynamics* (New York: Wiley)
[3] Brumer P and Shapiro M 1986 *Chem. Phys. Lett.* **126** 541
[4] Shapiro M and Brumer P 1987 *Faraday Discuss. Chem. Soc.* **82** 177
[5] Muller H G, Bucksbaum P H, Schumacher D W and Zavriyev A 1990 *J. Phys.* B **23** 2761
Potvliege R M and Smith P H G 1992 *J. Phys.* B **25** 2501
[6] Schafer K J and K C Kulander 1992 *Phys. Rev.* A **45** 8026
[7] Brumer P and Shapiro M 1992 *Ann. Rev. Phys. Chem.* **43** 257
[8] Bandrauk A D, Gauthier J M and McCann J F 1992 *Chem. Phys. Lett.* **200** 399
[9] Shapiro M and Brumer P 1993 *Chem. Phys. Lett.* **208** 193
[10] Ivanov M Yu, Corkum B P and Dietrich P 1993 *Laser Phys.* **3** 375
[11] Charron E, Guisti-Suzor A and Mies H F 1993 *Phys. Rev. Lett.* **71** 692
[12] Shapiro M and Brumer P 1994 *Int. Rev. Phys. Chem.* **13** 187
[13] Shapiro M and Brumer P 1997 *Trans. Faraday Soc.* **93** 1263
[14] Shapiro M and Brumer P 1999 *Advances in Atomic, Molecular and Optical Physics* vol 42, ed B Bederson and H Walther (San Diego: Academic) pp 287–343
[15] Gordon R J and Rice S A 1997 *Ann. Rev. Phys. Chem.* **48** 595
[16] Tannor D and Rice S A 1985 *J. Chem. Phys.* **83** 5013
[17] Tannor D J, Kosloff R and Rice S A 1986 *J. Chem. Phys.* **85** 5805
[18] Shi S, Woody A and Rabitz H 1988 *J. Chem. Phys.* **88** 6870
Peirce A P, Dahleh M A and Rabitz H 1988 *Phys. Rev.* A **37** 4950
[19] Shi S and Rabitz H 1989 *Chem. Phys.* **139** 185
[20] Kosloff R, Rice S A, Gaspard P, Tersigni S and Tannor D J 1989 *Chem. Phys.* **139** 201
[21] Peirce A P, Dahleh M A and Rabitz H 1990 *Phys. Rev.* A **42** 1065
[22] Jakubetz W, Manz J and Schreier H-J 1990 *Chem. Phys. Lett.* **165** 100
[23] Shi S and Rabitz H 1991 *Comp. Phys. Commun.* **63** 71
[24] Warren W S, Rabitz H and Dahleh M 1993 *Science* **259** 1581

[25] Yan Y, Gillilan R E, Whitnell R M and Wilson K R 1993 *J. Phys. Chem.* **97** 2320
Krause J L, Whitnell R M, Wilson K R, Yan Y and Mukamel S 1993 *J. Chem. Phys.* **99** 6562
[26] Kohler B, Krause J L, Raski F, Wilson K R, Yakovlev V V, Whitnell R M and Yan Y 1995 *Acct. Chem. Res.* **28** 133
[27] Bernstein R B (ed) 1979 *Atom-Molecule Collision Theory, A Guide for the Experimentalist* (New York: Plenum)
[28] Shapiro M and Brumer P 2001 *J. Phys. Chem.* **105** 2897
[29] Shapiro M 2000 *Adv. Chem. Phys.* **114** 123
[30] Judson R S and Rabitz H 1992 *Phys. Rev. Lett.* **68** 1500
[31] Bardeen C J, Yakovlev V V, Wilson K R, Carpenter S D, Weber P M and Warren W S 1997 *Chem. Phys. Lett.* **280** 151
[32] Yelin D, Meshulach D and Silberberg Y 1997 *Opt. Lett.* **22** 1793
[33] Assion T, Baumert T, Bergt M, Brixner T, Kiefer B, Seyfried V, Strehle M and Gerber G 1998 *Science* **282** 919
[34] Levis R J, Menkir G M and Rabitz H 2001 *Science* **292** 709
[35] Herek J L, Wohlleben W, Cogdell R J, Zeidler D and Motzkus M 2002 *Nature* **417** 533
[36] Shapiro M and Bersohn R 1980 *J. Chem. Phys.* **73** 3810
[37] Shapiro M 1986 *J. Phys. Chem.* **90** 3644
[38] Brumer P and Shapiro M 1999 *Coherent Control in Atoms, Molecules and Semiconductors* ed W Pötz and W A Schröder (Dordrecht: Kluwer)
[39] Cook D J and Hochstrasser R M 2000 *Opt. Lett.* **25** 1210
[40] Crim F F 1984 *Ann. Rev. Phys. Chem.* **35** 647
[41] Ticich T M, Likar M D, Dubal H, Butler L J and Crim F F 1987 *J. Chem. Phys.* **87** 5820
[42] Likar M D, Baggott J E, Sinha A, Ticich T M, Vander Wal R L and Crim F F 1988 *J. Chem. Soc. Faraday Trans.* **84** 1483
[43] Sinha A, Vander Wal R L and Crim F F 1989 *J. Chem. Phys.* **91** 2929
[44] Crim F F 1990 *Science* **249** 1387
[45] Vander R L Wal, Scott J L and Crim F F 1991 *J. Chem. Phys.* **94** 1859
[46] Arutsi-Parpar T, Schmid R P, Li R-J, Bar I and Rosenwaks S 1997 *Chem. Phys. Lett.* **268** 163
[47] Bar I and Rosenwaks S 2001 *Int. Rev. Phys. Chem.* **20** 711
[48] Shapiro M, Hepburn J W and Brumer P 1988 *Chem. Phys. Lett.* **149** 451
[49] Chen C, Yin Y-Y and Elliott D S 1990 *Phys. Rev. Lett.* **64** 507
Chen C, Yin Y-Y and Elliott D S 1990 *Phys. Rev. Lett.* **65** 1737
[50] Park S M, Lu S-P and Gordon R J 1991 *J. Chem. Phys.* **94** 8622
[51] Lu S P, Park S M, Xie Y and Gordon R J 1992 *J. Chem. Phys.* **96** 6613
[52] Kleiman V D, Zhu L, Li X and Gordon R J 1995 *J. Chem. Phys.* **102** 5863
[53] Zhu L, Kleiman V D, Li X, Lu S, Trentelman K and Gordon R J 1995 *Science* **270** 77
[54] Zhu L, Suto K, Fiss J A, Wada R, Seideman T and Gordon R J 1997 *Phys. Rev. Lett.* **79** 4108
[55] Wang X, Bersohn R, Takahashi K, Kawasaki M and Kim H L 1996 *J. Chem. Phys.* **105** 2992
[56] Gordon R J, Zhu L C and Seideman T 1999 *Acc. Chem. Res.* **32** 1007
[57] Kurizki G, Shapiro M and Brumer P 1989 *Phys. Rev.* B **39** 3435
[58] Schafer K J and Kulander K C 1992 *Phys. Rev.* A **45** 8026
[59] Potvliege R M and Smith P H G 1992 *J. Phys.* B **25** 2501
[60] Atanasov R, Haché A, Hughes L P, van Driel H M and Sipe J E 1996 *Phys. Rev. Lett.* **76** 1703
[61] Baranova B A, Chudinov A N and Ya Zel'dovitch B 1990 *Opt. Commun.* **79** 116
[62] Yin Y-Y, Chen C, Elliott D S and Smith A V 1992 *Phys. Rev. Lett.* **69** 2353
[63] Yin Y-Y, Shehadeh R, Elliott D and Grant E 1995 *Chem. Phys. Lett.* **241** 591
[64] Dupont E, Corkum P B, Liu H C, Buchanan M and Wasilewski Z R 1995 *Phys. Rev. Lett.* **74** 3596
[65] Sheehy B, Walker B and DiMauro L F 1995 *Phys. Rev. Lett.* **74** 4799
[66] Haché A, Kostoulas Y, Atanasov R, Hughes J L P, Sipe J E and van Driel H M 1997 *Phys. Rev. Lett.* **78** 306
[67] Charron E, Giusti-Suzor A and Mies F H 1995 *Phys. Rev. Lett.* **75** 2815
[68] Charron E, Giusti-Suzor A and Mies F H 1995 *J. Chem. Phys.* **103** 7359
[69] Aubanel E E and Bandrauk A D 1994 *Chem. Phys. Lett.* **229** 169
[70] Zuo T and Bandrauk A D 1996 *Phys. Rev.* A **54** 3254
[71] Ehlotzky F 2001 *Phys. Rep.* **345** 175
[72] Tannor D J and Rice S A 1988 *Adv. Chem. Phys.* **70** 441
[73] Tannor D J *Introduction to Quantum Mechanics: A Time Dependent Perspective* (Sausalito: University Science Press) submitted
[74] Levy I, Shapiro M and Brumer P 1990 *J. Chem. Phys.* **93** 2493
[75] Abrashkevich D G, Shapiro M and Brumer P 1998 *J. Chem. Phys.* **108** 3585

[76] Seideman T, Shapiro M and Brumer P 1989 *J. Chem. Phys.* **90** 7132
[77] Shapiro M and Brumer P 1993 *J. Chem. Phys.* **98** 201
[78] McCauley J C 1997 *Classical Mechanics* (Cambridge: Cambridge University Press)
[79] Brumer P 1990 *Encyclopedia of Modern Physics* ed R A Meyers (New York: Academic) p 205
[80] Brumer P 1981 *Adv. Chem. Phys.* **47** 201
[81] Pattanayak A and Brumer P 1996 *Phys. Rev. Lett.* **77** 59
[82] Wilkie J and Brumer P 1997 *Phys. Rev.* A **55** 27
Wilkie J and Brumer P 1997 *Phys. Rev.* A **55** 43
[83] Blümel R, Fishman S and Smilansky U 1986 *J. Chem. Phys.* **84** 2604
[84] Casati G and Chirikov B 1995 *Quantum Chaos: Between Order and Disorder* (Cambridge: Cambridge University Press)
[85] Gong J and Brumer P 2001 *Phys. Rev. Lett.* **86** 1741
[86] Moore F L *et al* 1995 *Phys. Rev. Lett.* **75** 598
Klappauf B G *et al* 1998 *Phys. Rev. Lett.* **81** 203
Ammann H *et al* 1998 *Phys. Rev. Lett.* **80** 111
[87] Blümel R and Reinhardt W P 1997 *Chaos in Atomic Physics* (Cambridge: Cambridge University Press)
[88] Gong J and Brumer P 2001 *J. Chem. Phys.* **115** 3590
[89] Haake F 1992 *Quantum Signatures of Chaos* (Berlin: Springer)
[90] Gong J, Woerner H J and Brumer P in preparation
[91] Krause J L, Shapiro M and Brumer P 1990 *J. Chem. Phys.* **92** 1126
[92] Shapiro M and Brumer P 1996 *Phys. Rev. Lett.* **77** 2574
[93] Holmes D, Shapiro M and Brumer P 1996 *J. Chem. Phys.* **105** 9162
[94] Abrashkevich A, Shapiro M and Brumer P 1998 *Phys. Rev. Lett.* **81** 3789
[95] Abrashkevich A, Shapiro M and Brumer P 1999 *Phys. Rev. Lett.* **82** 3002 (erratum)
[96] Brumer P, Abrashkevich A G and Shapiro M 2000 *Faraday Discuss. Chem. Soc.* **113** 291
[97] Brumer P, Bergmann K and Shapiro M 2000 *J. Chem. Phys.* **113** 2053
[98] Abrashkevich A, Shapiro M and Brumer P 2001 *Chem. Phys.* **267** 81
[99] Smith E T, Dhirani A A, Koborowski D A, Rubenstein R A, Roberts T D, Yao H and Pritchard D E 1998 *Phys. Rev. Lett.* **81** 1996
[100] Phillips W D 1998 *Rev. Mod. Phys.* **70** 721
[101] Weitz M, Young B C and Chu S 1994 *Phys. Rev. Lett.* **94** 2563
[102] Bethlem H L, van Roij A J, Jongma R T and Meijer G 2002 *Phys. Rev. Lett.* **88** 133003
[103] Gong J, Shapiro M and Brumer P 2003 *J. Chem. Phys.* **118** 2626
[104] Omnes R 1994 *The Interpretation of Quantum Mechanics* (Princeton: Princeton University Press)
Omnes R 1999 *Understanding Quantum Mechanics* (Princeton: Princeton University Press)
[105] Blum K 1981 *Density Matrix Theory and Applications* (New York: Plenum)
[106] Kupsch J 1996 *Decoherence and the Appearance of the Classical World* ed D Giulini *et al* (New York: Springer)
[107] May V and Kuhn O 2002 *Charge and Energy Transfer Dynamics in Molecular Systems* (Berlin: Wiley-VCH)
[108] Gong J and Brumer P 1999 *Phys. Rev.* E **60** 1643
[109] Caldeira A O and Leggett A J 1983 *Physica* A **121** 587
Unruh W G and Zurek W H 1989 *Phys. Rev.* D **40** 1071
Hu B L, Paz J P and Zhang Y 1992 *Phys. Rev.* D **45** 2843
Hu B L, Paz J P and Zhang Y 1993 *Phys. Rev.* D **47** 1576
[110] Jaffe C and Brumer P 1985 *J. Chem. Phys.* **82** 2330
[111] Eckhardt B, Hose G and Pollak E 1989 *Phys. Rev.* A **39** 3776
[112] Christoffel K M and Brumer P 1985 *Phys. Rev.* A **33** 1309
[113] Han H and Brumer P *Decoherence Effects in Reactive Scattering* in preparation
[114] Palma G M, Suominen K-A and Ekert A K 1996 *Proc. R. Soc.* A **452** 567
Duan L-M and Guo G-C 1997 *Phys. Rev. Lett.* **79** 1953
Duan L-M and Guo G-C 1998 *Phys. Rev.* A **57** 737
Zanardi P 1997 *Phys. Rev.* A **56** 4445
Zanardi P and Rasetti M 1997 *Phys. Rev. Lett.* **79** 3306
Lidar D A, Chuang I L and Whaley K B 1998 *Phys. Rev. Lett.* **81** 2594
Bacon D, Kempe J, Lidar D A and Whaley K B 2000 *Phys. Rev. Lett.* **85** 1758
[115] Nielsen M A and Chuang I L 2000 *Quantum Computation and Quantum Information* (Cambridge: Cambridge University Press)
[116] Demirplak M and Rice S A 2002 *J. Chem. Phys.* **116** 8028
[117] Iwaki L K and Dlott D L 2000 *J. Phys. Chem.* A **104** 9109

[118] Bardeen C J, Wang Q and Shank C V 1995 *Phys. Rev. Lett.* **75** 3410
[119] Brixner T, Damrauer N H, Niklaus P and Gerber G 2001 *Nature* **414** 57
[120] Shapiro M and Brumer P 1989 *J. Chem. Phys.* **90** 6179
[121] Allen L and Stroud C R Jr 1982 *Phys. Rep.* **91** 1
[122] Macomber J D 1976 *The Dynamics of Spectroscopic Transitions* (New York: Wiley)
[123] Cao J, Messina M and Wilson K R 1997 *J. Chem. Phys.* **106** 5239
[124] Cao J, Bardeen C J and Wilson K R 2000 *J. Chem. Phys.* **113** 1898
[125] Schirrmeister D H and May V 1997 *Chem. Phys.* **220** 1
Schirrmeister D H and May V 1998 *Chem. Phys. Lett.* **297** 383
[126] Batista V S and Brumer P 2002 *Phys. Rev. Lett.* **89** 143201
[127] Guillar V, Batista V S and Miller W H 2000 *J. Chem. Phys.* **113** 9510
[128] Campolieti G and Brumer P 1992 *J. Chem. Phys.* **96** 5969
Campolieti G and Brumer P 1994 *Phys. Rev.* A **50** 997
Campolieti G and Brumer P 1996 *Phys. Rev.* A **53** 2958
Campolieti G and Brumer P 1997 *J. Chem. Phys.* **107** 791
Campolieti G and Brumer P 1998 *J. Chem. Phys.* **109** 2999
McQuarrie B and Brumer P 2000 *Chem. Phys. Lett.* **319** 27
Batista V S and Brumer P 2001 *J. Phys. Chem.* **105** 2591
Batista V S and Brumer P 2001 *J. Chem. Phys.* **114** 10321
[129] Jiang X-P and Brumer P 1993 *Chem. Phys. Lett.* **208** 179
[130] Pattanayak A and Brumer P 1997 *Phys. Rev. Lett.* **79** 4131
[131] Sterling M, Zadoyan R and Apkarian V A 1996 *J. Chem. Phys.* **104** 6497
[132] Gershgoren E, Vala J, Kosloff R and Ruhman S 2001 *J. Phys. Chem.* A **105** 5081
[133] Jiang X-P, Shapiro M and Brumer P 1996 *J. Chem. Phys.* **104** 607
[134] Chen Z, Shapiro M and Brumer P 1995 *J. Chem. Phys.* **102** 5683
[135] Shnitman A, Sofer I, Golub I, Yogev A, Shapiro M, Chen Z and Brumer P 1996 *Phys. Rev. Lett.* **76** 2886
[136] Knight P L, Lauder M A and Dalton B J 1990 *Phys. Rep.* **190** 1
[137] Nakajima T, Elk M, Jian Z and Lambropoulos P 1994 *Phys. Rev.* A **50** R913
[138] Halfmann T, Yatsenko L P, Shapiro M, Shore B W and Bergmann K 1998 *Phys. Rev.* A **58** R46
[139] Cavalieri S, Eramo R, Fini L, Materazzi M, Faucher O and Charalambidis D 1998 *Phys. Rev.* A **57** 2915
[140] Baldwin K G H, Bott M D, Bachor H A and Chapple P B 2000 *J. Opt.* B **2** 470
[141] Barron L D 1982 *Molecular Light Scattering and Optical Activity* (Cambridge: Cambridge University Press)
[142] Woolley R G 1975 *Adv. Phys.* **25** 27
Walker D C (ed) 1979 *Origins of Optical Activity in Nature* (Amsterdam: Elsevier)
[143] For a discussion, see Barron L D 1986 *Chem. Soc. Rev.* **15** 189
For historical examples, see Bel J A 1874 *Bull. Soc. Chim. Fr.* **22** 337
Van't Hoff J-H 1894 *Die Lagerung der Atome im Raume* 2nd edn (Braunschweig: Vieweg) p 30
[144] Quack M 1989 *Angew. Chem. Int. Ed. Engl.* **28** 571
[145] Shapiro M and Brumer P 1991 *J. Chem. Phys.* **95** 8658
[146] Shapiro M, Frishman E and Brumer P 2000 *Phys. Rev. Lett.* **84** 1669
[147] Gerbasi D, Shapiro M and Brumer P 2001 *J. Chem. Phys.* **115** 5349
[148] Brumer P, Frishman E and Shapiro M 2001 *Phys. Rev.* A **65** 015401
[149] Salam A and Meath W J 1998 *Chem. Phys.* **228** 115
[150] Fujimura Y, Gonalez L, Hoki K, Manz J and Ohtsuki Y 1999 *Chem. Phys. Lett.* **306** 1
Fujimura Y, Gonalez L, Hoki K, Manz J and Ohtsuki Y 1999 *Chem. Phys. Lett.* **310** 578 (errata)
Fujimura Y, Gonzalez L, Hoki K, Kroener D, Manz J and Ohtsuki Y 2000 *Angew. Chem. Int. Ed. Engl.* **39** 4586
Hoki K, Ohtsuki Y and Fujimura Y 2001 *J. Chem. Phys.* **114** 1575
Hoki K, Kroener D and Manz J 2001 *Chem. Phys.* **267** 59
[151] Hoki K, Gonzalez L and Fujimura Y 2002 *J. Chem. Phys.* **116** 2433
[152] Maierle C S and Harris R A 1998 *J. Chem. Phys.* **109** 3713
[153] Shirley J H 1965 *Phys. Rev.* B **138** 979
[154] Brown A and Meath W J 1998 *J. Chem. Phys.* **109** 9351
[155] Shapiro M, Frishman E and Brumer P Enantiomeric purification of non-polarized racemic mixtures with coherent light *J. Chem. Phys.* submitted
[156] Hollas J M 1982 *High Resolution Spectroscopy* (London: Butterworths)
[157] Harris R A, Shi Y and Cina J A 1994 *J. Chem. Phys.* **101** 3459
Cina J A and Harris R A 1994 *J. Chem. Phys.* **100** 2531

[158] Segev E and Shapiro M 1980 *J. Chem. Phys.* **73** 2001
Segev E and Shapiro M 1982 *J. Chem. Phys.* **77** 5601
[159] Shapiro M 1972 *J. Chem. Phys.* **56** 2582
[160] Deretey E, Shapiro M and Brumer P 2001 *J. Phys. Chem.* A **105** 9509
[161] Hayashi M, Mebel A M, Liang K K and Lin S H 1998 *J. Chem. Phys.* **108** 2044
[162] Lochbrunner S, Schults T, Schmitt M, Shaffer J P, Zgierski M Z and Stolow A 2001 *J. Chem. Phys.* **114** 2519
[163] Gerbasi D, Shapiro M and Brumer P at press
[164] Brumer Y, Shapiro M, Brumer P and Balderidge K 2002 *J. Phys. Chem.* A **106** 9512
[165] Beumee J G B and Rabitz H 1990 *J. Math. Phys.* **31** 1253
[166] Aubanel E E and Bandrauk A D 1994 *Can. J. Chem.* **72** 673
[167] Cao J and Wilson K R 1997 *J. Chem. Phys.* **107** 1441
[168] de Araujo L E E and Walmsley I A 1999 *J. Phys. Chem.* A **103** 10409
[169] Král P, Amitay Z and Shapiro M 2002 *Phys. Rev. Lett.* **89** 063002
[170] Bergmann K, Theuer H and Shore B W 1998 *Rev. Mod. Phys.* **70** 1003
[171] Misra B 1977 *J. Math. Phys.* **18** 756
[172] Milburn G J 1988 *J. Opt. Soc. Am.* B **5** 1317
[173] Itano W M, Heinzen D J, Bollinger J J and Wineland D J 1990 *Phys. Rev.* A **41** 2295
[174] Knight P 1990 *Nature* **344** 493
[175] Frerichs V and Schenzle A 1991 *Phys. Rev.* A **44** 1962
[176] Kofman A G and Kurizki G 1996 *Phys. Rev.* A **54** R3750
[177] Facchi P and Pascazio S 1998 *Phys. Lett.* A **241** 139
[178] Kofman A G and Kurizki G 2000 *Nature* **405** 546
[179] Plenio M B, Knight P L and Thompson R C 1996 *Opt. Commun.* **123** 278
[180] Frishman E and Shapiro M 2001 *Phys. Rev. Lett.* **87** 253001
[181] Frishman E and Shapiro M Suppression of the spontaneous emission of atoms and molecules *Phys. Rev.* A submitted
[182] Autler S H and Townes C H 1955 *Phys. Rev.* **100** 703
[183] Friedrichs K C 1948 *Commun. Pure Appl. Math.* **1** 361
[184] Feshbach H 1967 *Ann. Phys.* **19** 287
Feshbach H 1967 *Ann. Phys.* **43** 410
[185] Fano U 1961 *Phys. Rev.* **124** 1866
[186] Levine R D 1969 *Quantum Mechanics of Molecular Rate Processes* (Oxford, UK: Clarendon)
[187] Cohen-Tannoudji C, Diu B and Laloë F 1977 *Quantum Mechanics* (New York: Wiley)
[188] Scully M and Zubairy M S 1997 *Quantum Optics* (Cambridge: Cambridge University Press)
[189] Loudon R *The Quantum Theory of Light* equations 4.111, 4.113, 5.140 and pp 174–9
[190] Harris S E 1989 *Phys. Rev. Lett.* **62** 1033
[191] Alonso-Medina A 1996 *J. Quant. Spectrosc. Radiat. Transfer* **55** 151
[192] Stevens W J, Hessel M M, Bertonicini P J and Wahl A C 1977 *J. Chem. Phys.* **66** 1477
[193] Schmidt I 1987 *PhD Thesis* Kaiserslautern University